MiCHe project

Multi-risk Hazard_ Norman Tower of Craco

Team Leader: Dora Foti

Collaborators: Mariella Diaferio

Michela Lerna

Maria Francesca Sabbà

Sommario

Introduction

The study and the mitigation of seismic risk in Italian Cultural and Historical Heritageis a problem that requires a multidisciplinary approach, as it integrates aspects of seismic hazard, vulnerability and exposure. Among these structures, the masonry ones constitute the main part. Masonry materials have low ductility, which can lead to rather fragile global behaviour; therefore, masonry structures are particularly vulnerable to dynamic actions.

The preservation of the Architectural Heritage, towards seismic actions, occupies a prominent place in our country. Following the collapses and damages recorded during the recent seismic events and to safeguard the Cultural Heritage, masonry buildings may be required to withstand horizontal forces.In past, in fact, the construction concept focused mainly on the action of vertical loads and not on force and ductility with respect to horizontal forces. So,in this field, the research goal isto analyse “ancient structures” in order to understand their structural behaviour and the related failure patterns. In recent years, their geometric characteristics have been a topic of discussion in various researches focused on evaluation methods to determine their dynamic behaviour [1-4] and on intervention solutions for structural repair and strengthening [5, 6]. Their behaviour is very poor for the purposes of resistance, especially if they are built in aggregates as shown in the literature [7, 8].

In this research the interest is centred on the Medieval City of Craco, near Matera and in particular on its tower [9]. This Norman structure was endowed with a defensive purpose and, for this reason, locatedon the highest point of the hill. The city has developed over time around it, thus creating the actual historic centre.

Today visiting Craco, the scenario is a village completely abandoned due to the damages atbuildings caused by serious landslidesdeveloped in the south-western part between 1959 and 1972, as shown in Figure 1.

FIGURE 1: VIEW FROM THE TOP OF THE HISTORIC CENTRE OF CRACO, INDICATING THE NORMAN TOWER (IN RED)

The propensity for landslides derives from the lithological composition and the geomorphological structure of the area. The upper part is made up of conglomerates, interspersed with sand, erodible and very permeable; while the underlying layers are mainly composed of relatively permeable sandy clay, which forms the bed of the water table. The swelling and plasticity of the clay on the contact surface causes the conglomerates and rubble to slide downstream in decay, triggering landslides

In Craco area there are several types of landslides: collapses due to the breaking of boulders in the north-eastern side, roto-translational shifts, earth flows and lateral expansions on the

southern side. Today's picture is made up of two scenarios: first, the still active landslide in South-East area near the "convent"; secondly the landslides currently inactive,of the "Historic centre" in the South-West andnear "Schools area " in the North-West.

The rapid evolution of landslides reactivated between the sixties and the seventies of the twentieth century, which caused collapses and large structural movements, gave rise to two evacuation orders issued the first in 1962 and the second in 1991 with the transfer of the inhabitants mostly towards the nearby valley.

The present study, through Visual inspection,Operational Modal Analysis(OMA) [10-12], (particularly suitable for this type of structure [13-19]) and Seismic Risck Analysis, aims to evaluate the real behaviour of the Norman Tower and to determine the effective stability of the structure in relation to a possible evolution of the landslide. Due to the uncertainties related to the properties of the material and the characteristics of the structural elements that make up the tower, the complete definition of a numerical model able to estimate the structural behaviour of the tower turns out to be quite complex.Also, an experimental test campaign was conducted, performing dynamic tests considering the environmental forces, in order to avoid the use of destructive tests that are not compatible with the historical character of the tower examined.Finaly to achieve an accurate Numerical Model on which it is possible to conduct further studies to evaluate the behaviour of the structure in relation to the evolution of the landslide, the data obtained from the test campaign will be compared with the previous dynamic characteristics evaluated by Finite Element Model (FEM).

FIGURE 2-3: SOUTH VIEW OF THE HISTORIC CENTRE OF CRACO AND NORMAN TOWER

FIGURE 4 - SOUTH-EAST VIEW OF THE HISTORIC CENTRE OF CRACO.

I. Mono-risk landslide hazard

I.1 The landslide

The municipality of Craco, in the province of Matera (Italy), is located in a hilly area between the Agri and Cavone rivers, which, further East, flow into the Gulf of Taranto.

The ancient inhabited center rises on the top of a hilly ridge that reaches the maximum elevation of 390 m on the sea level (o.s.l.) and extends in the direction NW-SE between the incisions of the Salandrella torrents to the North-East and Bruscata to the South-West. The landscape, typical of the clayey hills of the Matera area, is characterized by modest and isolated hills, on the peaks of which the oldest inhabited areas of the region are found.

The sides of the hills, almost everywhere, are scarce in vegetation due to the climate and the clayey nature of the soil, and the shapes that most characterize the landscape are the gullies, which can be seen in large areas along the slopes.

The morphology of the entire area, object of the present study, is very much affected by the complex tectonic structure. In fact, the relations existing between the alien tectonic units and the clay-sandy-conglomeratic units resting in angular disagreement on the previous ones and belonging to different cycles of Pliocene dispositions are visible in outcrop.

There are numerous mass movements that affect the whole area, but the particular development they take along the south-western slope of Craco is evident. This accentuated landslide appears to be closely related to the presence of a large movement, which can be traced back to a Deep Gravitative Slope Deformation. The continuous reactivations of this landslide complex along the slope, which from Craco degrades towards the Bruscata stream, have always threatened the stability of the town until it was reached the drastic decision of abandonment. In fact, the ancient country is currently uninhabited due also to laws that have required its evacuation, following the progressive deterioration of the conditions of stability in the area. To fully understand the main causes that led to the development of this landslide and the aggravation of the seismic hazard of the town, the geology and geomorphology

ofthis area will be analyzed, as well as the development of an analysis on the landslide evolution over the years.

I.2 Geology

Close to the buried front of the southern Apennine mountains, in particular just to the West, it rises the Craco ridge on which the town was built in the Middle Ages (Fig. 5a, b). In the area surfacing non-native units overwrite the plio-pleistocene clastic deposits of the Fossa Bradanica and covered in turn by conglomerates, sands and clays of Plio-Pleistocene age deformed by the continuous advancement of the front of the chain (Fig. 5c).

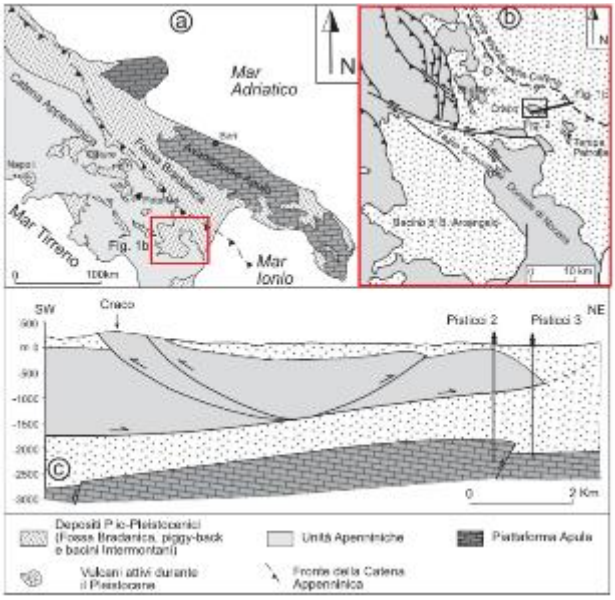

FIGURE 5 – A) REGIONAL GEOLOGICAL SCHEME OF THE SOUTHERN APENNINES. B) TECTONIC SCHEME OF THE FRONTAL PORTION OF THE SOUTHERN APENNINES, INCLUDING THE SCORCIABUOI FAULT AND THE SANT'ARCANGELO BASIN (MODIFIED BY PATACCA&SCADONE, 2001). C) GEOLOGICAL PROFILE ACROSS THE SOUTHERN APENNINE FRONT.

The non-native units are overwritten along a sub-horizontal surface, on the Plio-Pleistocene deposits of the Fossa Bradanica, in turn resting directly on the Apula Platform, lowered in steps by direct high-angle faults. For the development of the structural model it was fundamental to know the data relating to the surveys carried out for the oil exploration in the

area. From the data in possess it can be asserted that the advancement of allochthonous units took place until the middle Pleistocene, given that the overwritten units deposits of the lower Pleistocene have been found [19]. In particular, along the ridge of Craco, the non-native units emerge thanks to the presence of backflows linked to the deformation of the front of the Apennine mountains (Figs. 6 – 7a). From the stratigraphic point of view, allochthonous soils are represented by the Varicolor Clays which are extremely chaotic, due to tectonic and gravitational causes, and it is therefore impossible to reconstruct a stratigraphic succession, as well as to establish a lying; it is also difficult to evaluate the thickness of these coulters, whose formation dates back to the period from the Cretaceous to the Oligocene. This is evident in some points of the north-eastern slope of the Craco hill and in particular in the locality of Macinecchie, where along the ridge it can be observed the surface of discordance that separates the two depositional cycles and in particular the support in onlap of the deposits of the second cycle on the same surface (Fig. 7b).

The first cycle is composed of lenticular conglomerate bodies with sandy intercalations, bioclastic sands (“lower sands” in Fig. 6), marly clays with sandy horizons and finally bioclastic sands (“upper sands” in Fig. 6), with an overall thickness estimated at around 350 meters, while the second cycle is made up of gray marly clays with intercalation of sand and methyl thick tuff levels. The tectonic structures observed in the area of Craco are laterally discontinuous, as can be easily seen from the geological map (Fig. 6). The lateral variability in the geometry of the structures is partly linked to the presence of numerous faults with an anti-Apennine orientation that displace the contractional structures. The presence of these faults was verified by mapping in detail the main conglomerate horizons located at the base of the first cycle. Furthermore, important anti-Apennine faults are clearly visible between

Macinecchie and Tempa S. Lorenzo. In the area of Craco the Pliocene deposits and the Varicolor Clays form a monoclinal immersing towards the north-east (Fig. 6 and 7a), located on the roof of a main backstroke that brings the Varicolor Clays to the clays of the second cycle. The tectonic contact, tilted about 60 ° towards the North-East, is clearly visible from the Bruscata ditch, along the southern slope of the Craco hill. In turn the Varicolor Clays are covered by the basal conglomerate of the first cycle, which always immerses towards the North-East with inclinations of about 60 °. In addition to the left side of the Bruscata ditch, the Varicolored Clays also emerge on the north-eastern slope of the Craco hill, in the locality of Macinecchie, where they are apparently superimposed on the conglomerates and the lower sands. This anomalous situation can be explained with a second retrograde, which brings the Varicolor Clays over the lower sands or the marly clays of the first cycle, as indicated in the geological profile of Figure 7a. The data obtained from the surveys carried out in the Craco area allow to highlight the processes that have operated in the front part of the chain. In particular, it can be documented that the progressive deformation of allochthonous units occurred simultaneously with the sedimentation of Pliocene deposits, as evidenced by the support in onlap of the deposits of the second cycle on those of the first cycle (Fig. 7b).

The tectonic evolution of the area can be summarized as follows:

- the mélange formation process [20], responsible for the considerable internal deformation that characterizes the Varicolor Clays, occurred before the Pliocene succession was deposited. In fact, the deposits of the first cycle rest directly on the already deformed Varicolor Clays, which constituted the frontal portion of the accretionary prism of the southern Apennines;

- an intense tectonic activity characterized the end of the first cycle causing an oscillation towards the northeast of the whole succession;
- the deformation continued during the Pliocene – Lower Pleistocene with the genesis of overthrusts and backshells that deformed the clays of the summit Pliocene;
- starting from the end of the Lower Pleistocene – beginning of the middle Pleistocene, the area is affected by lifting phenomena [21] which led to the genesis of a series of marine terraces along the Gulf of Taranto [22].

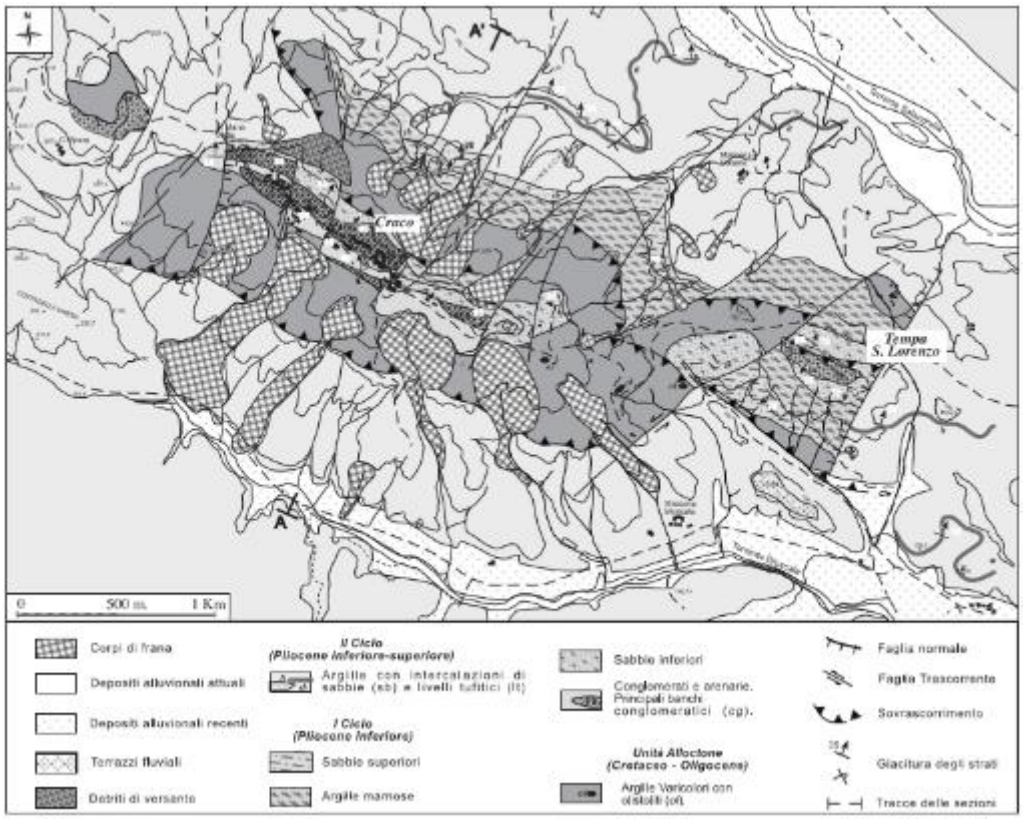

FIGURE 6 – GEOLOGICAL MAP OF THE CRACO AREA

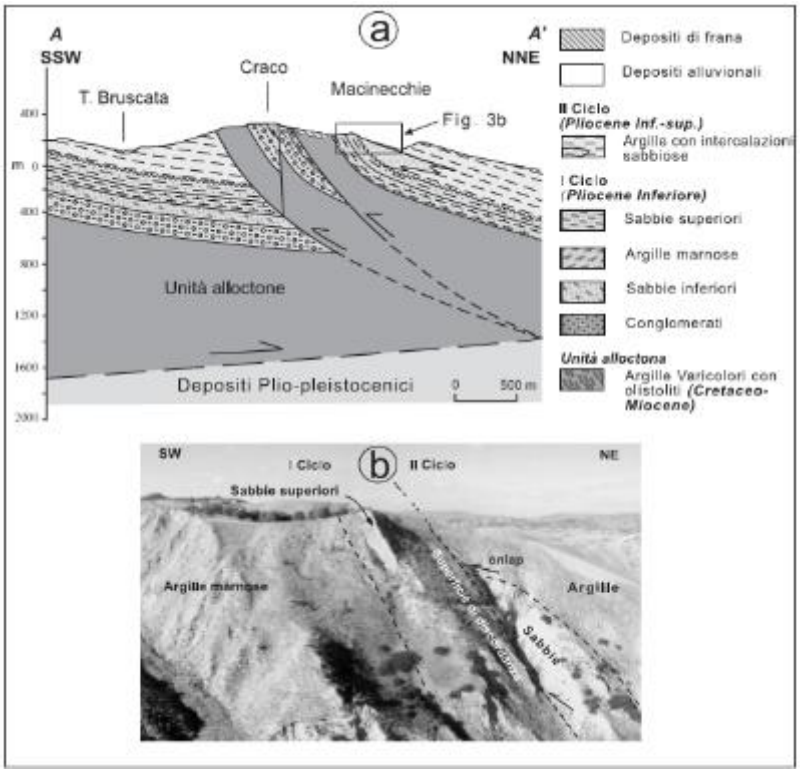

FIGURE 7 – A) GEOLOGICAL SECTION ILLUSTRATING THE MOST REPRESENTATIVE TECTONIC STRUCTURES OF THE CRACO AREA. B) SUPPORT IN ONLAP OF THE DEPOSITS OF THE SECOND CYCLE ON THE DISCONTINUITY THAT SEPARATES THE TWO CYCLES OF THE PLIOCENE SUCCESSION. THE TERMINATION OF THE SAND BODY LOCATED AT THE BASE OF THE SECOND CYCLE IS EVIDENT.

I.3 Geomorfology

The geomorphological analysis has highlighted the geometry, the state of activity of the landslides and the space-time relationships existing between them. Furthermore, all the elements useful for a morphological and chronological analysis were identified in order to establish the sequence of events that led to the current layout of the territory. To this end, particular attention was paid to the relationships between the deep gravitational slope movement, the morphology and the valley floor deposits.

The north-eastern slope of the ridge, on which Craco develops, has an average slope of about 13 ° and is affected by numerous landslides, some of which develop along the entire slope until it reaches the valley floor. Complex landslides were classified as sliding landslides, castings and more often landslides movements because they have a detachment zone at the foot of which there are trenches and counterslopes typical of landslides due to rotational sliding, while downstream they develop with lobes and undulations typical of landslides, castings [23]. The slopes are affected by gully shapes that sometimes develop for several hundred meters as in the northern part of the Macinecchia district, which are often subject to landslides, such as collapses.

These phenomena mainly occur along the northern slope of the hills, where the steep conglomerate rock walls are located. In these areas local collapses can be observed that occur due to the state of fracturing of the cluster, of the alteration and erosion due to atmospheric agents. Isolated prisms of conglomerate are identified by the presence of structural discontinuities, and their stability is influenced by the laying conditions of these discontinuities with respect to the exposure and slope of the hill. The volumes of the observable unstable blocks are of modest dimensions, ranging from a few tens of cubic decimetres to, at most, a few cubic meters.

A fundamental contribution to the geomorphological study of the territory of Craco and to the production of a cartography related to it was provided by the observation of aerial photos of the site under study.

FIGURE 8 – DETACHMENT SURFACES OF COLLAPSES ALONG THE CONGLOMERATE WALLS OF THE NORTH-EASTERN SLOPE.

I.4 State of the art for the study and management/mitigation of Landslide Risk

I.4.1 Assessment of hazards

Landslide hazard depends on numerous concurrent factors: morphology, geology, tectonics, hydrogeology, vegetation cover, land use, etc. Based on the type of approach used to evaluate it we have:

- **relative hazard (susceptibility)**: through the application of heuristic methods (based on qualitative and subjective estimates) or indirect statistical methods (based on the areal frequency of the landslides), generally used for spatial forecasting on a regional scale;
- **absolute hazard**: through the use of direct deterministic or statistical methods (based on the cause-effect relationship), whose reliability is strictly connected to the quantity and quality of the data and, therefore, generally guaranteed only for reduced territorial

scales (eg.Single slope). The evaluation of absolute hazard is often a step consequent to that of the relative hazard, which thus assumes the purpose of identifying the most dangerous areas on which to concentrate subsequent studies.

It is therefore clear that the techniques for assessing landslide hazard differ substantially in relation to the scale of analysis. In relation to the type of landslide phenomenon, some intuitive criteria are suggested:

- a landslide that has already occurred will tend to reactivate with the same typology;
- areas with characteristics similar to those in which existing landslides have been detected will be susceptible to similar phenomena;
- the geological, hydrological and geomorphological set-up can provide indications on the typology of potential instability phenomena (a clay slope with a moderate slope will not be subject to landslides).

I.4.2 Regional risk assessment methods

The following are the main methods for evaluating macro-hazard (eg 1: 25,000 or 1: 15,000):

Indirect statistical methods: they are based on the use of bi-varied or multivariate statistical analysis techniques; starting from the cartography of different factors determinant for landslide hazard (weighed according to their relative importance) and the past landslide map, the critical combinations (in terms of landslide frequency) of the various factors are identified (previously divided into classes of values), extrapolating the information also to areas currently not affected by landslides, thus circumscribing the potentially most dangerous areas. In this context, the correct identification of the basic territorial units, i.e. of a spatially homogeneous and objectively mappable domain, to which to refer in the implementation of the GIS, plays a fundamental importance. They can be:

- geomorphological units: natural limits (lithology, morphology, ongoing processes) →these are subjective representations, with manual acquisition of the data, which, however, has a significant physical meaning;
- sub-basins and main slopes: geomorphologically significant subdivision, implementable with algorithms starting from an accurate digital elevation model of the ground;
- unique condition units (homogeneous units): deriving from overlapping operations and intersection of thematic maps (GIS) →poor compliance with the spatial territory;
- elementary cells: discretization using a regular grid (pixel) → poor compliance with the spatial territory.

These indirect statistical methods [24], which have had considerable diffusion over the past years, generally refer to the following factors:

- geological factors:
  - lithology,
  - structural arrangement (faults, fractures, stratification, etc.);
- geomorphological factors:
  - inclination of the slopes,
  - relative height,
  - relative height difference
  - proximity to major landslides,
  - distance from the nearest ridges;
- hydrology and climatology;
- vegetation;

- analysis of existing or past landslides.

The process of cartographic representation (scale 1: 15.000) of these methods is articulated as follows (Fig 9):

1. divide the area under examination into units, for example through a grid;
2. a weight is attributed to each of the factors mentioned above according to their relative importance as a cause of landslide;
3. a map of past landslides is constructed, to then be superimposed on the thematic maps of the single factors to identify the units in which landslides have already occurred and then carry out a statistical analysis;
4. each factor is subdivided into classes and a numerical evaluation is assigned to each class according to the areal frequency of the landslides;
5. the thematic maps of each factor are superimposed and, through a weighted sum operation, a numerical index representing the degree of danger is attributed to each unit of territory.

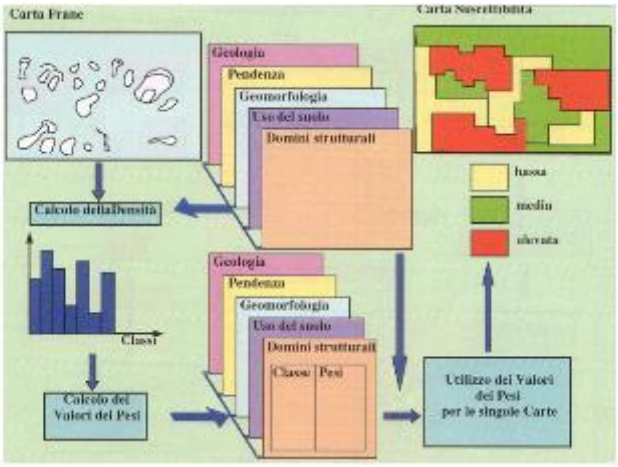

FIGURE 9EXAMPLE OF EVALUATION OF THE DANGER OF AN AREA BY MEAN OF INDIRECT STATISTICAL METHODS (VAN WASTEN, 1996).

The main advantage of these methods evidently consists in being able to analyze large portions of territory in a relatively short time. Among the limitations of this approach, in addition to subjectivity in the choice of the parameters and their weight, the low resolution (depending on the density of the available information) and the fact that the danger thus obtained is expressed in a relative scale is emphasized. In large-scale studies, the analysis of the interactions between underground water circulation and slope stability is generally limited to the definition of rainfall thresholds for the triggering of superficial landslides, ignoring the effects of water circulation on the deeper landslides; this simplification obviously derives from the complexity of the processes that govern the phenomenon, as well as from the frequent difficulty in finding sufficient hydrogeological data. To overcome these limits it is necessary to combine indirect methods with detailed analysis, to be carried out at the scale of the single slope.

Simplified deterministic models[25-27]: they are based on the use of a GIS in which extremely simplified geotechnical (indefinite slope) and hydrological models are implemented (models infiltration and trigger thresholds), which allows to identify potentially unstable areas; the results can then be validated by comparing the instability mapping. The great advantage of this approach is to provide an absolute hazard assessment over large areas; on the other hand, its major limitation is inherent in the extremely simplifying hypotheses that form the basis of the models used and which make it possible to take into account only the superficial forms of instability (translational slips, soil slips, surface flows).

I.4.3 Methods for hazard assessing on a slope scale

For the estimation of landslide hazard (generally expressed in absolute terms) on a slope scale, reference can be made to two approaches:

Direct statistical approach: it is based on the statistical analysis of cause-effect relationships between the triggering of a landslide and its causal factors; it consists, for example, of reconstructing the probability distribution of the safety factor F_s (using Monte Carlo simulations) as a function of the probability distribution of the various strength parameters, interstitial pressures, etc. and, therefore, calculate the probability of breaking as (Fig. 2):

$p_f = p(F_s \leq 1)$

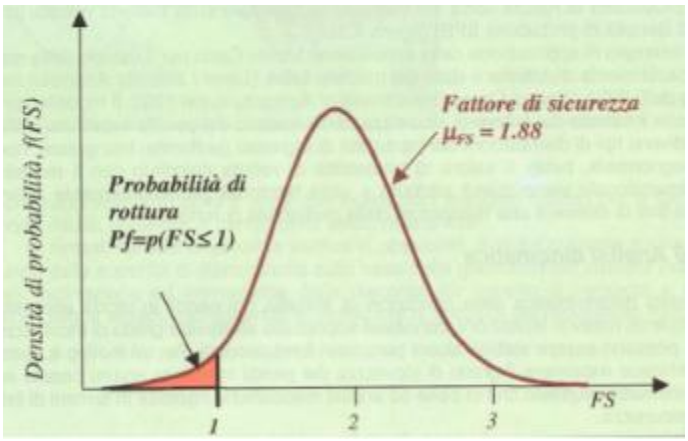

FIGURE 10– EXAMPLE OF HAZARD EVALUATION D_I IN TERMS OF PROBABILITY OF FAILURE.

Much more complex and, to date, little applied (if not in the field of scientific research) is the temporal forecasting of the event according to the historical series of past events (often schematized, for recurrent events, through a Poisson distribution), possibly in combination with historical series of trigger factors (human activity, erosion, precipitation, earthquakes, etc.); in this case the hazardis expressed in terms of conditional probability:

$$P[evento_i | indicatore] = \frac{P[evento_i] * P[indicatore | evento_i]}{\sum_{i=1}^{n} P[indicatore | evento_i] * P[evento_i]}$$

Prob. evento stimata in base a serie temporale

Prob. indicatore quando si verifica l'evento

Such an approach presupposes:

- an analysis of the time series of events,
- an analysis of the time series of trigger factors (eg.Rains, earthquakes, etc.),
- monitoring of the area.

The main difficulty in making temporal forecasts of this type derives from the fact that often catastrophic landslides are mono-episodic; moreover, even for recurrent landslides, it is often difficult to find the historical series of events (depending on their intensity) and, above all, the various indicators. Deterministic approach: it is based on the use of functions (eg.Safety factor) or, more often (given the complexity of the phenomena), physical-mathematical models able to predict the evolution in space and time of the landslide, identifying their areas of expansion and accumulation. The type of model to be used is chosen based on the kinematics being examined, for example: the simulation of the slope-deformation behavior of slopes in earth and in rock, respectively,the modeling of landslides of collapse, the reconstruction of dynamics (triggering, propagation and stop with relative expansion areas) of debris flows. The application of these models evidently requires the knowledge of punctual and specific geotechnical or geo-mechanical data for the different types of instability and, therefore, the execution of tests on the site and in the “ad hoc” laboratory. Consequently, the deterministic models are listed for types of disasters that can be easily schematized, such as for example translational slips and colonies, or on specific sites and for particular details (a slope scale). The simulations can be conducted taking into account the different intensity of the event, different cause predisposed and triggering (among which the underground water circulation is particularly important, as already mentioned previously) and, possibly, also to

the resistance parameters of the material. With a sufficient number of simulations, it is possible not only to predict the spatial and temporal evolution of the instability, but also to stimulate its probability of priming and the risk associated with the expansion and accumulation zones. This evaluation is of fundamental importance especially for landslides characterized by high speed (egCollapse) and considerable spreading distance (eg Castings). Through the topographical reconstruction of the slope and the calibration of the geo-mechanical parameters it is possible to construct on the slope scale an absolute hazard map (Fig. 11) as a function of the probability of detachment of the boulder and of the subsequent dynamic fall.

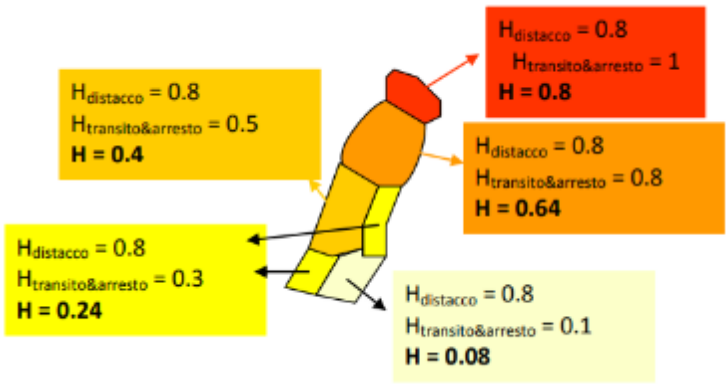

FIGURE 11. EXAMPLE OF AN ABSOLUTE HAZARD CHART AT A SLOPE SCALE FOR A CROSSO LANDSLIDE.

I.5 Assessment of risk elements

Evaluation of the elements at risk means, first of all, the quantification of the elements at risk, in terms of:

- number of discrete units (N) for buildings, commercial activities, etc.;
- surface unit (S) for lands, residential lots, etc.

The further step consists in calculating the value to be attributed to the various elements exposed to the risk, which can be carried out through: the calculation of a discrete value of the single elements: the comparison between the different types is possible only if a reference value is chosen, eg.An insurance evaluation, otherwise, there are relative values;

- the use of utility functions;
- the use of empirical formulas;
- the qualitative estimate of the total value for a certain area, for example with reference to urban planning instruments.

For example, using the utility functions for each element identifies the trend of social or individual utility u (x_i) and gives it a weight w_i(Fig. 12):

$U = \Sigma w_i * u(x_i)$

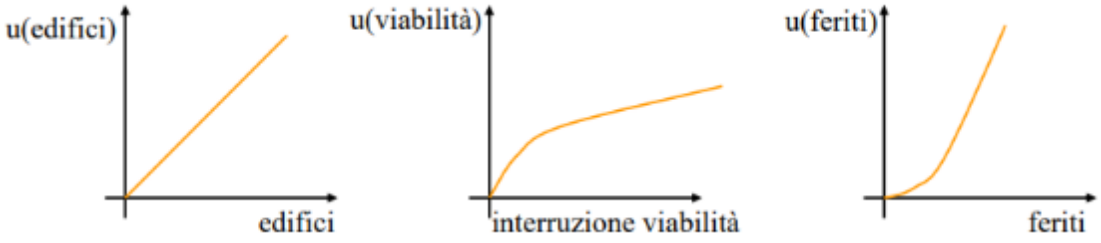

FIGURE 12 EXAMPLE OF THE USE OF UTILITY FUNCTIONS IN THE EVALUATION OF ELEMENTS AT RISK (REGIONELOMBARDIA, 2001).

Vulnerability is one of the most critical aspects of risk assessment. In fact, the vulnerability of an element to different dangerous phenomena must be evaluated differently; the approach can be of both qualitative-quantitative and heuristic. Through a qualitative approach the vulnerability is estimated as being between 0 and 1 for each element at risk; the overall

vulnerability is given by the distribution density function f (V) of the single values with mean E(V). The calculus of the vulnerability of the single elements must take into account:

- intensity I of the phenomenon (variable in space, Fig. 13) (Flageolett, 1999),
- constitution and structure of the element (Fig. 14),
- position (orientation) of the element with respect to the phenomenon (Fig. 15),
- presence of any protections.

ELEMENTS AT RISK	URBAN AREAS
E1	wooded area, extensive agricultural area, public state property
E2	special agricultural area public infrastructure (non-strategic municipal roads), environmental protection area, public equipped green, public parks
E3	public infrastructures (strategic state, provincial and municipal roads, railways, lifelines: oil pipeline, power line, aqueduct) areas for technological systems and landfills of solid urban waste or aggregates, quarry areas
E4	urban centers, rural core minor of particular value, urban completion areas, urban expansion zones, craft area, industrial and commercial public services, main public and strategic infrastructures, special or toxic-harmful landfill areas, hotel zone area for campsites and tourist villages

TABLE 1 – EXAMPLE OF QUALITATIVE EVALUATION OF RISK ELEMENTS BASED ON THE MUNICIPAL MASTER PLAN (REGIONELOMBARDIA, 2001).

It is therefore evident the need to integrate different skills, combining heterogeneous quantities of difficult determination. For this reason, in practice we often use qualitative assessments (based on subjective estimates or evaluation matrices, Table 1), which are easy to apply but which compromise a rigorous risk assessment.

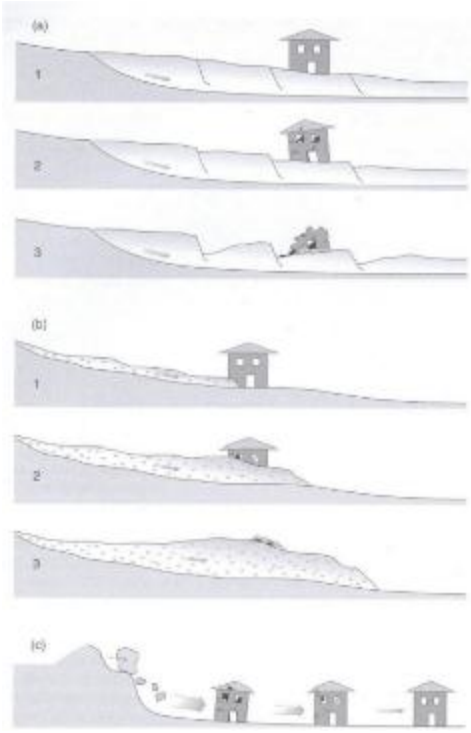

FIGURE 13 – EXAMPLE OF VARIATION IN THE VULNERABILITY OF A BUILDING ACCORDING TO THE TYPE OF LANDSLIDE PHENOMENON, ITS INTENSITY AND DISTANCE (FLAGEOLLETT, 1999).

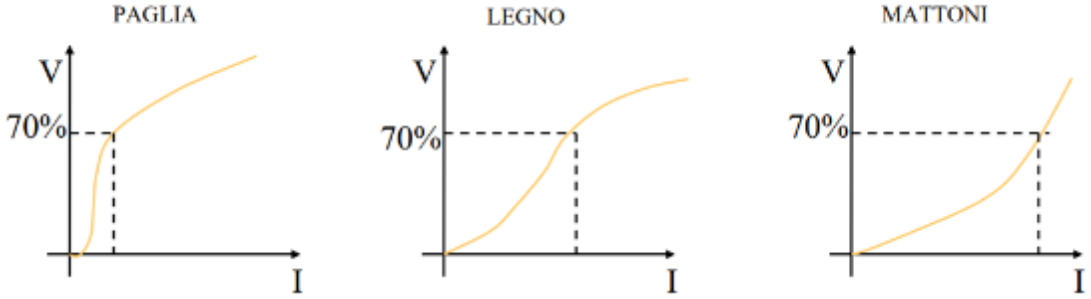

FIGURE 14 – EXAMPLE OF THE USE OF UTILITY FUNCTIONS FOR THE ASSESSMENT OF THE VULNERABILITY OF ELEMENTS AT RISK ACCORDING TO THEIR CHARACTERISTICS (REGIONELOMBARDIA, 2001).

The wall is torn down No damage

FIGURE 15 EXAMPLE OF VARIABILITY OF VULNERABILITY ACCORDING TO THE ORIENTATION OF THE ELEMENT AT RISK WITH RESPECT TO THE DANGEROUS PHENOMENON (REGIONELOMBARDIA, 2001).

Grade of damage	% valueof the construction	Type of damage
1	Some %	Non-structural light damage. Stability not affected
2	10-30 %	Wallcracks
3	50-60 %	Important deformations. Open cracks and subsequent necessary evacuation
4	70-90 %	Partial failure of the floors, crumbling in the walls, disarticulation of the walls. Immediate evacuation
5	100 %	Total destruction and impossible recovery

TABLE. 2EXAMPLE OF DAMAGE CLASSES FOR VULNERABILITY ASSESSMENT (REGIONELOMBARDIA, 2001)

I.6 Risk management

By integrating the results of the previously described processing it is possible to draw up a map of risk (in particular of the specific risk, if only H and V are considered), characterized by a variable degree of detail depending on the scale of analysis. Being:

$$R_s(I,E) = H(I)*V(I,E)$$

the risk will be higher where there is a high hazard in the presence of anthropic structures; vice versa, the risk tends to cancel itself out in areas characterized by low danger or low vulnerability (Fig. 16). The cartography thus obtained constitutes an important decision-making tool (Fig. 17) for the purposes of planning the territory (on a regional scale) and the planning of the interventions on the slope (slope scale). Since the choice of interventions is conditioned by various factors, often in contrast with one another (effectiveness, costs, environmental impact, etc.), it is suggested to use formalized methods such as, for example, the multicriteria analysis which, in addition to rationalizing and to make the decision-making process in question transparent, can help to identify the optimal alternative for the case in

question. As regards, instead, the most strictly inherent aspects of land planning and management, the integration of a Geographic Information System with the numerical analyzes and the previously described modeling guarantees the development of a complete and flexible tool, which can provide the competent authorities with valid indications for the purpose of drawing up an intervention plan. In summary, always bearing in mind that zero risk does not exist, for the purpose of risk reduction it can be done the following:

- reduction of hazard: action is taken on the triggering factors of the phenomenon (impossible for earthquakes and volcanoes) or on their propagation of active and passive accommodations
- reduction of vulnerability: the degree of damage is reduced with structural interventions on the elements (seismic building) or social education of the population
- reduction of the exposure of the elements at risk: territorial planning and emergency management, with warning and rescue systems
- reduction of the value of the elements at risk: planning.

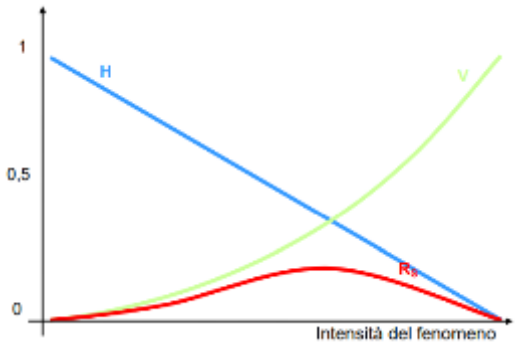

FIGURE 16 EXAMPLE OF DANGER, VULNERABILITY AND SPECIFIC RISK TRENDS DEPENDING ON THE INTENSITY OF THE PHENOMENON (REGIONELOMBARDIA, 2001).

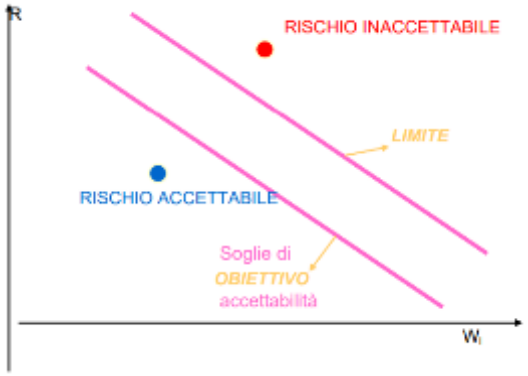

FIGURE 17 EXAMPLE OF TREND OF RISK ACCEPTABILITY THRESHOLDS BASED ON THE VALUE OF THE ELEMENTS EXPOSED TO RISK (REGIONELOMBARDIA, 2001).

Risk reduction interventions can generally be divided into two categories:

NON-STRUCTURAL:

- inhibitory and precautionary constraints relating to the use of the land and the construction of buildings, imposed by codes;
- insuranceagainstcatastropherisks.

STRUCTURAL:

- works intended to make the territory and populations safe (hydraulic-forestry arrangements or consolidation)

The various risk mitigation measures are adopted at different decision levels:

- code level (eg.Prescriptions on construction techniques),
- planning level (eg. PRG, safeguard measures, etc.),
- technical-scientific level (eg.New technologies),
- information level (education of operators and population).

I.7 Study of the Landslide Risk of Craco (by Enea) [28]

The methodology described was used by ENEA for the Craco case study, in particular deterministic analyzes.

I.7.1 Inventary of the Landslide Phenomena

In the study found in the literature various phenomena of instability that develop along the Craco hill are identified; they are distinguished by type and state of activity and are represented in the inventory map (Board 1).

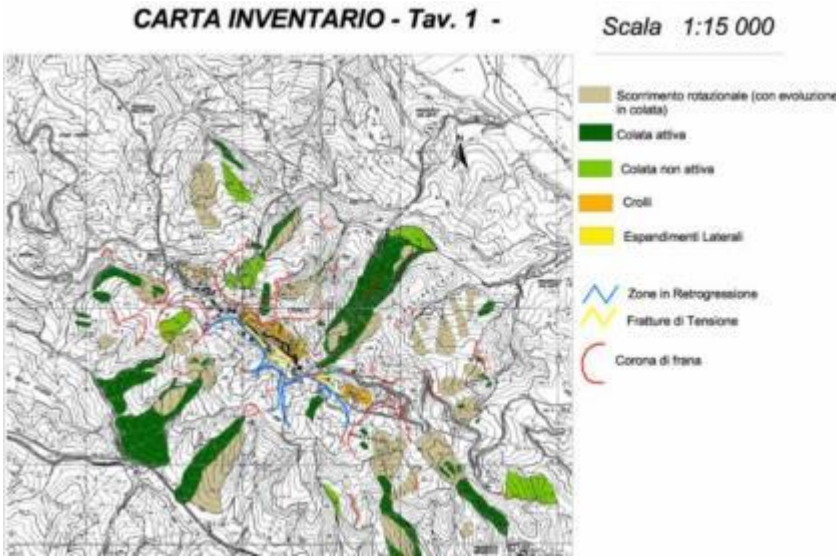

BOARD 1INVENTARY CHART [28]

Four different types of landslides affecting the slopes have been recognized, some of which appear as complex systems, that is composed of a set of several simple landslides. The most extensive movements in terms of areas and volumes involved can be considered as landslide systems, composed of rotational slides in the upper part of the slope and by castings that face in the accumulation areas of the previous movements.

I.7.1.1 Geomorphological analysis from aerial photos

A fundamental contribution to the geomorphological study of the territory of Craco and to the production of a cartography related to it, was provided by the observation of aerial photos of the site under study.

The analysis of the current state of the territory was carried out through photographic images provided by the company Geotec of Matera, relating to a flight of 1997 at a scale of 1: 14,000. This material allowed an accurate observation of the areas in failure and the drafting of a Geomorphological Map at 1: 10,000 scale (Board 4), consistently with the scale of the basic cartography. In addition to the data obtained through aerial observation, the analysis carried out by ENEA included four direct survey campaigns in the territory, in June, September and November 2000 and in February 2001, which provided additional data relating to the condition developments in the area.

The geomorphological analysis consisted in identifying all the areas that have characteristics linked to the processes of modification and modeling of the territory, such as:

- areas in superficial erosion, mainly gullies;
- landslides in progress and areas with signs of surface instability;
- linear erosion along the hydrographic network.

Following the study of the recent morphological situation, the ENEA conducted a multi-temporal analysis through the observation of two previous air flights, respectively in 1955 and 1972, provided by the Military Geographic Institute.It was therefore possible to create a geomorphological map relating to each of the flights (Board 2 and 3), to analyse the state of the territory at different times. Thus, the evolution of slope processes has been observed and interpreted, especially to the dynamics of instability affecting the area.

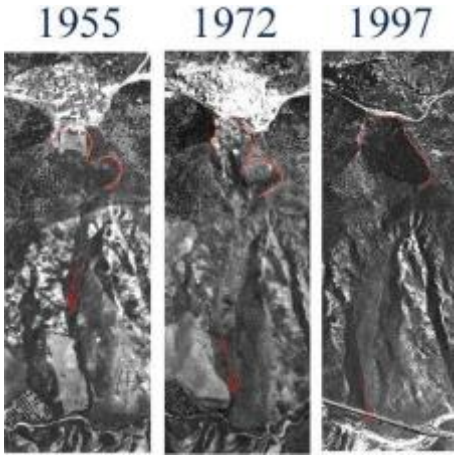

FIGURE 18 LANDSLIDE IN THE HISTORIC CENTER IN THE THREE DIFFERENT YEARS; IN RED THE DETACHMENT PARTS ARE HIGHLIGHTED AND THE ARROWS INDICATE THE PROGRESS OF THE LANDSLIDE CASTING [28].

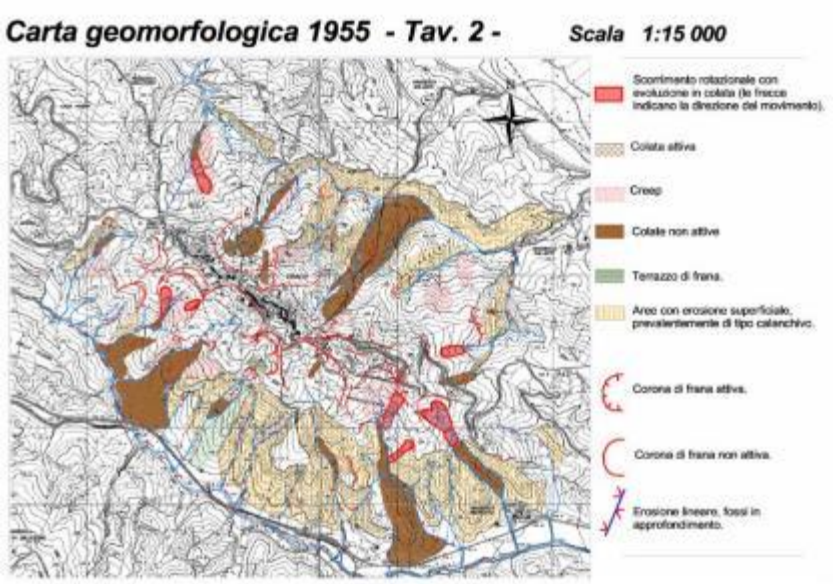

BOARD 2- GEOMORPHOLOGICALMAP OF 1972[28]

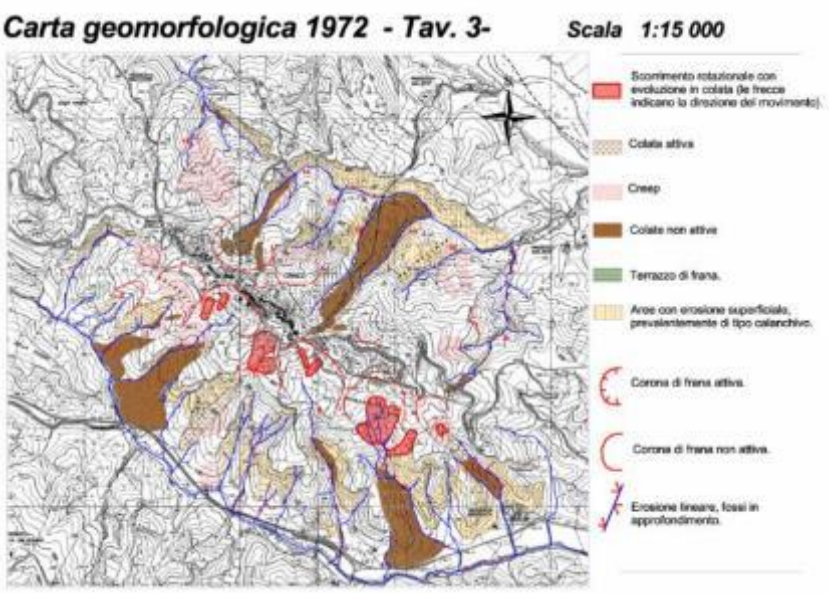

BOARD 3- GEOMORPHOLOGICAL MAP OF 1972 [28]

The results of the aerial observations will be presented below in chronological order, consistent with the temporal evolution of the area.

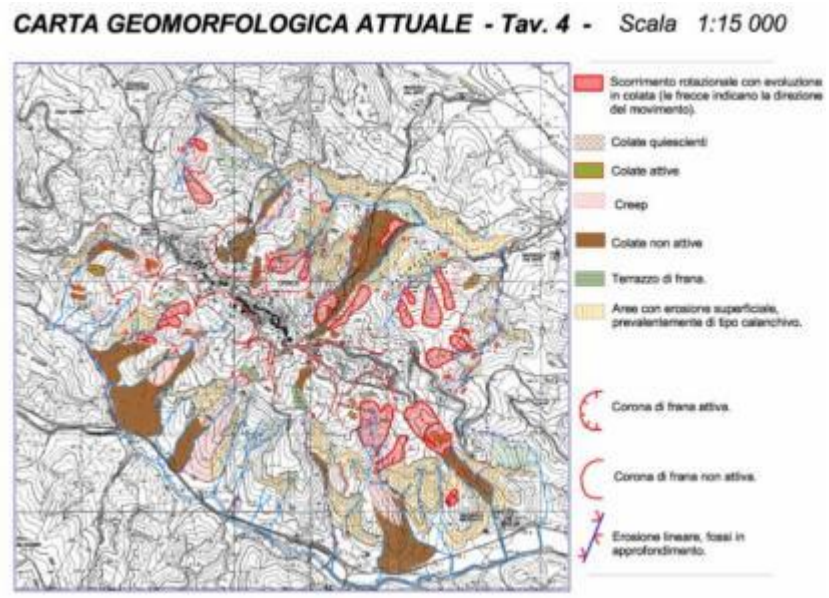

BOARD 4- CURRENTGEOMORPHOLOGICALMAP[28]

I.7.1.2 Multi-temporalanalysis

The surveys carried out in the countryside and the aerial images made it possible to observe the evolution of the slopes of the Craco ridge over a period of about 50 years. In this period the area that has undergone major modifications is the one below the center of the inhabited area of Craco, due to the reactivation of the landslide in the historic center, in 1959, 1965 and 1971, the last of which can be observed from the flight plane performed a few months later. Unlike this phenomenon of vast dimensions, the other niches produced by ancient landslides do not seem to have progressed towards the town. Despite this, most of the summit areas of the ditches, especially in the southern slope, have been affected by minor movements, which in any case testify to the high propensity to damage the clayey soils present in the upper part of the ridge.

The investigations carried out led to a selection within the four typologies of landslide phenomena initially identified, present in the inventory map (Board 1), operated on the basis of the actual capacity of each of these to determine conditions of instability.

The modest danger of both collapses, due to the prevalence of the slow disintegration process of the sandy-conglomerate body with respect to the billing and detachment of isolated blocks, and of the phenomenon of lateral spreading, due to the very low speed of development, has determined the choice of focus attention on the flow phenomena and on the flows. Consequently, the considerations that follow, relating to the predisposing parameters, the triggering factors and the evolutionary dynamics, are mainly directed to these two types of landslide.

I.7.2 Present Factors

The analysis of the single landslide phenomena has allowed the identification of the geomorphological, geological, geotechnical, hydrological/hydrogeological and land use characteristics that in different measure have contributed to determine the propensity to collapse. The distribution of the various parameters allowed a distinction based not on the typology but on the dimension of the phenomena. A direct relationship was observed between the depth of the phenomena, the flows and the different predisposing parameters identified.

a.Slides and superficial castings

• Prevailing lithology: various color clays
• Slopes between 10 ° and 20 °
• Absorption and desiccation
• Contrast of permeability between surface blanket and substrate
• Presence of creep
• Surface erosion (gullies and rill erosion)
• Land use, land sown annually

b. Deep flows and large flows

• Prevailing lithology: various color clays
• Contrast of competence and permeability between the sandy-conglomerate body and the underlying clays
• Presence of large niches predisposing to instability in the upstream area

c. Presence of extensive upstream rotational scrolling

I.7.2.1 *Susceptibility analysis to superficial landslides*

Surface phenomena include those phenomena of instability that develop within the superficial blanket of soils, for depths not exceeding 4-6 m.

For this first class, lithology, slope class, land use, and slope exposure were considered as predisposing factors; these parameters can be represented in vector form through homogeneous polygons and expressed in information layers digitalized through the GIS. In this way the susceptibility can be represented and generalized through the integration of the data related to each of the predisposing parameters, through the identification of homogeneous territorial units (UTO) that contain or not the parameters themselves.

To obtain the UTO an intersection of the vectorial themes relative to the individual predisposing parameters was performed, obtaining a new information layer composed of a series of polygons, each of which homogeneous with respect to the information relating to each parameter.

A weight has been assigned to the individual classes of each parameter (for example, for the lithology, the various colored clays must have a different weight from the Pliocene clays). The univariate statistical method of the Conditional Analysis was used to assign weights. Based on this methodology, the individual information layers (*layers*) relating to the predisposing parameters were superimposed to the surface landslide map, and from the corresponding database, the areas related to the polygons thus obtained were calculated. In this elaboration the single polygons of each information layer, constitute the basic units (UTO) in which the class to which they belong within the layer is defined as a distinctive homogeneous characteristic. As an example, in the "lithology" information layer, the

individual UTOs are represented by the polygons that compose it, each of which is defined by a distinct class, represented by the particular geological formation. Therefore, to assign a weight to each class of each individual information layer, the conditional probability (P) of the presence of instability (D) within each class (C) was adopted, given by:

P(D/c) = area of the class that results in landslide / total area of the class

The resulting probability values were then used as representative class weights. (Tab.3, 4, 5, 6)

Geology				
tipology	**Total area**	**Landslide areas**	**Stable areas**	**A slide/A tot**
floods	233627	0	233627	0,000
varicolored clays	2325499	155879	2169620	0,067
landslide bodies	561914	60647	501267	0,108
Clays of thePlioc sup	2661602	25496	2636106	0,010
conglomerates	165240	0	165240	0,000
sand-clays	375117	6673	368444	0,018

TABLE3 - ASSIGNMENT OF THE WEIGHT TO THE GEOLOGY[28]

Esposure				
class	**Total area**	**Landslide areas**	**Stable areas**	**A slide/A tot**
horizontal	438475	3620	434855	0,008
N	719826	42022	677804	0,058
NE	662638	29230	633408	0,044
E	752674	43623	709051	0,058
SE	763249	13304	749945	0,017
S	792934	18247	774687	0,023
SO	1119267	18111	1101156	0,016
O	666408	50660	615748	0,076
NO	407168	29877	377291	0,073

TABLE 4 - ASSIGNMENT OF THE WEIGHT TO THE EXPOSURE [28]

Land use				
tipology	**Total area**	**Landslide areas**	**Stable areas**	**A slide/A tot**
areas with sparse vegetation	2268544	59757	2208787	0,026
coniferousforests	23243	0	23243	0,000
annual crops associated with permanent crops	297777	20007	277770	0,067
olive groves	531057	4335	526722	0,008
abandoned country	44577	0	44577	0,000
pasture	552186	52996	499190	0,096
arable	2534479	111599	2422880	0,044
discontinuous urban fabric	70775	0	70775	0,000

TABLE 5- ASSIGNMENT OF THE WEIGHT TO THE DIFFERENT CLASSES OF LAND USE [28]

slope				
class	**totalarea**	**Landslide areas**	**Stable areas**	**A slide/A tot**
0-5°	758728	6579	752149	0,009
5-15°	2393715	123981	2269734	0,052
15-25°	2400577	113202	2287375	0,047
25-35°	722948	4933	718015	0,007
35-40°	15223	0	15223	0,000
40-70°	31446	0	31446	0,000

TABLE 6- ASSIGNMENT OF THE WEIGHT TO THE SLOPE CLASSES [28]

Once the weights were assigned to each class of each of the information layers considered, a combination of the same weights was carried out, in order to assign a final value to each homogeneous element present in the final information layer.

For this purpose, two distinct linear functions have been considered, the first as summation type and the second as product type.

In the two cases a distinct distribution of the final values attributed to the UTOs was obtained, as can be seen from the graphs of Figures 20 and 21.

FIGURE 20DISTRIBUTION OF THE SUSCEPTIBILITY VALUE CALCULATED WITH THE SUM FUNCTION FOR ALL UTOS [28]

In the case of the sum function, the distribution has two inflections, and a wide band in which the distribution is linear. It was initially decided to identify the separation values of the three susceptibility classes (high, average and low), corresponding to the inflections. On the basis of this choice it was found that the band relating to the class of average susceptibility was excessively wide, especially based on the distribution in the territory. This band has therefore been reduced by increasing the separation value between in low and average classes, choosing it equal to 15, and decreasing the separation value between the middle and high classes, choosing it equal to 20. In this way we obtained a map of susceptibility (Board5) closer to the characteristics of the territory in question.

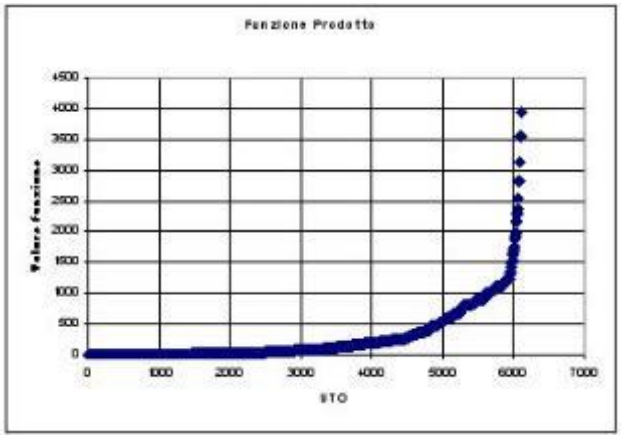

FIGURE 21DISTRIBUTION OF THE SUSCEPTIBILITY VALUE CALCULATED WITH THE PRODUCT FUNCTION FOR ALL UTOS

As far as the product function is concerned, the distribution of the susceptibility values is exponential, and separator values between the classes have been chosen for the values 200 and 500.

In the two cases analyzed, the percentages of areas of the basin falling into the three distinct susceptibility classes are different. In the case of the sum function, 45% of the basin has a low susceptibility, 24% falls into the intermediate class and the remaining 31% is highly susceptible (Tab.7)

	area[mq]	% to total area
low	2820280	44,61
average	1523363	24,10
high	1978999	31,30
tot	6322642	

TABLE 7 - TOTAL AREAS AFFECTED BY THE THREE CLASSES [28]

In the second case we observe an increase in the areas falling in the two extreme classes and a reduction in the areas subject to average susceptibility, the percentages are 59%, 17% and 24%, respectively for the low middle and high classes (Tab. 8)

	area mq	% to total area
low	3733778	59,05
average	1046170	16,55
high	1542694	24,40
tot	6322642	

TABLE 8 -TOTAL AREAS AFFECTED BY THE THREE CLASSES [28]

Also with regard to the percentages of landslide areas that fall into the different classes, the two cases present differences, it is possible to observe that through the summation function, 74% of the landslide areas fall into the high susceptibility class, while only 3.3% of them fall into areas defined as low susceptibility (Tab.9). However, with this type of function, formations occur in the average or high susceptibility classes that, in the area, do not detect the presence of this type of phenomena.

	area[mq]	% to total area
low	8257	3,32
average	55534	22,33
high	184904	74,35
tot	248695	

TABLE 9 - LANDSLIDE AREAS THAT FALL INTO DIFFERENT CLASSES [28]

Through the multiplicative function, the distribution of landslide areas falling into the three classes is as follows: 49% and 39%, respectively, for the middle and high classes, and 12% for the low susceptibility class. In this case, the formations that are not susceptible to superficial breakdowns, fall entirely into the low susceptibility class.

The study concludes by saying that in the first case (sum function) we obtain a card of susceptibility of a conservative type with respect to the phenomena of superficial instability, which presents a wide range of territory recognized as having average susceptibility, including land on which these phenomena are not are registered.

The multiplicative function, on the other hand, provides more restrictive results than the previous one, since the product renders null the value attributed to a single UTO that has only one of the zero weights. In this case the distribution according to the lithology distinguishes the different lands more clearly. It is agreed to adopt as a reference susceptibility map the one related to the sum function (Board5).

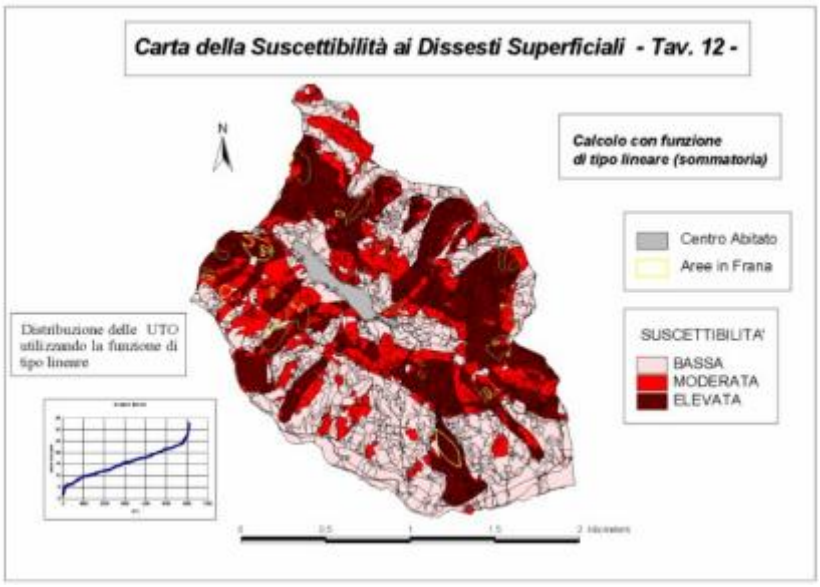

BOARD5 SUSCEPTIBILITY TO SURFACE DISRUPTIONS MAP [28]

I.7.2.2 *Susceptibility analysis to deep landslides*

With regard to the deep instability phenomena that over time have been reactivated in the Craco area, the methodology set out above is not effective for defining susceptible areas, for the following reasons: the main one is attributable to the potential of this method with respect to the evaluation of those areas, currently stable, but which may manifest potential instability phenomena in the future. In the area under examination, the deep phenomena are essentially produced by reactivating disasters that have already occurred in the past, with

retrogression in the summit parts and enlargement in the middle portions of the slopes. In summary, the development and evolution of these phenomena occurs only in areas that are already in landslide and therefore would not have meant searching for new susceptible areas.

The second problem identified in the application of the methodology concerns the choice of the predisposing parameters. In addition to lithology, which fundamentally conditions phenomena, another factor is the local stratigraphic structure, characterized by the presence of a more permeable formation above a slightly permeable one. All the phenomena are, in fact, produced in the areas of contact between the sands and the conglomerates and the underlying clay formations. This type of parameter is difficult to reconstruct and represent on the GIS, in light of the investigative potential available in this study. In this case it is therefore not possible to apply an intersection of themes and obtain homogeneous units, the basis for the analysis by GIS.

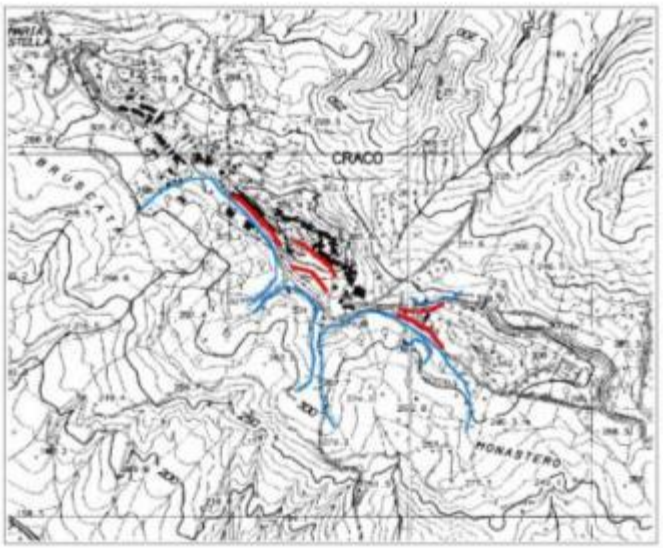

FIGURE 19 IDENTIFICATION OF AREAS SUSCEPTIBLE TO DEEP LANDSLIDES ACCORDING TO THE RESULTS OF THE GEOMORPHOLOGICAL ANALYSIS [28]

The possible methodologies are one of a geomorphological type and a deterministic one of a single phenomenon scale. As far as the first approach is concerned, all the areas upstream of those already affected by landslides in the past are identified as susceptible, since a future reactivation of the rotational flow phenomena, given the retrogressive tendency identified by the previous analyzes, would produce a progress towards upstream of collapse areas. In this regard, all those areas that already show signs of mobilization, such as tensilecracks or areas of land in counter-slope, are considered to be extremely at risk, as it has been observed in numerous areas within the area of the ancient settlement.

I.7.3 Trigger factors and relative return periods

As regards to the factors that influence the triggering of landslides, from an initial analysis of historical reports, it appears evident the active role of extreme rain events that hit the area in the periods immediately preceding the most important landslides.

The rain gauge analysis related to landslide events highlights the difficulty of determining possible critical trigger thresholds for landslides. In the cases analyzed by the study, it is possible to distinguish two different pluviometric regimes that contribute to triggering the slope movements.

The first concerns the events that occurred in November 1959 and January 1972: they, in fact, are directly linked to exceptional rainfall phenomena, of an alluvial type, which began a few days before the collapse. In these two cases, the rains of the previous months do not appear to be significant for the purpose of triggering, since, in both cases, they are below the average seasonal values. In all other cases, the instability cannot be caused by rainy events of particular entity; what is observed is the presence of precipitation above the average over long periods, with higher frequencies recorded for durations from 3 to 5 months (Fig. 20).

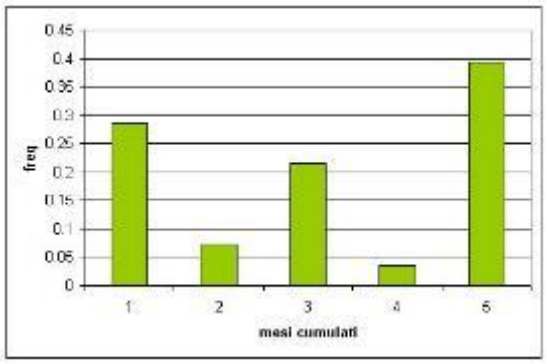

FIGURE 20 FREQUENCIES OF THE CUMULATIVE MULTI-MONTH PERIODS THAT RECORD THE MAXIMUM RETURN PERIOD; THE HIGH VALUES FOR THE ONE-MONTH CUMULATIVE REFER TO THE FLOOD EVENTS OF 1959 AND 1972 [28]

Thus, the influence of long-term rainfalls is denoted, which, however, do not present characters of exceptional intensity, as evidenced by the analysis of the return periods, which never exceed 8 years, and that most remain under 3 years (Fig. 21).

Often, long-term rains are associated with periods of a few consecutive rainy days, in the days prior to the collapse. Therefore, it emerges that to observe a dependence of landslides on rainfall, it is necessary to go back to the rains that occurred even in distant periods of time, as evidenced by the higher concentrations of the T_r peak around the previous three-five month periods.

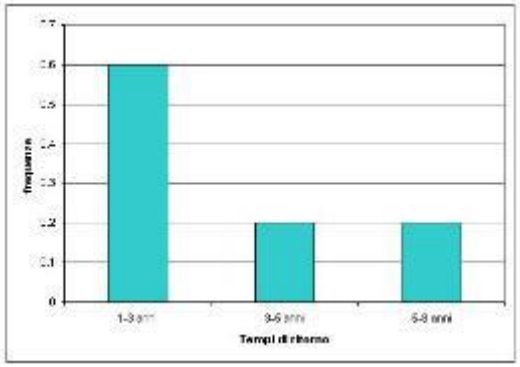

FIGURE 21 FREQUENCY OF RETURN PERIODS FALLING IN THE THREE CLASSES; VALUES RELATING TO FLOOD EVENTS ARE NOT INCLUDED [28].

However, even modest rainfall distributed over several consecutive days makes the slope stability conditions critical.

These observations are in accordance with the lithological characteristics of the formations concerned. In fact, apart from exceptional rainfall cases, the permeability of soils is such as to allow a saturation of the coulters in rather long periods of time. Generally, disruptions are observed between November and January, when the rainy season is at its peak and the rains of the previous months have allowed the soils to be saturated in depth.

The study failed to define intensity values appropriately, so only a form of spatial hazard, based on the phenol-morphological cartography of Board 5, was evaluated. Also the modalities and times of evolution of the phenomena at the moment can be evaluated exclusively in a qualitative way both for superficial and deep phenomena.

I.7.4 Typological classification of exposed elements

The object of the analysis of the elements exposed to risk by the numerous different landslides is the whole urban area of Craco. This analysis was therefore aimed at defining the exposure index of buildings, now abandoned, generating a sort of hierarchization based on mainly historical-cultural parameters. The abandonment of the country facilitated the analysis of the exposure, precisely because it was not necessary to face the most difficult element to assess: the population.

Although focused on architectural objects, the study was conducted in respect of the places crossed as historical heritage. The objective of the classification is a map that shows the set of buildings in the country distinguished by exposure index, indicative of the set of historical-cultural and economic-touristic characteristics. The index also contains information about the complexity of any restoration work that could theoretically be necessary.

The study was conducted starting from the environmental and hazard conditions, to select, as a basic unit for the exposure analysis phase, the individual buildings, i.e. those architectural elements characterized by an evident structural independence.

First, the cadastral cartography was retrieved from the Municipality. Subsequently, in order to classify the assets present in the area of the historic center and the Convent of Craco, the application of a structured form was envisaged following the principles of the italiansurvey card of ICR (Consolidation and Restauration Institute) relating to the part of the architectural elements.

The data collected were subsequently processed to get at the identification of the exposure index through three orders of operations:

- **Hierarchical**, for those parameters for which the belonging to the relative class of values was established in the survey phase (representativeness, integrity, state of preservation, presence of decorative elements and assets, current use, accessibility);
- **Statistical**, through an elaboration of the database associated with GIS (.dbf file) for the definition of the frequency of the different types present in the set of elements considered;
- **Spatial**, through GIS processing, to define the planimetric and volumetric indexes necessary for a complete view of the characters of the different elements.

The elaboration of these parameters led to the evaluation of the following three indicators:

INDICATOR A – HISTORICAL / CULTURAL
- Representativeness
- Typological frequency
- Presence of interventions
- Presence of decorative elements and goods

INDICATOR B – ECONOMIC TOURIST
- Current use
- Volumetric index

INDICATOR C – RESTORATION COMPLEXITY

- State of preservation
- Presence of decorative elements
- Volumetric index

The state of abandonment that characterizes the current use, which can be generalized to the totality of the buildings of the historical center, has induced to leave out the ***B*** indicator and to evaluate exclusively the other two. Once the values for each individual building have been defined and calculated, the exposure index has been defined as the algebraic sum of the indicators ***A*** and ***C***, hypothesizing in first approximation a simple superposition of the effects.

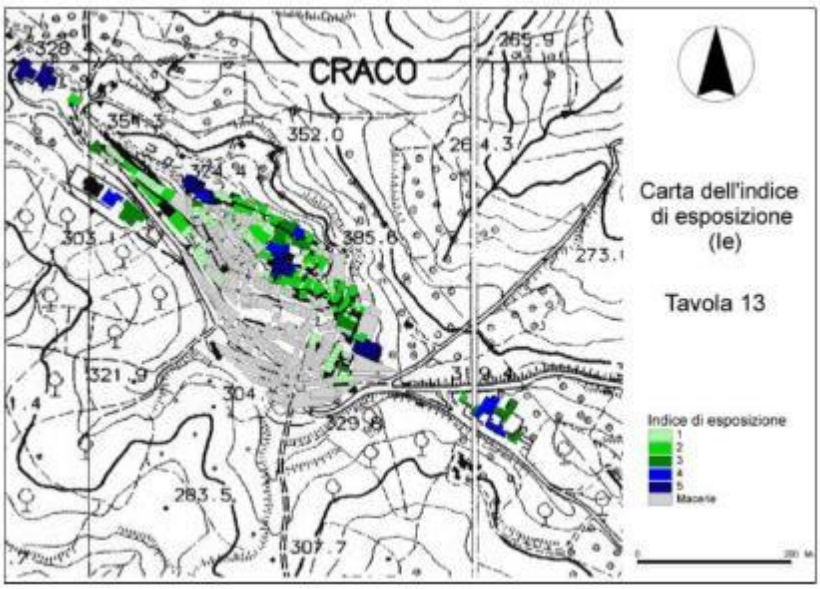

BOARD 6 EXPOSURE INDEX MAP[28]

I.8 Vulnerability analysis: static-structuralconditions[28]

The state of conservation of the buildings in the town of Craco is affected by a series of factors. First of all, assuming that the country was in normal conditions prior to the

evacuation measures, the landslide caused the disappearance of the outermost and recent portion of the buildings on the southern slope. At the same time, the landslide movement caused conditions of instability in the portion upstream of the landslide crown, causing serious injuries in the nearest buildings that reduce in the direction of the ridge of the relief and therefore of the highest part of the inhabited area.

To this damage caused directly by the landslides, other two factors were added, the abandonment and the 1980earthquake; the first is directly consequential, while the second is due to a coincidence only tragically accidental. Both causes, however, led to a worsening of the condition of the buildings in a uniformly distributed manner over all the buildings of the town.

The procedure for the assessment of the vulnerability consisted in the survey of the static-structural conditions carried out on all the elements of the investigation area consisting of the historical center and the buildings of the Convent. It would have been possible to evaluate only a portion of the buildings and subsequently extrapolate, through a correlation and the definition of iso-vulnerability curves, the evaluation of the conditions on the remaining part. However, a rigorous extrapolation process should have related the static-structural conditions to the process that is at the origin of the degradation of each building. Since the processes at the origin of the degradation differ (landslides, earthquakes and abandonment) and are difficult to evaluate in a way distinct from each other, it would have been difficult to make a direct correlation between landslide and injuries. Extending the census to the totality of the elements of the set under consideration it was avoided to carry out such extrapolation operations.

The analytical approach was also conditioned by the presence of deeply damaged areas where there is often nothing left but portions of the perimeter walls and accumulations of rubble. Faced with these conditions it was not considered appropriate to proceed with the definition of the crack pattern of the buildings and apply an assessment that referred to the presence of injuries. Instead, it was considered more practical to assess the state of conservation of each building by referring to the classification shown in Table 10.

TYPE OF DAMAGE	**class**	***% damage***
No damage	0	None
Light non-structural damages. Stability is not affected	1	Some %
Wall cracking. Slight structural damage	2	10 – 40 %
Important deformations. Broadly open cracks.	3	40 – 60 %
Partial subsidence of the floors, breaches in the walls, disarticulation of the walls.	4	60 - 90 %
Structure from very damaged to totally destroyed. Impossible recovery	5	90 – 100 %

TABLE 10 ESTIMATION OF THE STATIC-STRUCTURAL CONDITIONS [28]

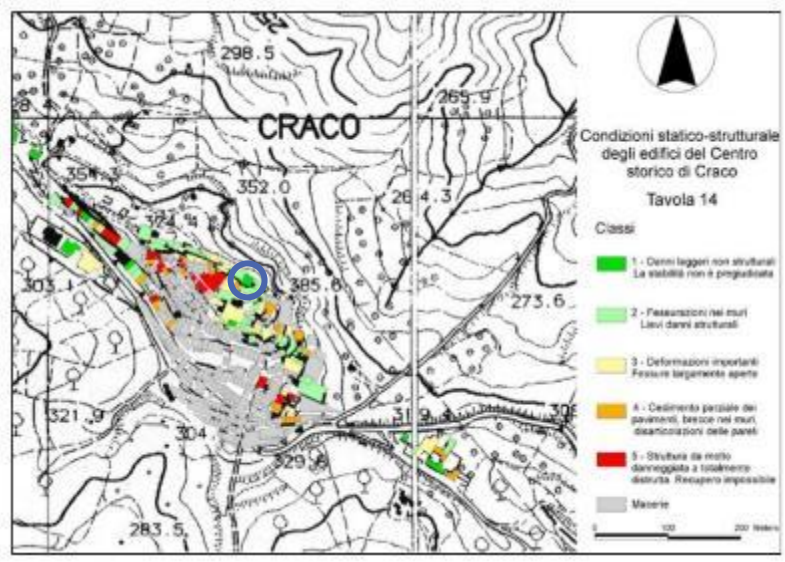

BOARD 7 STATIC-STRUCTURAL CONDITIONS MAP [28]

Therefore it was considered sufficient to assimilate the static-structural conditions to the state of vulnerability of the buildings (simplified methodology described in the Guidelines)

proceeding therefore to the drawing up of a cartography (Board 8) comparable with the informative level relative to the hazard at the end of a conclusive risk analysis.

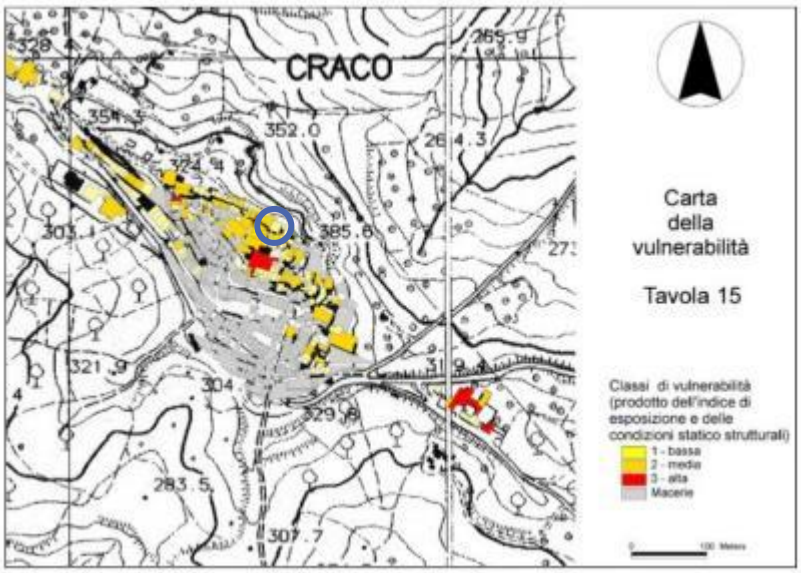

BOARD 8 VULNERABILITYMAP[28]

The relationship between the distribution of the static-structural conditions with the parameters related to the location of the exposed element with respect to the spatial evolution of the phenomenon, allows to define different possible scenarios of isovulnerability.

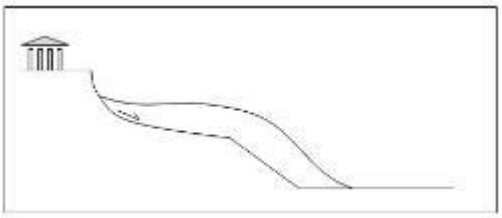

FIGURE 21 CULTURAL HERITAGE LOCATED UPSTREAM OF THE LANDSLIDE [28]

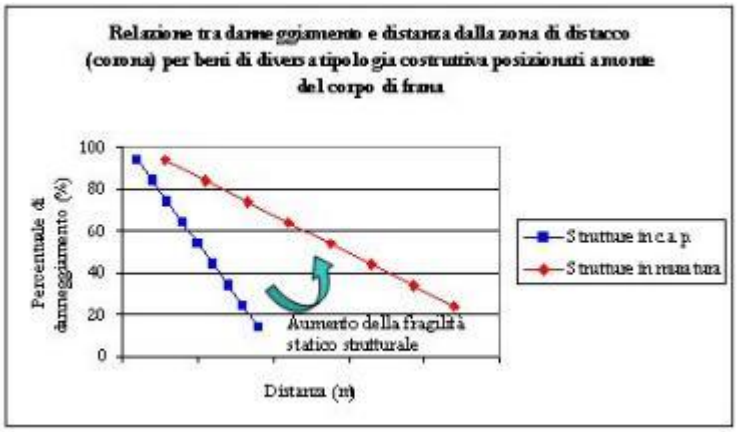

FIGURE 22 RELATIONSHIP BETWEEN DAMAGE AND LANDSLIDE **[28].**

he buildings located upstream of the landslide area (Fig. 21), the parameter that governs the vulnerability is the distance of the property from the area of the landslide crown (Fig.22).

I.9 Riskanalysis: evaluation of dame propensity [28]

The determination of the risk in the area of the Historical Centre of Craco was carried out through the analysis of three components necessary for a complete evaluation (danger, vulnerability and exposure index of the elements at risk) that were determined according to qualitative scales, carried out on the expert knowledge base. Therefore, one can speak, in reality, in a more rigorous way of assessing the propensity to **damage**.

The overlap of the information layers created within the GIS project, however, allowed to identify the main emergencies of the area. In fact, from the analysis of the cartography produced (Board8) it can be seen that the most valuable and most vulnerable elements, highlighted in Board 9, are in different HAZARD conditions. Therefore, the main church or the baronial palace, for example, even if they are elements of great value, are in lesser risk

conditions than the Convent that results in a particularly active area and positioned in the maximum danger class

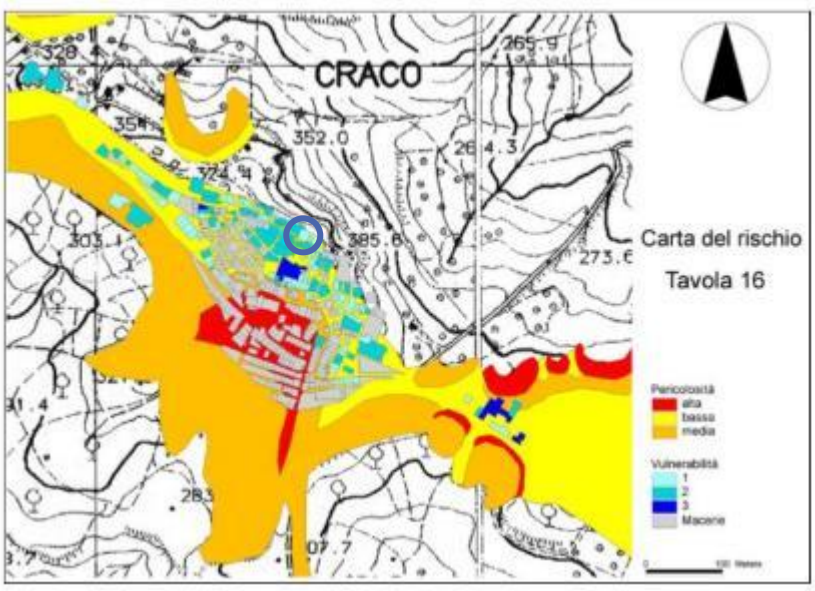

BOARD 9 LANDSLIDERISK MAP[28]

I.10 Mosaic of landslide hazard (PAI)

I.10.1 Plan for Hydrogeological Structure (or PAI)

The Plan for the Hydrogeological Structure (or PAI) is a fundamental tool of the spatial planning policy outlined for the first time by Law 183/89 [29]. It was started in each region for basin planning and constitutes the first thematic and functional section. PAI has the value of a Territorial Sector Plan and is the cognitive, regulatory and technical-operational tool through which the actions, interventions and rules of use concerning the defense against the hydrogeological risk of the territory are planned. Following the entry into force of the

Consolidated Act on the Environment (Legislative Decree 152/2006) [30] the subject is regulated by articles 67 and 68.

Inside there is also the Inventory Chart of Landslide and Erosive phenomena.

I.10.2 Methodological aspects

ISPRA (Italian “Higher Institute for Environmental Protection and Research”), in order to update the landslide hazard map throughout the country, in 2017proceeded to the new national Mosaicization (v. 3.0 – December 2017) of the hazardous areas of the Hydrogeological Planning – PAI. The mosaicization activity was carried out in the framework of the agreement stipulated between MATTM and ISPRA on 10/16/2016 for the monitoring, control and verification of the implementation and consistency with the planning, of the hydrogeological risk mitigation measures on the National territory. This mosaic was used for the production of new landslide risk indicators. The newlymosaic ISPRA activityincluded the followingphases:

- Request to the district Basin Authorities for updated data on hazardous areas (July 2017);
- Data analysis:
    - analysis of the methodology (Par. 1.3) and of the classification of landslide hazard adopted by each Basin Authority, using the information contained in the General Reports of PAIs and in the cartographic attachments;
    - analysis of the Implementation Standards of PAI that define the constraints of land use and the requirements;
    - interlocutions, technical clarifications and in-depth analysis with the officials of the District Basin Authorities on the data transmitted by uploading on ISPRA platform;
- Data homogenization:

  - use of the hazard classification for the entire national territory in 5 classes: very high hazard P4, high P3, average P2, moderate P1 and areas of attention AA, taking into account the Guidance and coordination Act for the identification of criteria relating to the obligations pursuant to art. 1, paragraphs 1 and 2, of the decree-law 11 June 1998, n. 180 (DPCM September 29, 1998);
  - use of a reclassification table of the landslide hazard for each Hydrogeological Plan in order to attribute the aforementioned national classes to PAI polygons;
- Data mosaicization:
  - re-projection of the files in a single reference system (WGS84 UTM fuse 32);
  - topology check
  - elimination of any overlapping geometries, giving priority to the highest hazard classification
- Evaluation of the homogeneity of PAI

The results of the mosaicization obtained by ISPRA are given on the following territorial levels: national, regional, provincial, municipal, macro-geographical areas and distribution of structural funds. A set of national landslide risk indicators that identify areas with different hazard levels – very high P4, high P3, average P2, moderate P1 and areas of attention AA-. Has been published by ISTAT, in collaboration with ISPRA, INGV and MiBACT, on the platform http://www.istat.it/it/mappa-rischi [31].

The hazard identified in the Craco area is visible in the image below (Fig. 23). The areas identified coincide perfectly with the areas outlined in the “IFFI Project” map (Fig. 24), where the acronym IFFI stands for Inventory of Landslide Phenomena in Italy, which collects and lists landslides at the typological level.

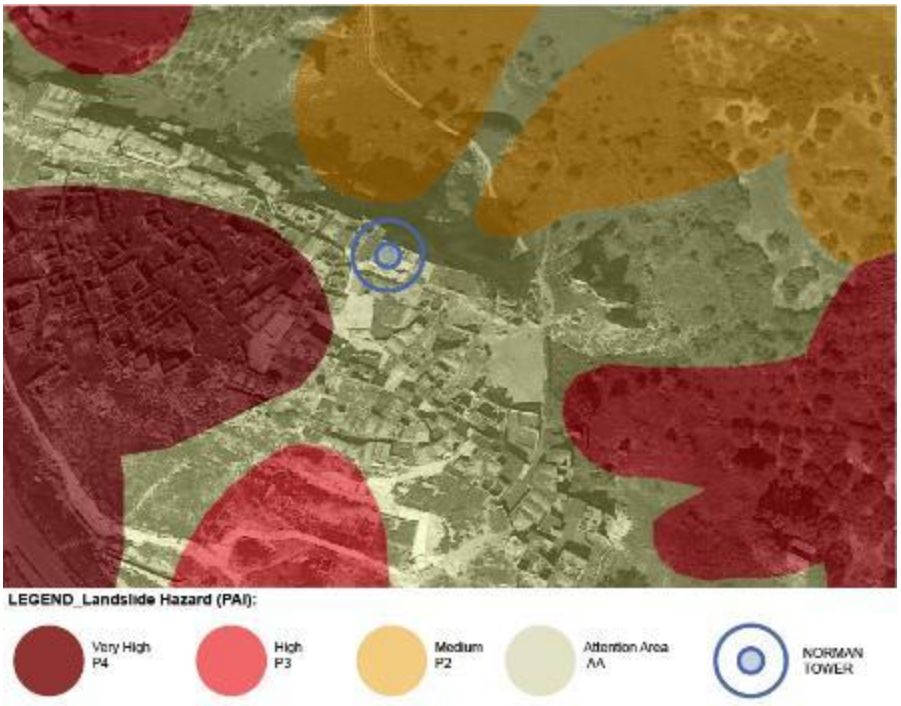

FIGURE 23 MAP OF PAI, LANDSLIDE HAZARD : CRACO.

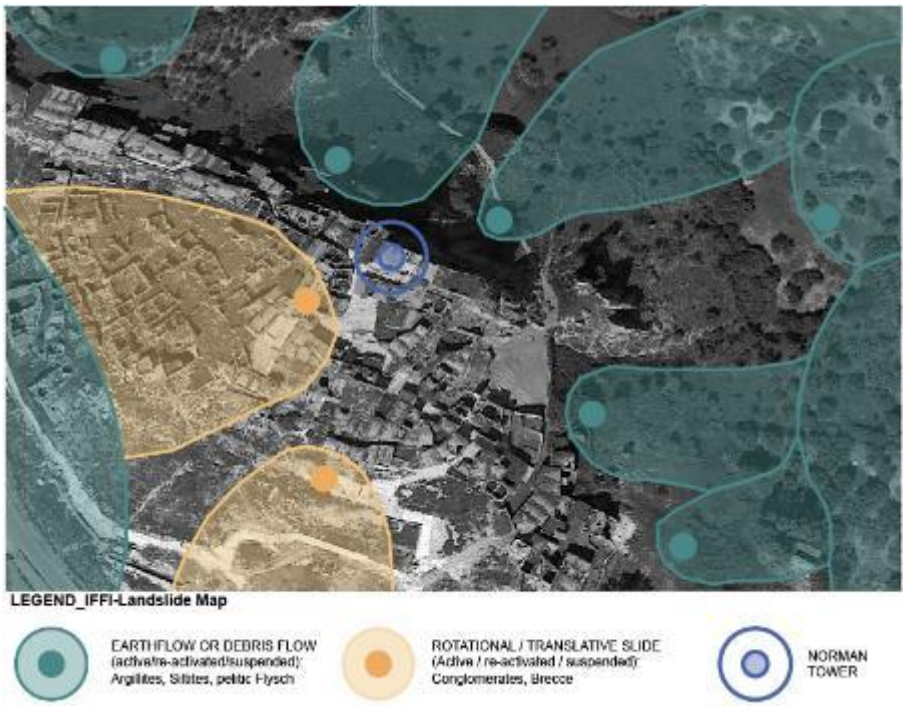

FIGURE 24 MAP OF THE "IFFI PROJECT"

The areas at greatest risk for Craco are those situated to South-West and to East where the convent is located and, in particular, concern two types of landslide, the “Earthflow or Debris flow” and the “Rotational / translational Slide”.

The Norman Tower area of grounds is subject to a low level of danger, being included in the zoning “AA-Area of attention” in the PAI Cartography.

I.11Studies comparison

The comparison of the PAI cartography and the study of the Landslide Risk performed by ENEA shows the same areas at greatest risk, those to: South-West and the Convent area; the scenario that emerges is comparable and the area under study is in an area of low risk and/or danger. These indications (areas of relevance) have been taken into consideration for the subsequent Multi-risk analysis.

II. Mono-risk Earthquake Hazard

II.1 Dynamic monitoring of the Norman tower of Craco

II.1.1 Description of the tower

The Norman tower, object of study, is one of the few structures remained unharmed by the effects of the landslide, until today. The building, dating back to medieval times, rises in the highest part of the hill on which the town stands and the historic centre was built around it.

The defensive character of the tower is underlined by its robust appearance and by a quadrangular structure in compact masonry of 11x11 m size, with an architrave opening on the East side at the first level, which allows access and arched openings on the second level (12.5 m), one for each side, with the exception of the one facing North. Cracks arranged in three rows at the height of the crown (triangular in the lower rows and quadrangular in the third row) mark the horizontal closure placed at 20 m from the ground level; while the basement has a truncated pyramid shape.

Originally the structure had two masonry vaults, a barrel one (no longer existing) on the first floor and a cruise (still visible) on the second level and connected by an internal staircase that had been destroyed. The inside of the tower has been subjected, in relatively recent times, to manipulations that have affected the general state of conservation. In fact, the demolition of the barrel vault and the staircase dates back to 1949, for the installation of a municipal tank of water with a cylindrical form in reinforced concrete, thus undermining the stability and function of the building; the cistern is not connected to the tower, but at some levels it is perfectly adherent to it.

From the relief of the thickness of the wall (about 2.15 m at the base and about 1.70 m at the top) and from the visual inspection of the two sides, external and internal, it is assumed a

two-pitch masonry with a sand-interposed core. Externally the masonry base consists of a set of irregular river stones and shows conditions of advanced decay; the upper part of the tower, apparently in good conditions, consists of sandstones of varying sizes, with the exception of the cantons where cut stone blocks prevail, used for the double rings of the arched openings. The knowledge of materials and construction techniques is certainly useful to discern the weaknesses of the structure, to be considered in the numerical modeling. [32]

FIGURE 25 - SW-NE VIEW OF CRACO WITH NORMAND TOWER.

FIGURE 26 – EAST SIDE OF THE NORMAN TOWER.

FIGURE 27 – INTERIOR DETAIL OF THE TOWER WITH TANK. FIGURE 28 – CROSS VAULT OF THE TOWER.

II.2 Description of the tower

Experimental observation through structural monitoring plays a central role in the diagnostic process as it constitutes the essential information base for identifying the causes of the failure and in the analysis and evaluation of the seismic vulnerability.

The measurement chain typically used in dynamic monitoring activities in the structural field is composed of:

- 16 seismic piezoelectric accelerometers (National Instruments)
- multi-channel signal conditioning system and sensor power supply
- high frequency sampling card

The experimental test campaign was conducted with the objective of direct monitoring of environmental vibrations, subsequently the results were analyzed and compared with the data obtained from the finite element numerical model.

This technique is particularly suitable for tower buildings because, as indicated in the DPCM on the Assessment and reduction of seismic risk of cultural heritage [33], if subjected to vibrations, even at low intensity, they produce easily measurable signals, unlike structurally non-independent buildings and then aggregated with others [34].

The boundary conditions of the tower and the mechanical properties of the masonry can be defined by dynamic identification based on experimental recordings in situ, by monitoring only environmental vibrations. In this way it is possible to evaluate the characteristics of the materials and the conditions of constraint of the structure, in order to define reliable numerical models and to identify the modes of vibration of the structure, the natural frequencies and the damping ratio on the real data [35] .

The architectural survey and direct observation were the preliminary operations to the data acquisition phase.

Module	Channel	Serial Number
1	1	35205
1	2	35122
1	3	35035
2	1	35212
2	2	35203
2	3	35204
3	1	35098
3	2	35092

TABLE 11– DATA RELATING TO THE DAQ 1 POSITIONED AT A HEIGHT OF 12.50 M.

Module	Channel	Serial Number
1	1	35211
1	2	35208
1	3	35090
2	1	35201
2	2	35119
2	3	35120
3	1	35089
3	2	35083

TABLE 12 – DATA RELATING TO DAQ 2 POSITIONED AT A QUOTE OF 21,00 M.

During the tests carried out, the main stresses acting on the structure were caused by the wind.

During the monitoring carried out on the Norman tower of Craco they were used:

- 2 NI9188 chassis modules, one located at a height of 12.5 m and one at a height of 21 m, with NI9232 modules connected according to the following tables (Fig. 28);
- Acquisition units or PBC piezoelectric accelerometers of National Instruments, each with a sensitivity of about 1000 mV/g; appropriate rectangular blocks have been designed and manufactured to ensure a perfect orthogonality of the accelerometers

at each point of application: the accelerometers have been inserted with screws in the threads made on the perpendicular faces of the blocks (Fig. 29);

- Coaxial cables with low impedance and variable length from 4 to 15 m.
- A portable computer with NI acquisition software installed.

The management of data acquisition and archiving takes place through software developed in a Labview environment [36].

FIGURE 29 – CHASSIS MODULE NI9188 WITH 8 SLOTS FOR DAQ CARD.

FIGURE 30 PIEZOELECTRIC ACCELEROMETERS PBC OF THE NATIONAL INSTRUMENTS, ORTHOGONAL BETWEEN THEM.

II.3 Positioning of the accelerometers inside the tower

For the tests 16 piezoelectric accelerometers were used, with a sensitivity of about 1000 mV/g, positioned at different points within the tower.

In particular, 8 accelerometers were placed in pairs of two mutually orthogonal, at a height of 12.5 m from ground level, arranged at the four corners of the tower. (Fig. 31)

While the other 8 accelerometers, equally coupled and arranged like the first, were positioned at a height of 21 meters, at the roof level of the tower. (Fig. 32)

The OXYZ global reference system, taken into consideration to determine the coordinates of the accelerometers, has as its origin a point of the external masonry of the tower, belonging to the South-West corner at the ground level; in the origin, then, the three Cartesian axes intersect: the X axis in the East direction, the Y axis in the North direction and the Z axis facing the other (as shown in Figures 31 and 32). The Cartesian axes are orthogonal to each other and not entirely coincident with the walls of the tower due to the imperfect orthogonality of the latter. In fact, it was decided to position the Y axis aligned and adherent to the North-West side of the tower; while the X axis, orthogonal to the first, deviates slightly from the South wall of the structure.

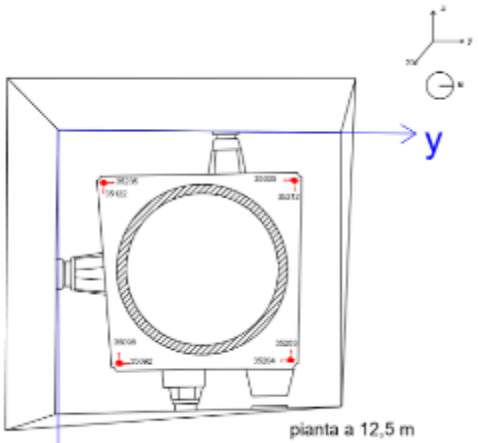

CANALI	MODULI 1	2	3
1	35205	35212	35098
2	35122	35203	35092
3	35036	35204	

FIGURE 31POSITIONING OF THE ACCELEROMETERS (IN RED) IN PLAN AT 12.5 M; TABLE WITH INDICATION OF THE CHANNELS POSITIONED ON DAQ1.

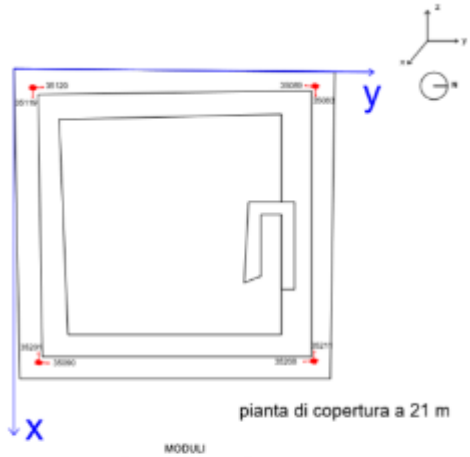

CANALI	MODULI 1	2	3
1	35211	35201	35089
2	35208	35119	35083
3	35090	35120	

FIGURE 32 POSITIONING OF THE ACCELEROMETERS (IN RED) IN PLAN AT 21 M; TABLE WITH INDICATION OF THE CHANNELS POSITIONED ON DAQ2

FIGURE 33 PIEZOELECTRIC ACCELEROMETERS POSITIONED AT THE SOUTH-WEST CORNER OF THE TOWER AT 12.5M

FIGURE 34 DAQ 1 (DATA ACQUISITION MODULE) LOCATED AT 12.5 M.

FIGURE 35 PIEZOELECTRIC ACCELEROMETERS POSITIONED AT THE SOUTH-EAST CORNER OF THE TOWER ROOF AT A QUOTE OF 21 M

FIGURE 36 DAQ 2 (DATA ACQUISITION MODULE) SET AT 21M

The following tables show the coordinates of the 16 accelerometers divided on the two levels of the tower.

MODULE	CHANNEL	SERIE	X (cm)	Y (cm)	Z (cm)	ACCELEROMETER DIRECTION
1	1	35205	200	176	1250	y
1	2	35122	200	176	1250	x
1	3	35035	187	911	1250	- y
2	1	35212	187	911	1250	x
2	2	35203	885	900	1250	- x
2	3	35204	885	900	1250	- y
3	1	35098	900	235	1250	- x
3	2	35092	900	235	1250	y

TABLE 13 – COORDINATES OF THE ACCELEROMETERS AT 12,5 M QUOTE

MODULE	CHANNEL	SERIE	X (cm)	Y (cm)	Z (cm)	ACCELEROMETER DIRECTION
1	1	35211	1110	1150	2100	- x
1	2	35208	1110	1150	2100	- y
1	3	35090	1120	96	2100	y
2	1	35201	1120	96	2100	- x
2	2	35119	72	72	2100	x
2	3	35120	72	72	2100	y
3	1	35089	57	1157	2100	- y
3	2	35083	57	1157	2100	x

TABLE 14 – COORDINATES OF THE ACCELEROMETERS AT 21 M QUOTE

During the experimental investigations 6 series of acceleration recordings were carried out in the points indicated above, due to environmental vibration; each recording lasted 15 minutes.

The acquisitions were carried out at a frequency of 1028 Hz, while the data obtained from these acquisitions were sampled with a frequency of 128 Hz.

Analyzing the six different recordings, it was noted that some accelerometers showed anomalies, probably due to external factors that could not be identified with certainty. For this reason, only four of the six registrations were considered, specifically acquisitions 2, 3, 5, 6, thus excluding registrations 1 and 4 for the reasons indicated above.

However, in all the tests, channels 352011 and 35208 relating to two of the accelerometers present at the second level (roof plan), showed anomalies due to interference or external causes that could not be exactly deciphered.

The following diagrams illustrate some plots relating to the acquisitions of the accelerometers, in the time, referred to the tests No. 5 and No. 6.

The graphs show an almost constant acceleration trend in accelerometer 35090 placed on the roof level, unlike the other two accelerometers positioned at a height of 12.5 m, in which acceleration peaks appear throughout the duration of the tests, variously arranged as a function of time.

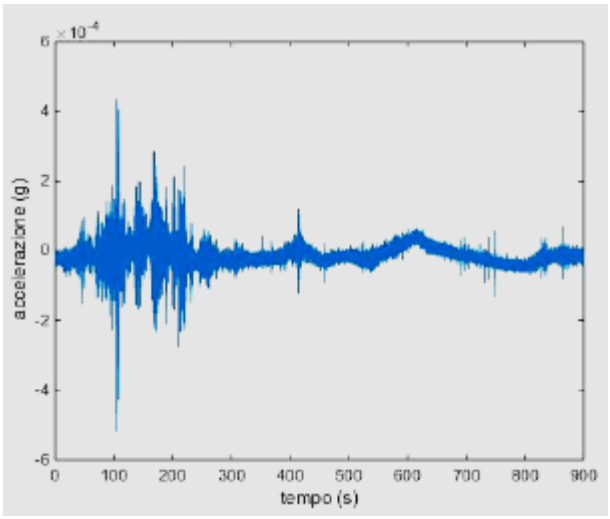

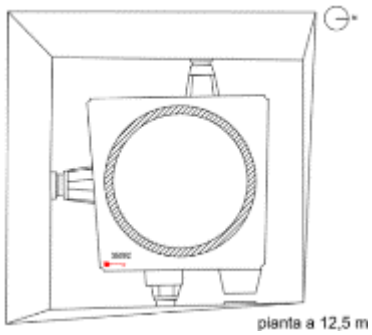

FIGURE 37 – DIAGRAM RELATING TO ACCELEROMETER 35203 DURING TEST N ° 5 WITH INDICATION OF THE POSITION IN PLAN.

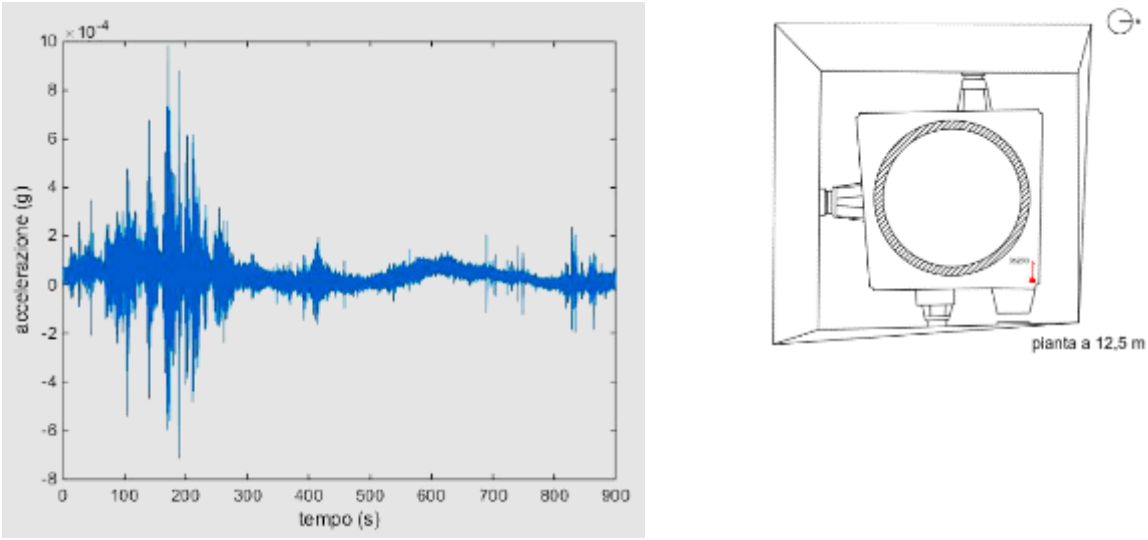

FIGURE 38 – DIAGRAM RELATING TO THE ACCELEROMETER 35092 DURING TEST N ° 5 WITH INDICATION OF THE POSITION IN PLAN.

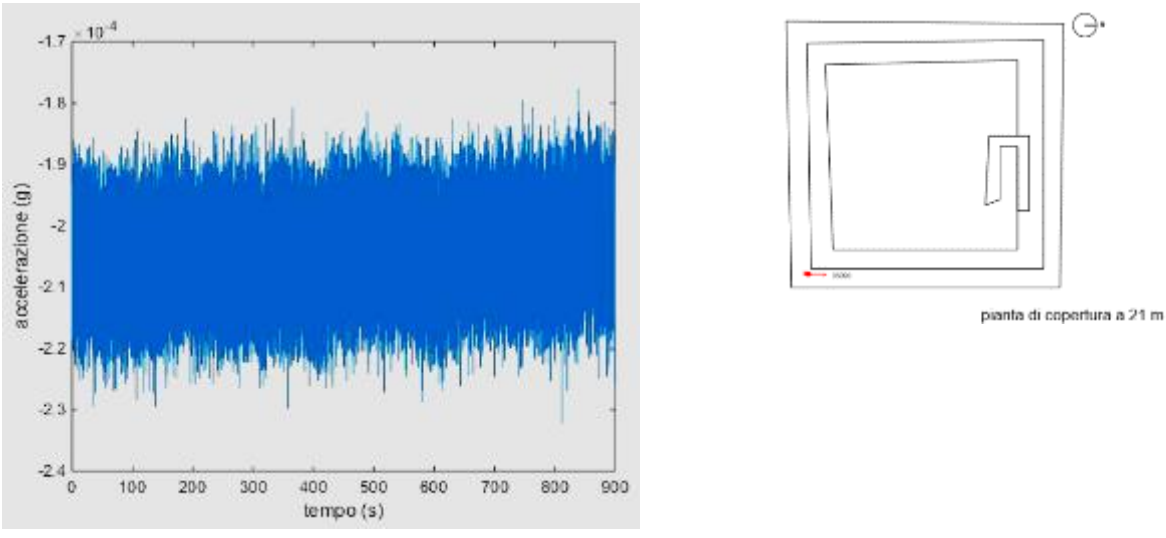

FIGURE 39– DIAGRAM RELATING TO THE ACCELEROMETER 35090 DURING TEST N ° 5 WITH INDICATION OF THE POSITION IN PLAN.

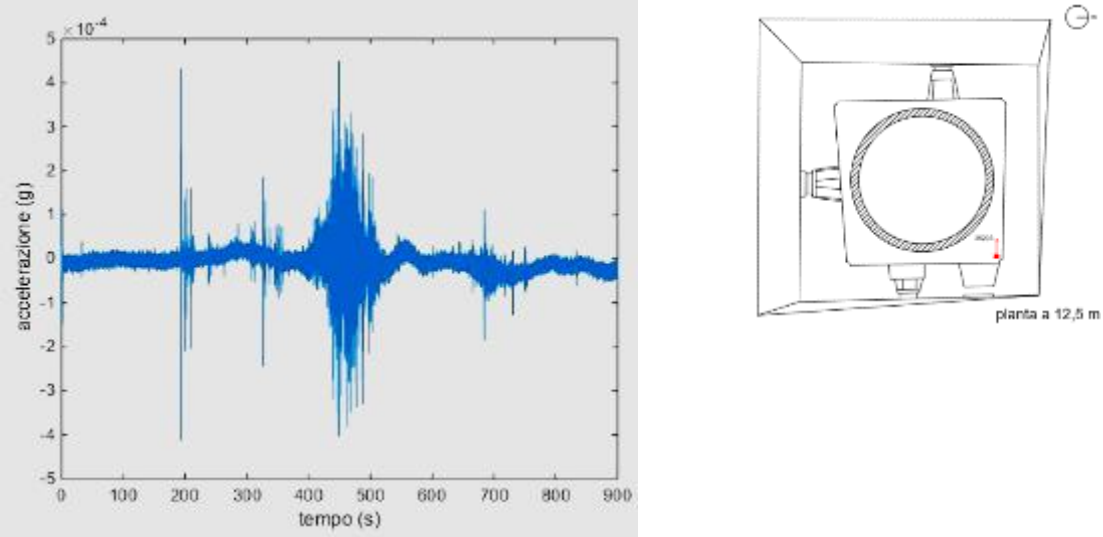

FIGURE 40– DIAGRAM RELATING TO THE ACCELEROMETER 35203 DURING TEST N ° 6 WITH INDICATION OF THE POSITION IN PLAN.

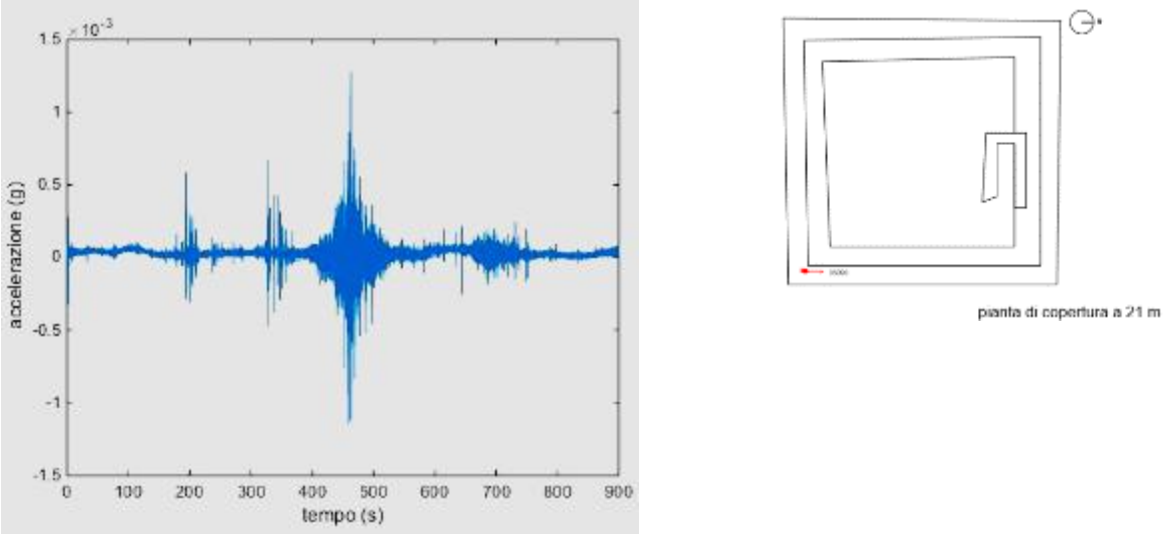

FIGURE 41– DIAGRAM RELATING TO THE ACCELEROMETER 35092 DURING TEST N ° 6 WITH INDICATION OF THE POSITION IN PLAN.

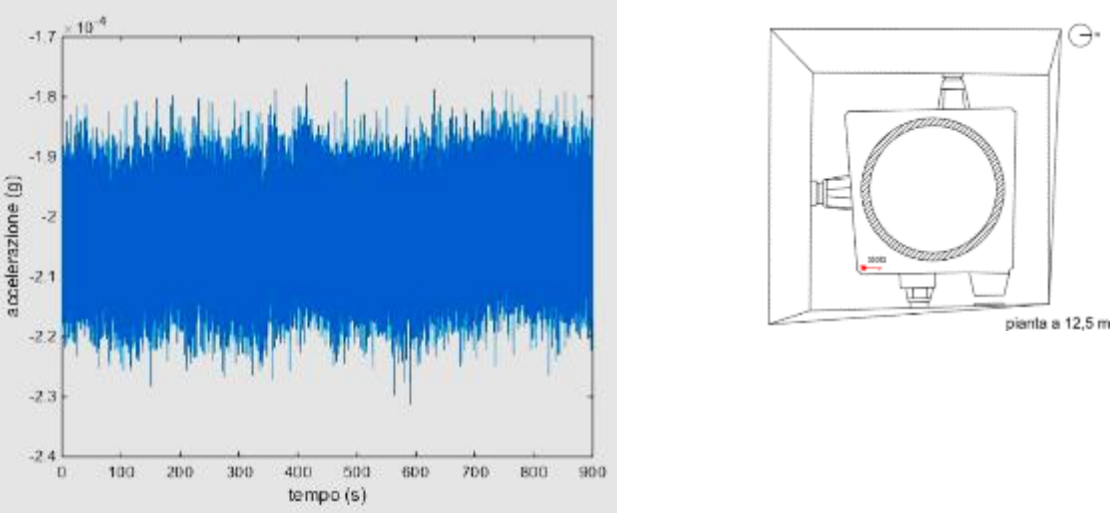

FIGURE 42– DIAGRAM RELATING TO THE ACCELEROMETER 35090 DURING TEST N ° 6 WITH INDICATION OF THE POSITION IN PLAN.

II.4 Finite element numerical model of the Normand tower

Following the data obtained from the archive researches, the geometric survey and the visual inspection, it was possible to develop a three-dimensional finite element preliminary model, in order to evaluate the structural behavior of the tower. This model was created using Straus7 software [37], (Fig. 43)

For the modeling of the structure quadrangular flat elements of the Quad4 type were used for a total of 14,382 elements, with a uniform distribution along the whole height of the tower, maintaining the length of the side of each quadrangular flat element of about 30 cm; in addition, 17,050 nodes and 46 vertices were used to model the entire geometry of the tower. The model also included 3,266 springs to model the constraint offered by the buildings surrounding the tower.

In order to make the final numerical model as true as possible, several models have been generated that take into account the different elements that compose it, and therefore, the different constraints and the mechanical characteristics of the different elements. The models considered were No. 3:

1. Complete model, in which the concrete tank inside the tower was also modeled, taking into account appropriate simplifications: the latter was created from a cylinder, modeled with triangular flat elements of the Tri3 type and bound to the base as totally fixed. (Figs. 44 and 45)

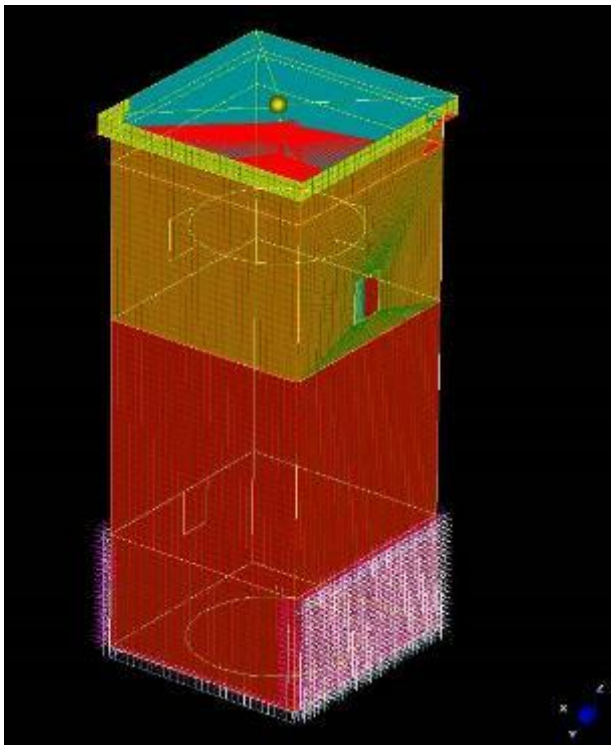

FIGURE 43 – SOUTH-EAST VIEW OF THE FINITE ELEMENT MODEL OF THE TOWER AND VISUALIZATION OF THE PLANAR ELEMENTS.

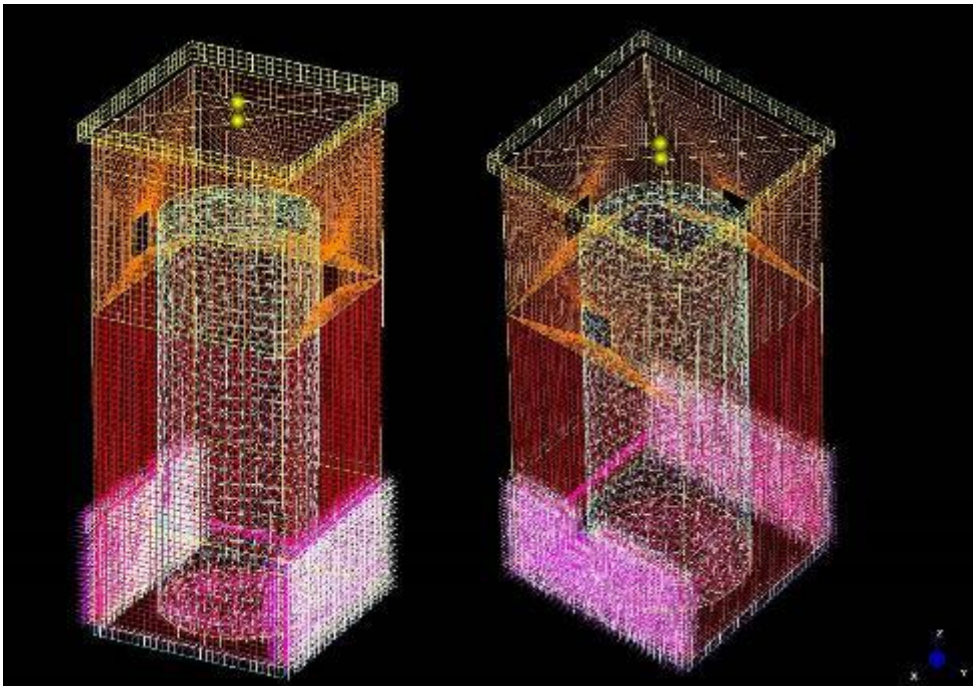

FIGURE 44 – NORTH-WEST VIEW OF THE COMPLETE NUMERICAL MODEL OF THE TOWER WITH DISPLAY OF THE INTERNAL TANK; WIREFRAME VIEW (ON THE LEFT) _ FIGURE 45 – SOUTH-WEST VIEW FROM ABOVE OF THE COMPLETE NUMERICAL MODEL OF THE TOWER WITH DISPLAY OF THE INTERNAL TANK; WIREFRAME. VIEW (ON THE RIGHT)

2. Model with only masonry, to evaluate the natural frequencies of the structure without the cistern, and at a later stage the possible hammering of the two elements that compose it during a seismic event. Both in this model and in the previous one, the masonry of the tower was modeled taking into account the geometric and mechanical properties visually detected.

   In the figures shown above, we notice the different colors that correspond to the change in thickness of the masonry: with the red color we mean the thickness of 215 cm, almost constant up to the height of 12.5 m, above the thickness takes on a value

of 170 cm, and finally, in yellow the thickness equal to 85 cm. (Figs. 43, 44, 45, 46 and 47).

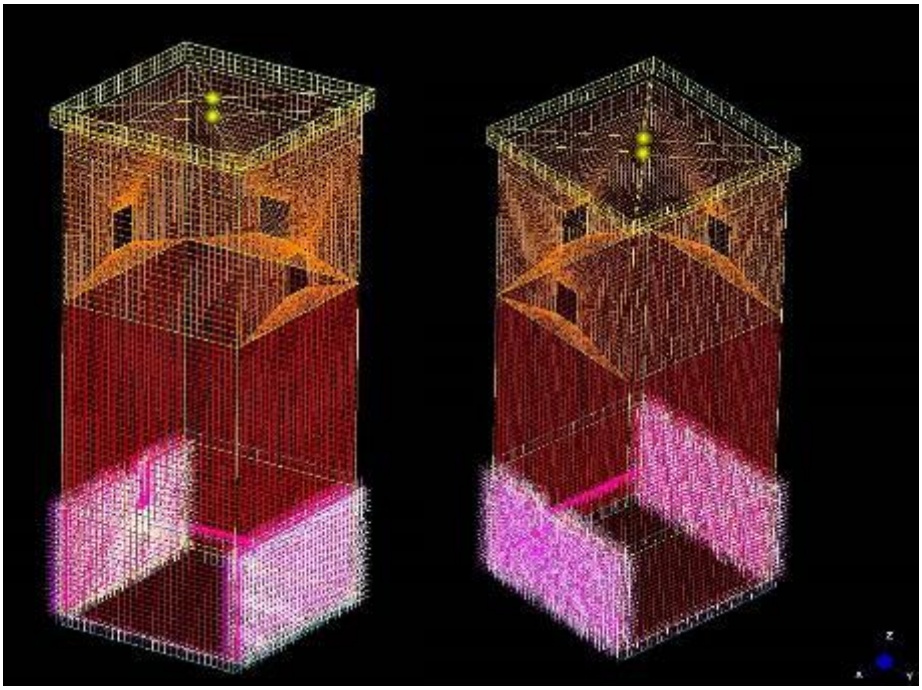

FIGURE 46 NORTH-WEST VIEW OF THE NUMERICAL MODEL OF THE TOWER COMPOSED OF ONLY MASONRY; WIREFRAME VIEW (ON THE LEFT). - FIGURE 47 SOUTH-WEST VIEW FROM ABOVE OF THE NUMERICAL MODEL OF THE TOWER COMPOSED OF ONLY MASONRY; WIREFRAME. VIEW (ON THE RIGHT).

3. Model with the only tank, created by a cylinder, modeled with triangular flat elements of the Tri type and bound to the base by fix joints.

   At a later phase, after having developed the analyzes and individually compared the data of the three numerical models studied, it was found that for the optimization it is sufficient to take into consideration only the first model, that is the complete model.

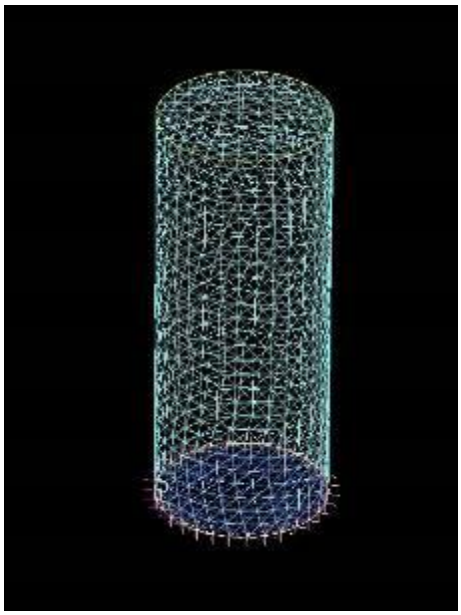

FIGURE 48 NORTH-WEST VIEW FROM THE TOP OF THE NUMERICAL MODEL OF THE TANK COMPOSED OF ONLY CONCRETE; WIREFRAME VIEW. (ON THE RIGHT)

II.4.1 Choice of the mechanical properties of the model

The mechanical properties of the masonry used for FEM analysis are:

- Elastic modulus E = 1050 MPa
- Poisson's Modulus v = 0.2
- Average specific weight of the masonry w = 19 kN/m^3

The value of the elastic modulus has been obtained based on the Wall Quality Index (IQM) of the tower.

From the substantial difference between the internal and external masonry, and from the consistent thickness of the entire wall, it can be imagined that a core is interposed between the two, which cannot be directly inspected.It was therefore necessary to identify an internal

and an external IQM. The final value of the elastic modulus was assumed to be equal to the average of the elastic modules resulting in relation to each Wall Quality Index.

In Tables 5 and 6 the type of wall quality corresponding to each soliciting action and the mechanical parameters relating to the masonry and dependent on the IQM are indicated.

Internal IQM			
Category	**Vertical**	**Out-of-the-plane**	**In the plane**
Point method	C	C	C
LMT (section)		130	
IQM	2	2	1
Mechanical parameters MIN-MAX values	**f_m (N/cm^2)**	**E(N/mm^2)**	**τ_0 (N/cm^2)**
	150-260	780-1150	2,4-3,7

TABLE 5 – PARAMETERS RELATIVE TO THE INTERNAL MASONRY OF THE TOWER

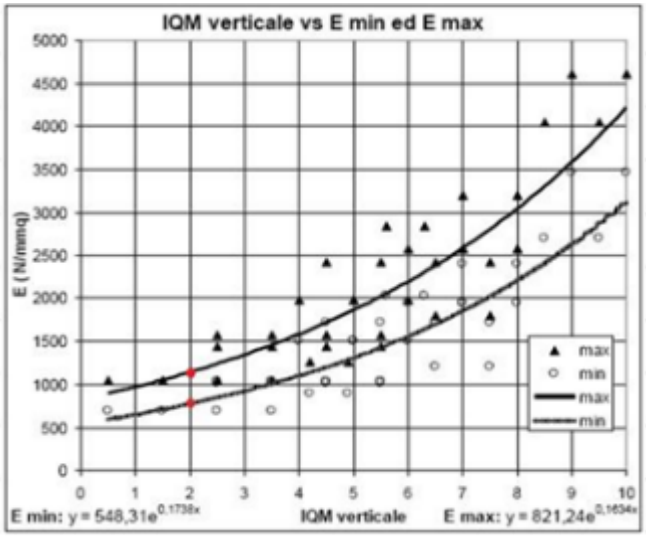

FIGURE 40 –POSITION (IN RED) OF THE MIN AND MAX VALUES OF THE ELASTIC MODULUS REFERRED TO THE INTERNAL MASONRY, ON THE E-IQM GRAPH.

External IQM			
Category	**Vertical**	**Out-of-the-plane**	**In the plane**
Point method	B	C	C
LMT (section)		130	
IQM	3	2	2,5
Mechanical parameters: MIN-MAX values	**f_m (N/cm^2)**	**E(N/mm^2)**	**τ_0 (N/cm^2)**
	185-310	920-1350	3,2-5

TABLE 6 - PARAMETERS RELATIVE TO THE EXTERNAL MASONRY OF THE TOWER

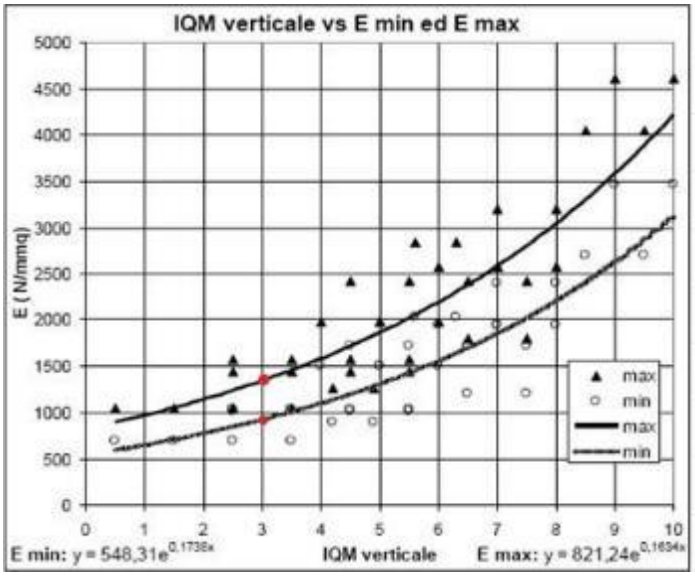

FIGURE 41 - POSITION (IN RED) OF THE MIN AND MAX VALUES OF THE ELASTIC MODULUS REFERRED TO THE EXTERNAL MASONRY, ON THE E-IQM GRAPH.

According to current code, in order to determine the mechanical properties of materials forming part of existing buildings, it is necessary to conduct experimental investigations in situ.

In the specific case of the Norman tower, limited in situ investigations have been carried out. The results of the tests are then used in combination with the contents of Table C8A.2.1 according to the level of knowledge acquired during the investigations.

In relation to this level of knowledge, the average values of the mechanical parameters and the confidence factors (CF) can be defined. In this case the level of knowledge corresponds to a level LC1, which is intended to be reached when the geometric survey has been carried out, limited in situ checks on construction details and limited investigations on the properties of the materials; the corresponding confidence factor FC is 1.35.

With an LC1 level of knowledge, the average values of mechanical parameters can be defined as follows [37]:

▪ Resistances: the minimums of the intervals reported in Table C8A.2.1 for the type of walls under consideration

▪ Elastic modules: the average values of the intervals reported in Table C8A.2.1.

Tabella C8A.2.1 - Valori di riferimento dei parametri meccanici (minimi e massimi) e peso specifico medio per diverse tipologie di muratura, riferiti alle seguenti condizioni: malta di caratteristiche scarse, assenza di ricorsi (listature), paramenti semplicemente accostati o mal collegati, muratura non consolidata, tessitura (nel caso di elementi regolari) a regola d'arte; f_m = resistenza media a compressione della muratura, τ_0 = resistenza media a taglio della muratura, E = valore medio del modulo di elasticità normale, G = valore medio del modulo di elasticità tangenziale, w = peso specifico medio della muratura

Tipologia di muratura	f_m (N/cm^2)	τ_0 (N/cm^2)	E (N/mm^2)	G (N/mm^2)	w (kN/m^3)
	Min-max	min-max	min-max	min-max	
Muratura in pietrame disordinata (ciottoli, pietre erratiche e irregolari)	100 180	2,0 3,2	690 1050	230 350	19
Muratura a conci sbozzati, con paramento di limitato spessore e nucleo interno	200 300	3,5 5,1	1020 1440	340 480	20
Muratura in pietre a spacco con buona tessitura	260 380	5,6 7,4	1500 1980	500 660	21
Muratura a conci di pietra tenera (tufo, calcarenite, ecc.)	140 240	2,8 4,2	900 1260	300 420	16
Muratura a blocchi lapidei squadrati	600 800	9,0 12,0	2400 3200	780 940	22
Muratura in mattoni pieni e malta di calce	240 400	6,0 9,2	1200 1800	400 600	18
Muratura in mattoni semipieni con malta cementizia (es.: doppio UNI foratura ≤ 40%)	500 800	24 32	3500 5600	875 1400	15
Muratura in blocchi laterizi semipieni (perc. foratura < 45%)	400 600	30,0 40,0	3600 5400	1080 1620	12
Muratura in blocchi laterizi semipieni, con giunti verticali a secco (perc. foratura < 45%)	300 400	10,0 13,0	2700 3600	810 1080	11
Muratura in blocchi di calcestruzzo o argilla espansa (perc. foratura tra 45% e 65%)	150 200	9,5 12,5	1200 1600	300 400	12
Muratura in blocchi di calcestruzzo semipieni (foratura < 45%)	300 440	18,0 24,0	2400 3520	600 880	14

FIGURE 42 – TABLE C8A.2.1. INDICATION IN RED OF THE ELEMENTS TO BE TAKEN INTO CONSIDERATION

At this point it is possible to obtain the value of the elastic modulus (E) which will be used in the finite element model. After having calculated the average values between the minimum and the maximum of E referred to the internal and external masonry (see Table 1 and Table 2), we considered the average value between these two values, equal to 1050 MPa.

It is now possible to compare this value with those in the code table, in order to determine the other unidentified mechanical properties in the experimental tests.

With the value of 1050 N/mm^2 of the elastic module, the first two rows of the table can be taken into consideration, which correspond largely to the type of masonry of the tower.

The specific weight of the masonry was considered equal to 19 kN/m^3, thus restricting the choice of the mechanical properties to be adopted, to the first line.

The average compressive strength of masonry, f_m, was calculated starting from the f_m minimum values:

- f_m = 150 N/cm^2 for interior walls

- f_m = 185 N/cm^2 for external masonry

the average value between the two, reduced by the Confidence Factor equal to 1.35, represents the final value of the resistance used in the numerical model and equal to 124 N/cm^2.

I.4.2 Constraint conditions of the structure

The structure, object of study, rests its foundations on a rocky ground quite resistant and not directly affected by the landslide. On the basis of these data, it was decided to consider the tower embedded at the base.

On the other hand, the different conditions of constraint that characterize the structure on the North-West and South-East sides in contact with other small structures, have been modeled with local elastic springs.

These elastic springs have been distributed up to 4.7 m, going to cover, in this way, the area of contact between the tower and the structures adjacent to it.

Finally, the stiffness of the springs is equal to 400,000 N/mm^2.

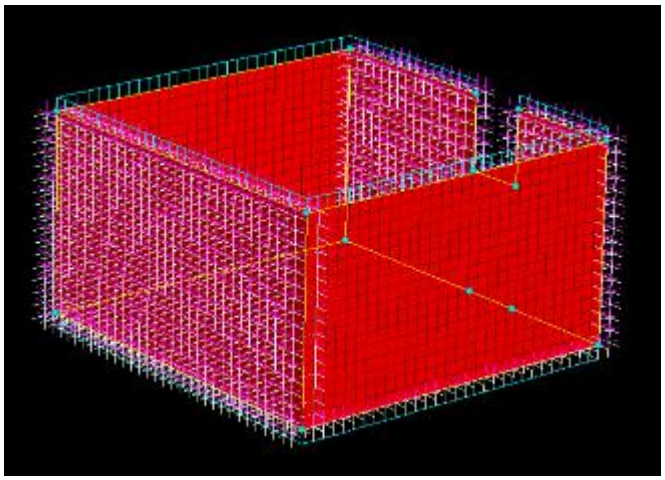

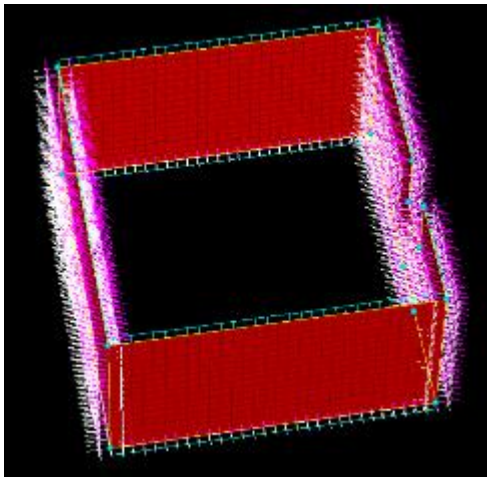

FIGURES 43, 44 BEAMS ELEMENTS IN THE NUMERICAL MODEL ACTING AS SPRINGS

In addition, a rigid plane constraint on top of the tower (*load pach*) was inserted to model the rigid behavior of the roof surface.

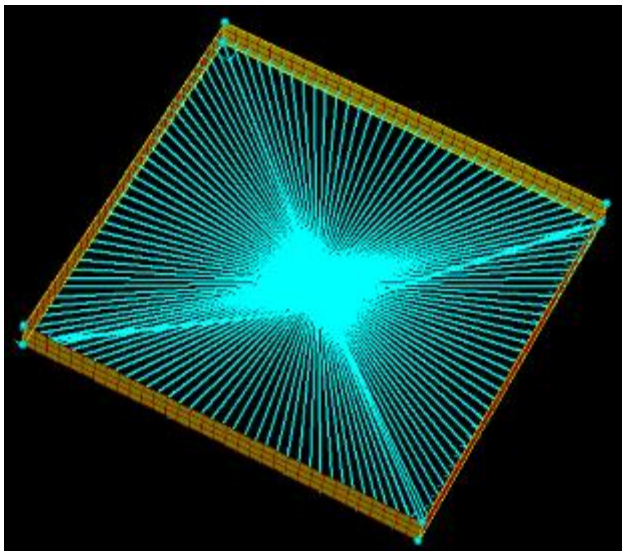

FIGURE 45 – RIGID TOP PLANE.

II.5 Dynamic linear analysis

After the modeling of the tower the modal analysis was carried out, by mean of Straus7 software, with the aim of obtaining the relative modes of vibrating and comparing them with those identified on the basis of the data acquired during the test campaign previously conducted on the structure.

With reference to what stated in the code regarding the participating mass of each vibrating mode, in Fig..46 andFig. 47 the frequencies and the participating masses of the first 25 modes of vibration of the tower are shown.

TOTAL MASS (MX,MY,MZ) : (3.130866E+03, 3.130866E+03, 0.000000E+00)

MODE PARTICIPATION FOR TRANSLATIONAL EXCITATION

Mode	Frequency (Hz)	Modal Mass (Eng)	Modal Stiff (Eng)	PF-X (%)	PF-Y (%)	PF-Z (%)
1	2.6435E+00	8.9887E+05	2.4798E+08	0.001	71.557	0.000
2	3.1350E+00	5.9616E+05	2.3132E+08	49.177	0.002	0.000
3	5.0349E+00	9.8685E+05	9.8764E+08	0.001	0.155	0.000
4	7.1541E+00	6.5488E+05	1.3232E+09	0.004	12.011	0.000
5	1.0165E+01	1.8344E+06	7.4831E+09	0.052	0.154	0.000
6	1.0585E+01	3.7858E+05	1.6746E+09	11.626	0.002	0.000
7	1.0851E+01	1.2449E+05	5.7865E+08	5.999	0.962	0.000
8	1.0854E+01	1.2447E+05	5.7884E+08	0.963	5.999	0.000
9	1.1782E+01	3.3993E+05	1.8629E+09	2.023	0.003	0.000
10	1.2961E+01	1.3162E+05	8.7286E+08	0.000	1.653	0.000
11	1.4176E+01	1.0133E+06	8.0388E+09	0.048	0.055	0.000
12	1.7204E+01	1.4295E+05	1.6704E+09	0.249	0.409	0.000
13	1.7979E+01	3.2259E+05	4.1167E+09	0.157	0.081	0.000
14	1.8196E+01	3.0459E+05	3.9812E+09	0.007	0.017	0.000
15	1.9089E+01	2.1236E+05	3.0551E+09	0.135	0.075	0.000
16	2.0319E+01	2.1817E+05	3.5562E+09	0.895	0.247	0.000
17	2.1008E+01	1.5760E+05	2.7461E+09	1.642	0.020	0.000
18	2.1210E+01	2.0623E+05	3.6626E+09	0.003	0.005	0.000
19	2.3134E+01	9.4985E+03	2.0069E+08	0.222	0.152	0.000
20	2.3270E+01	8.9804E+04	1.9198E+09	0.000	0.000	0.000
21	2.3305E+01	1.1318E+05	2.4269E+09	0.000	0.000	0.000
22	2.3597E+01	9.0642E+03	1.9925E+08	0.022	0.115	0.000
23	2.3752E+01	1.4403E+04	3.2078E+08	0.067	0.004	0.000
24	2.4791E+01	2.1942E+04	5.3240E+08	0.000	0.653	0.000
25	2.5104E+01	4.5612E+03	1.1348E+08	0.082	0.050	0.000
TOTAL TRANSLATIONAL MASS PARTICIPATION FACTORS				73.374	94.381	0.000

FIGURA 46 – RISULTATI DELL'ANALISI MODALE: VALORI DELLE FREQUENZE

MODE PARTICIPATION FOR ROTATIONAL EXCITATION

Mode	Frequency (Hz)	Modal Mass (Eng)	Modal Stiff (Eng)	PF-RX (%)	PF-RY (%)	PF-RZ (%)
1	2.6435E+00	8.9887E+05	2.4798E+08	86.433	0.002	68.625
2	3.1350E+00	5.9616E+05	2.3132E+08	0.003	81.900	0.406
3	5.0349E+00	9.8685E+05	9.8764E+08	0.682	0.001	0.004
4	7.1541E+00	6.5488E+05	1.3232E+09	0.174	0.001	13.035
5	1.0165E+01	1.8344E+06	7.4831E+09	0.017	0.013	0.180
6	1.0585E+01	3.7858E+05	1.6746E+09	0.003	3.008	0.167
7	1.0851E+01	1.2449E+05	5.7865E+08	1.194	7.439	0.539
8	1.0854E+01	1.2447E+05	5.7884E+08	7.439	1.194	6.498
9	1.1782E+01	3.3993E+05	1.8629E+09	0.011	0.748	0.035
10	1.2961E+01	1.3162E+05	8.7286E+08	0.227	0.000	1.462
11	1.4176E+01	1.0133E+06	8.0388E+09	0.009	0.008	0.004
12	1.7204E+01	1.4295E+05	1.6704E+09	0.001	0.009	0.404
13	1.7979E+01	3.2259E+05	4.1167E+09	0.002	0.004	0.043
14	1.8196E+01	3.0459E+05	3.9812E+09	0.017	0.001	0.035
15	1.9089E+01	2.1236E+05	3.0551E+09	0.007	0.011	0.023
16	2.0319E+01	2.1817E+05	3.5562E+09	0.000	0.096	0.217
17	2.1008E+01	1.5760E+05	2.7461E+09	0.000	0.335	0.080
18	2.1210E+01	2.0623E+05	3.6626E+09	0.008	0.001	0.011
19	2.3134E+01	9.4985E+03	2.0069E+08	0.003	0.025	0.219
20	2.3270E+01	8.9804E+04	1.9198E+09	0.000	0.000	0.000
21	2.3305E+01	1.1318E+05	2.4269E+09	0.000	0.000	0.000
22	2.3597E+01	9.0642E+03	1.9925E+08	0.005	0.001	0.151
23	2.3752E+01	1.4403E+04	3.2078E+08	0.014	0.005	0.009
24	2.4791E+01	2.1942E+04	5.3240E+08	0.002	0.001	0.674
25	2.5104E+01	4.5612E+03	1.1348E+08	0.001	0.005	0.074
TOTAL ROTATIONAL MASS PARTICIPATION FACTORS				96.253	94.812	92.896

FIGURE 47 – RESULTS OF THE MODAL ANALYSIS: VALUES OF THE PARTICIPATING MASS FOR EACH MODE OF VIBRATION

For the comparison with the data acquired from the experimental tests, only the first five vibration modes were taken into consideration.

	Frequency [Hz]	Frequency [rad/s]	Period [s]
1° mode	2,643	16,609	0,38
2° mode	3,1435	19,697	0,31
3° mode	5,034	31,635	0,19
4° mode	7,154	63,869	0,14
5° mode	10,016	66,508	0,10

TABLE 7 – FREQUENCY AND PERIOD VALUES REFERRING TO THE FIRST 5 VIBRATION MODES.

The first two modes of vibration appear to be of a flexional type, the first directed towards the y-axis in a North-South direction and the second directed towards x with an East-West direction (Figures 48a and b); the third mode of vibrating is a torsional one (Fig. 48c), while the fourth is a bending one in the y direction (Fig. 48 d) and the fifth mode is a torsional one (Fig. 48 e).

Given the quadrangular geometry of the tower, the first two modes of vibrating are very close in terms of period and frequency. The sides arranged along the x axis, however, have a greater rigidity due to the presence of the small structures annexed to the tower, which favors the trend of the first mode of vibrating along the y axis. In these first five modes of vibrating the cistern inside the tower is not involved, starting to vibrate from the seventh mode on, with higher frequencies of the tower.

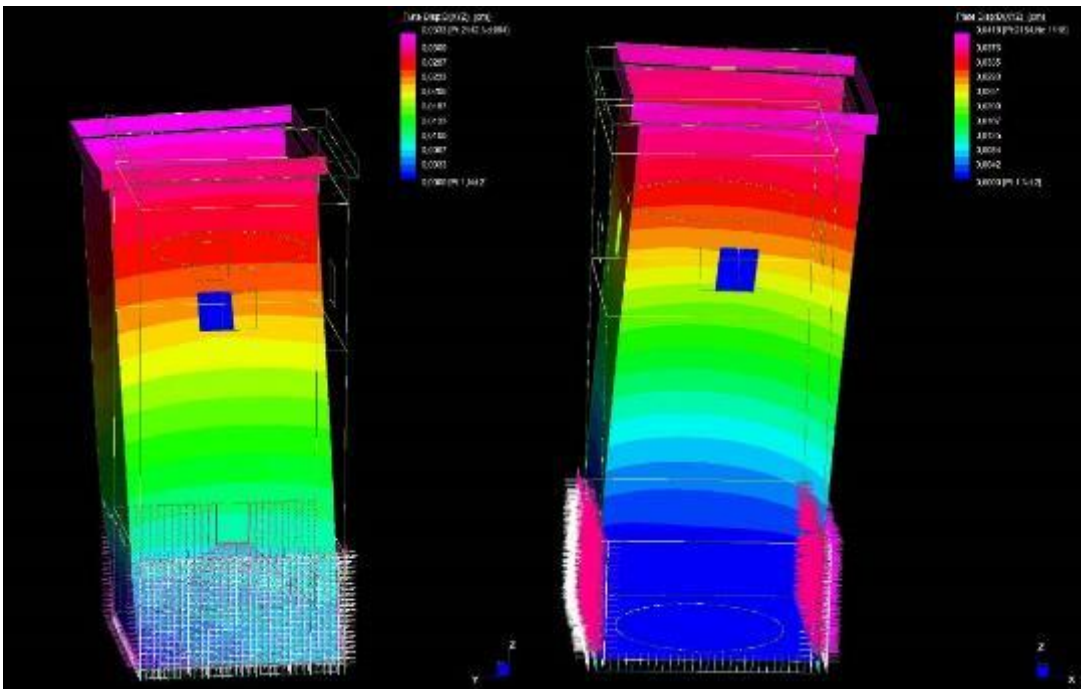

a) **b)**

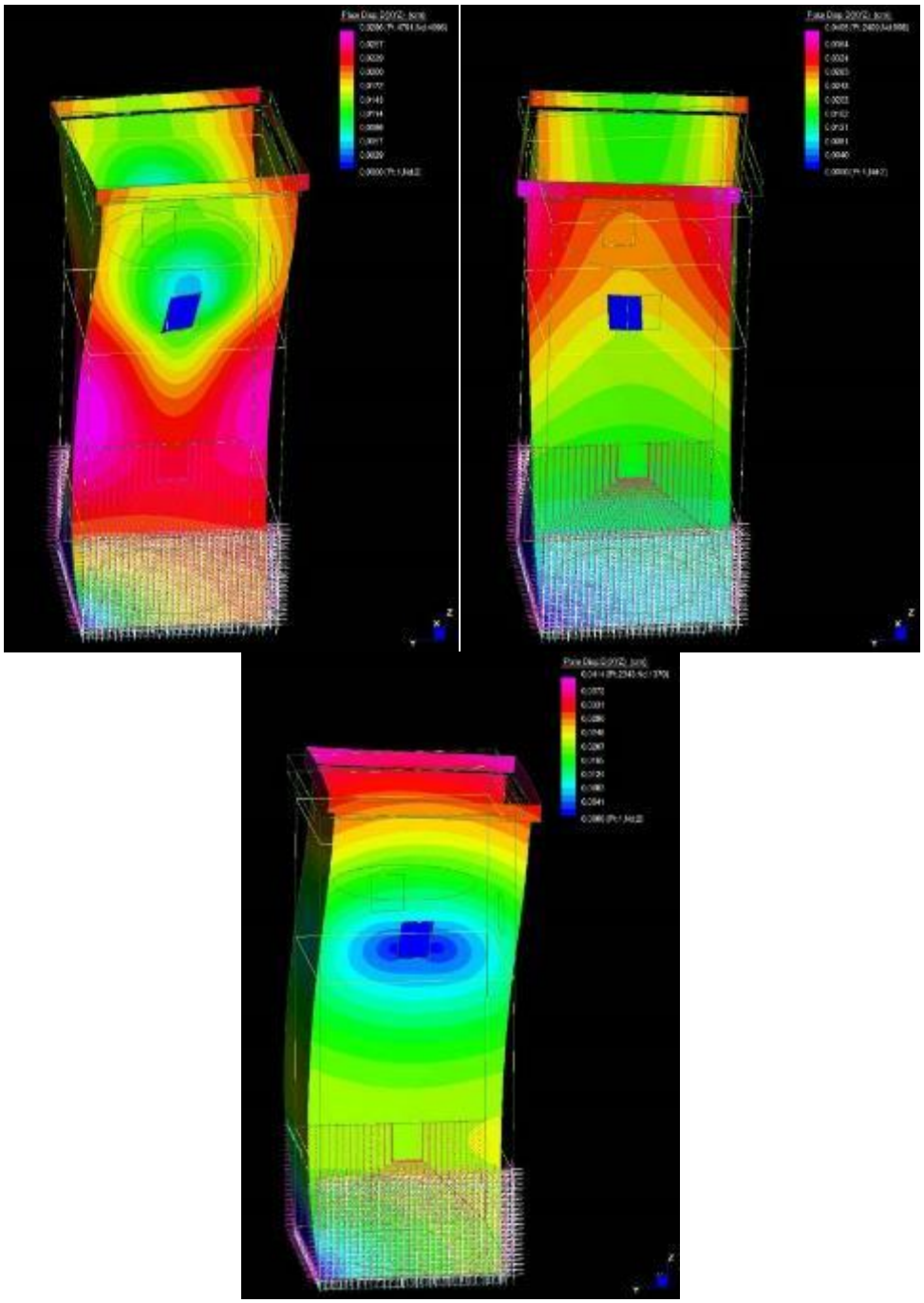

c) **d)** **e)**

FIGURE 48. FIRST FIVE MODES OF VIBRATING OBTAINED FROM THE NUMERICAL ANALYSIS OF THE TOWER OF CRACO.

Below in Fig. 49 and Tab. 8 we report the modal deformations relating to the first 5 vibration modes for the three different models analyzed: complete model, model consisting of masonry structure only and model of the cylindrical tank.

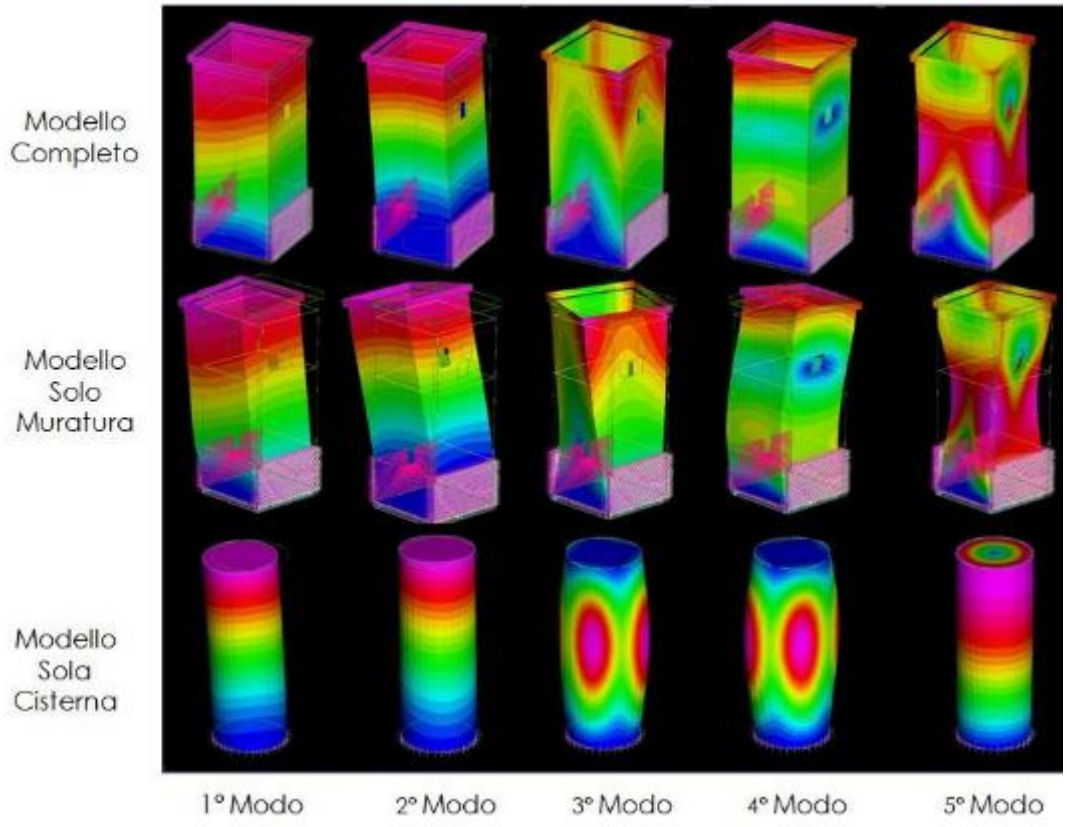

FIGURE 49. FIRST FIVE MODES OF VIBRATING OBTAINED FROM THE NUMERICAL ANALYSIS OF THE THREE DIFFERENT MODELS CONSIDERED.

		Mode of Vibrating				
	Models	**1**	**2**	**3**	**4**	**5**
Frequencies	**Compleate Model**	2,64 Hz	3,14 Hz	5,03 Hz	7,15 Hz	10,17 Hz
	Mansory Structure Model	2,64 Hz	3,14 Hz	5,03 Hz	7,15 Hz	10,17 Hz
	RC Tank Model	10,85 Hz	10,86 Hz	23,27 Hz	23,30 Hz	30,53 Hz

TABLE 8. FREQUENCIES OF FIRST FIVE MODES OF VIBRATING OBTAINED FROM THE NUMERICAL ANALYSIS OF THE THREE DIFFERENT MODELS CONSIDERED.

II.6 The Operational Modal Analysis:comparison between the FE model and the experimental data

The data acquired during the experimental test campaign using accelerometers arranged at specific points in the tower, were then processed through the Artemis software according to the Modal Operational Analysis procedures, with the aim of deriving the structural dynamic response to the environmental actions on the Norman tower.

The ultimate goal of this analysis is to determine the dynamic properties of the structure in question, so that they can then be compared to the dynamic properties, acquired by the modal analysis of the finite element model of the structure itself. Subsequently the FEMtools software was used for the update of the numerical model.

As previously explained, 6 recordings of the 15-minute accelerometers were made; only four of the six trials were taken into consideration for the Operational Modal Analysis (Test n ° 2, n ° 3, n ° 5, n ° 6). Furthermore, for each of the four recordings only the most significant channels were chosen and where the signal was the cleanest. In particular, channels 35211 and 35208 have been eliminated in all the records due to interference in the signal attributable to causes that cannot be defined with certainty.

TEST N°2		
	Frequency (Hz)	**Mode shape**
1°mode	2.974	Bending along Y
2°mode	3.064	Bending along X
3°mode	5.973	torsional
4°mode	8.023	Bending along Y
5°mode	10.5	torsional

TEST N°3		
	Frequency (Hz)	**Mode shape**
1°mode	3.025	Bending along Y
2°mode	3.152	Bending along X
3°mode	6.025	torsional
4°mode	8.985	Bending along Y
5°mode	-	torsional

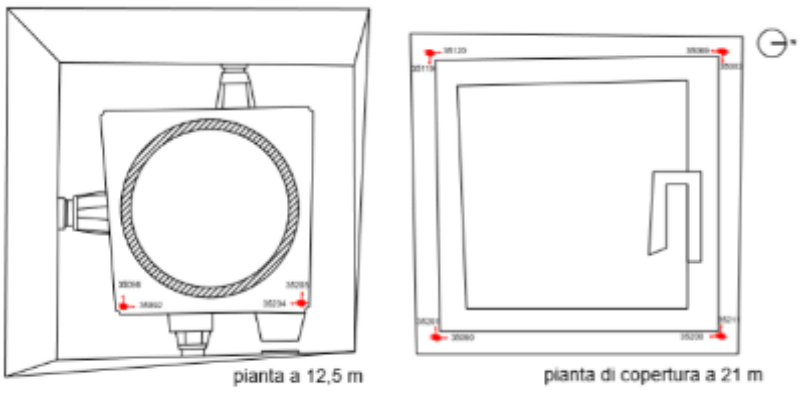

FIGURE 50 – POSITIONING OF THE CHANNELS USED WITH REFERENCE TO TEST N ° 2

In test n ° 2 channels 35205, 35122, 35035 and 35212 were eliminated for modal analysis, all positioned at the first level at a quote of 12.5 m.

TEST N°5		
	Frequency (Hz)	**Mode shape**
1°mode	2.935	Bending along Y
2°mode	3.071	Bending along X
3°mode	5.882	torsional
4°mode	8.846	Bending along Y
5°mode	10.47	torsional

TEST N°6		
	Frequency (Hz)	**Mode shape**
1°mode	3.04	Bending along Y
2°mode	3.255	Bending along X
3°mode	6.065	torsional
4°mode	8.879	Bending along Y
5°mode	-	torsional

Following the data acquired from registration no. 3, channels 35119 and 35083 were placed for the Modal Operational Analysis, both positioned at a height of 21 m (figure 50).

From test n ° 5, on the other hand, all the channels were suitable for the modal analysis.

Also, for this last test only channels 35119 and 35083 have been imposed.

On the basis of the data obtained from the Operational Modal Analysis performed for each of the four chosen tests, a statistical analysis was performed on the frequency values resulting from the modal analysis(Fig. 51). For each mode of vibration, the minimum, maximum and average values between the values previously obtained from the four experimental tests have been identified.

Referring to the average values, the update of the finite element model was performed.

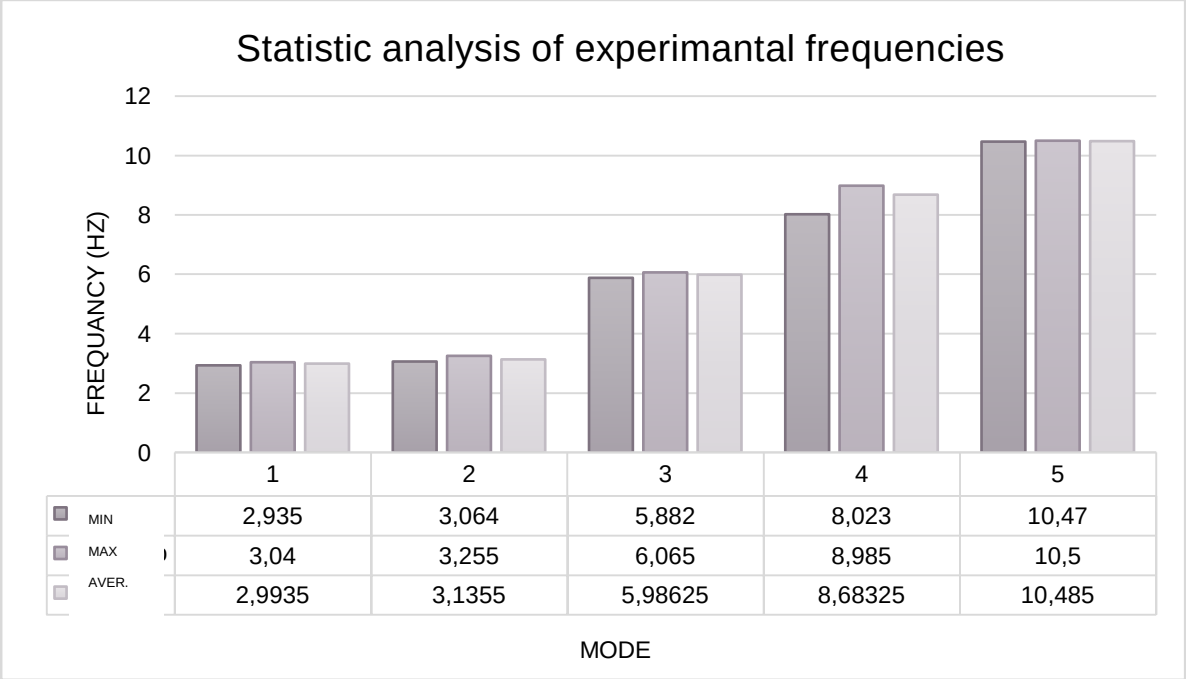

FIGURE 51. STATISTICAL ANALYSIS OF THE FIRST FIVE EXPERIMENTAL FREQUENCIES.

Mode	Model Frequencies FE (Hz)	Experimental Frequencies (Hz)		
		Mean	*Minimum*	*Maximum*
1	2.643	2.9935	2.935	3.04
2	3.135	3.1355	3.064	3.255
3	5.034	5.98625	5.882	6.065
4	7.154	8.68325	8.023	8.985
5	10.058	10.485	10.47	10.5

TABLE 9. COMPARISON OF EXPERIMENTAL FREQUENCIES WITH THOSE RELATING TO THE FINITE ELEMENT MODEL.

From the direct comparison between the experimental frequencies and those relating to the finite element model, values are observed that are rather close together (Table 9). In

particular, it is evident that the frequencies of the model are particularly close for the first two ways of vibrating, at the values of the experimental frequencies, with respect to the values relative to the last three modes of vibration that are more different.

Table 10 shows the differences between the experimental frequencies and those of the numerical model.

Modes	Model Frequencies	Average experimental Frequencies	d_i
1	2.643	2.994	0.351
2	3.135	3.136	0.001
3	5.034	5.986	0.952
4	7.154	8.683	1.529
5	10.016	10.485	0.469

TABLE 10. COMPARISON OF EXPERIMENTAL FREQUENCIES WITH THOSE RELATING TO THE ELEMENT MODEL

d_i represents the difference between the values acquired in the two methods. If D indicates the mean of the values of d_i and N is the number of samples considered, which in the case in question corresponds to the five modes of vibrating the tower, it is possible to determine s_D:

$$s_D = \sqrt{\frac{\sum(d_i - \underline{D})^2}{(N-1)}}$$

From the values of d_i shown in Table 10, the value of D is equal to 0.126; therefore considering the Student distribution (Student's *t*) it results:

$$\pm t_{calc.} = \frac{D}{s_D} \times \sqrt{N}$$

In this case, $t_{calc.}$ is equal to 1.15. Table 11 shows the values of the factor relative to the different confidence intervals.

Gradi di libertà	Fattore relativo all'intervallo di fiducia				
	80%	90%	95%	99%	99,9%
1	3.08	6.31	12.70	63.70	637
2	1.89	2.92	4.30	9.92	31.6
3	1.64	2.35	3.18	5.84	12.9
4	1.53	2.13	2.78	4.60	8.60
5	1.48	2.02	2.57	4.03	6.86
6	1.44	1.94	2.45	3.71	5.96
7	1.42	1.90	2.36	3.50	5.40
8	1.40	1.86	2.31	3.36	5.04
9	1.38	1.83	2.26	3.25	4.78
10	1.37	1.81	2.23	3.17	4.59
11	1.36	1.80	2.20	3.11	4.44
12	1.36	1.78	2.18	3.06	4.32
13	1.35	1.77	2.16	3.01	4.22
14	1.34	1.76	2.14	2.89	4.14
	1.29	1.64	1.96	2.58	3.29

TABLE 11. VALUES OF THE FACTOR RELATIVE TO THE DIFFERENT CONFIDENCE INTERVALS

Taking into consideration $t_{95\%}$ and $t_{99\%}$ with 5 degrees of freedom, that is 5 specimens, a comparison is made witht_{calc}. As t_{calc}= 1,15 < $t_{95\%}$ = 2.57 and t_{calc}= 1.15 < $t_{99\%}$ = 4.03 it is possible to affirm that the results of the frequencies obtained from the two modal analyses are statically independant.

In Figures 52-54 are shownthe modal shapes relating to the first three modes of vibration acquired during test n ° 5. The geometric model doesn't consider the cylindrical concrete tankbecause the results of the FE model, previously studied, show that the frequencies of the first five shape of vibrating depend only on the masonry structure; so the Reinforced Concrete element doesn't contribute to them.

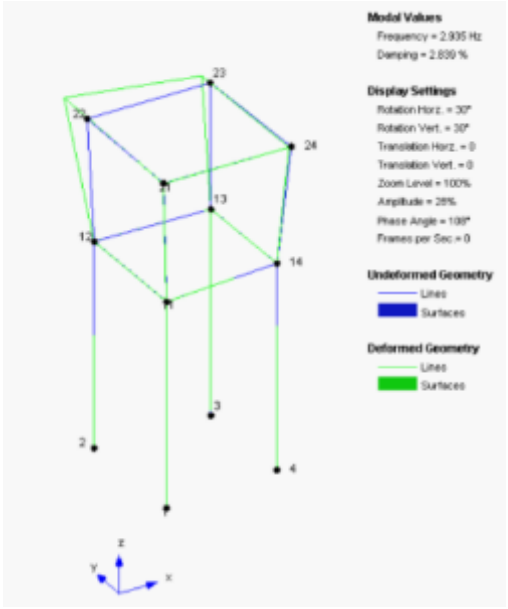

FIGURE 52 – FIRST WAY OF VIBRATING – BENDING ALONG Y = 2,643 HZ

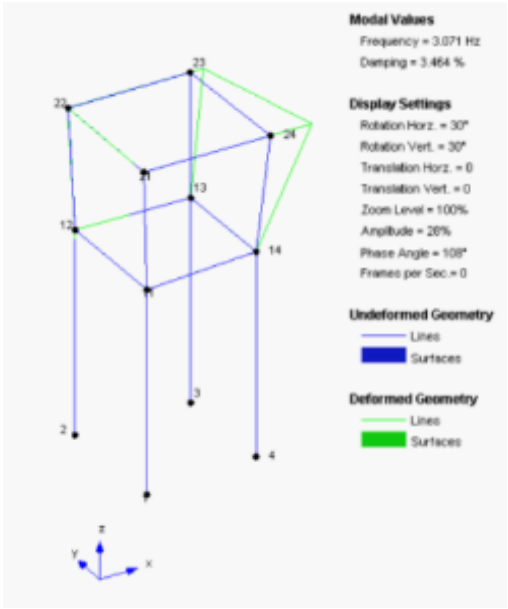

FIGURE 53 – SECOND MODE OF VIBRATING – BENDING ALONG X = 3,135 HZ

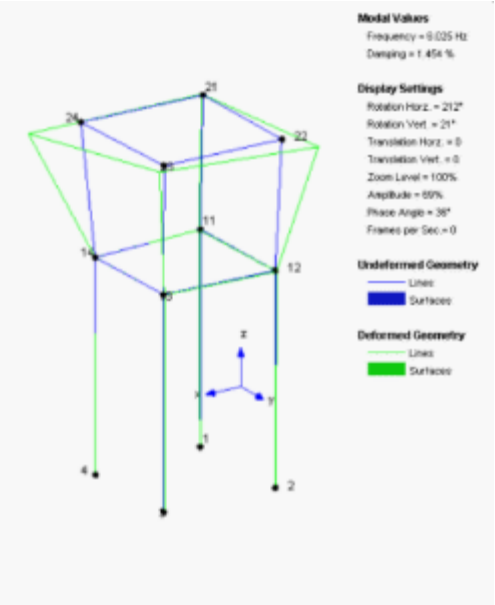

FIGURE 54 – THIRD MODE OF VIBRATING – TORSIONAL = 5,034 HZ

As indicated in the preceding tables, the first mode of vibrating corresponds to a flexional type along the y direction; the second mode, also of a flexional type, is directed more towards the x-axis, while the third mode of vibrating is torsional.

In the figures, the geometry of the tower (in green) seems to deform only at the top; in fact, the portion in question corresponds to the part of the structure between 12.5 m and 21 m. They represent the accelerometers positioning quotas, consequently the structure shows its deformation only in the part in which the accelerometers have acquired the accelerations of the structure, subject to environmental excitation

II.7Structural earthquake response

The seismic classification of the national territory has introduced specific technical regulations for the geographical areas characterized by the same seismic risk. The

Municipality of Craco (MT) falls under the Order of the President of the Council of Ministers, OPCM n. 3274/2003, updated with the Resolution of the Regional Council of Basilicata n. 731 of 11.11.2003, in seismic zone 2, or "Zone with average seismic hazard where strong earthquakes can occur". In the scenario of a multi-risk analysis, therefore, it is necessary to evaluate the vulnerability of the Norman tower both from a hydro-geological and seismic point of view, considering the risk of landslides, possible soil erosion and earthquakes in the area.

The seismic risk assessment was performed through a modal analysis with response spectrum, having the natural frequencies and the vibrating modes of the structure available from the previous phase. The modal analysis, in fact, allows to analyze in seismic combination, complex structures with multiple degrees of freedom, since it operates simplifications, facilitating the resolution of the structural problem, in order to calculate the single modes of vibration, the period of oscillation and the participation masses of any modal form. In particular, this analysis reduces structures with multiple degrees of freedom in several simple oscillators (with only one degree of freedom and the same dynamic properties of the mode of vibration), analyzing response spectra that associate the vibration period of each simple oscillator, that is, in any way, at the maximum seismic acceleration that it will undergo. The maximum seismic action that solicits the single oscillator, that is the cutting action at the base in the event of an earthquake, will be nothing but the maximum acceleration of the mode of vibrating multiplied by its participating mass. Once the seismic action has been obtained for each mode of vibrating, these are distributed in the original structure to several degrees of freedom, in order to obtain the relative stresses that act on the entire structure and, through SRSS probabilistic methods (“Square Root of Sum of

Squares ”) Or CQC (“ Complete Quadratic Combination ”) which also consider the damping of the structure, obtaining an assessment of the seismic risk.

The modal analysis with response spectrum was performed with the Straus7 software, in which it was possible to load the recording of the "accelerating response spectrum" of the L'Aquila earthquake of 2009 (Event ID "L_AQUILA") processed and downloaded from the Itaca INGV website (National Institute of Geophysics and Volcanology) (see Fig. 55). The spectrum, divided into three spectra, one for each direction of the analytical model or according to its x, y and z axes, is processed for the three models described above, the complete one, the only masonry and only the cistern and for each model the results for the 25 modal shapes obtained previously were obtained.

The study was carried out considering only the 10 modal shapes of the complete model and the model with the only masonry and the first four modal shapes of the cistern alone. From the modeling of the cistern alone it emerged that the latter results to have frequencies too high and not comparable with the other two models, in fact the first modal form of the cistern is found at 10.058 Hz, a frequency much higher than the other first two, which are coincident because they concern only the masonry. This makes it possible to state that for very low frequencies the stressed mass affects only the masonry part of the structure.

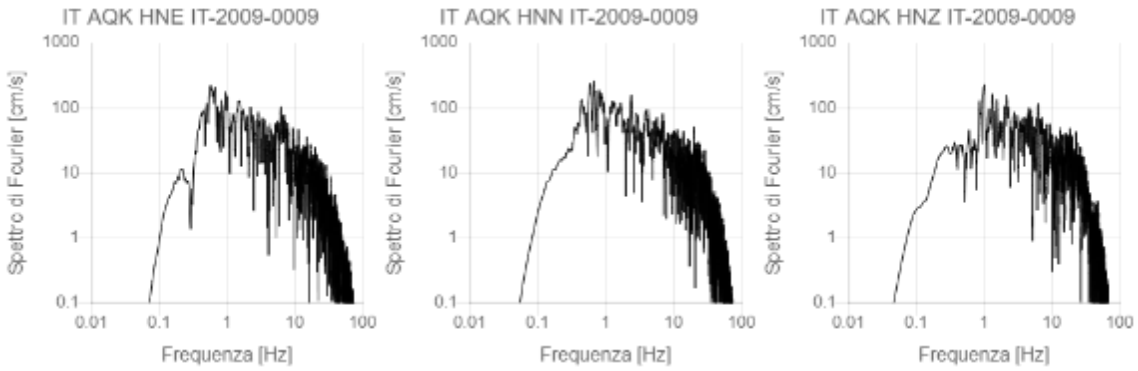

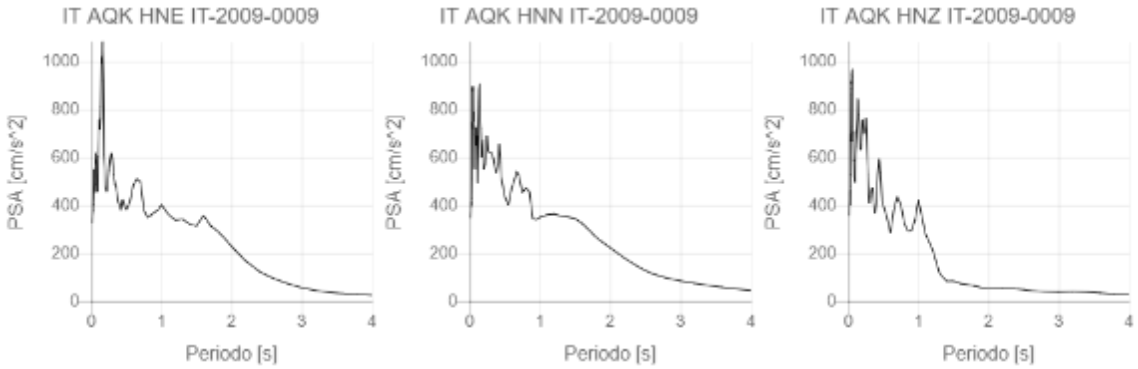

FIGURE 55 – FOURIER SPECTRA (SEE ABOVE) AND RESPONSE SPECTRA IN PSEUDO ACCELERATION (PSA) DAMPED AT 5% RELATIVE TO THE RECORDED SEISMIC EVENT (L'AQUILA).

Subsequently, through the same program, the seismic combination set by the NTC2018 standard was set, which takes into account the simultaneous presence of the earthquake in both the x and y directions, and therefore of a prevalent seismic action and a 30% reduced one. In the specific case of the Norman tower, the accidental eccentricities were not considered, as there are no accidental permanent loads; the tower, which contains a cistern inside it, is not accessible to the public. Thus, there will be only 8 combinations, 2 for each position of the masses, i.e.:

+Ex + 0,3 Ey (Fig. 55)
+Ex – 0,3 Ey (Fig. 56)
-Ex + 0,3 Ey (Fig. 57)
-Ex – 0,3 Ey (Fig. 58)
+0,3 Ex + Ey (Fig. 59)
+0,3 Ex – Ey (Fig. 60)
-0,3 Ex + Ey (Fig. 61)
-0,3 Ex – Ey (Fig. 62)

Below the deformations of the tower in the event of an earthquake that consider the weight and theseismic action with the different combinations are reported(Figg. 56-62).

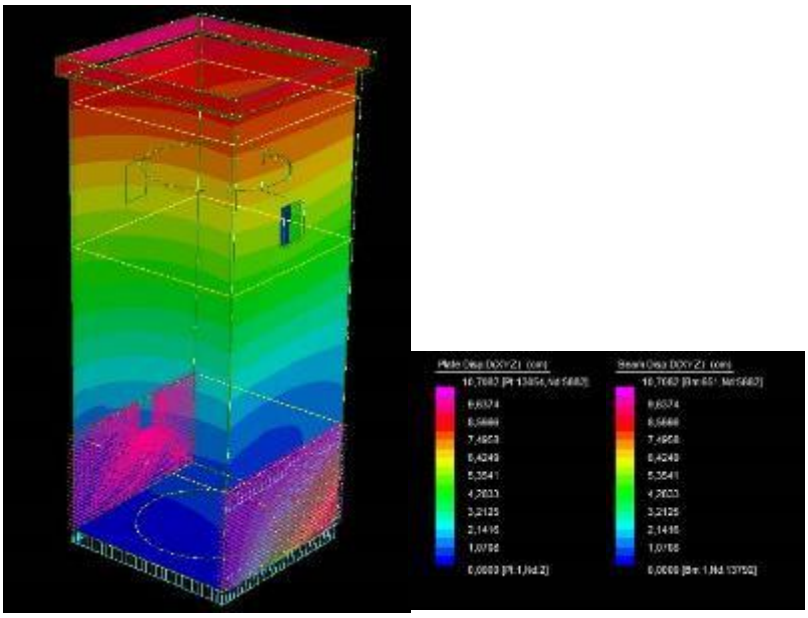

FIGURE 56 – NORTH-WEST VIEW OF THE TOWER, DEFORMATION WITH SEISMIC COMBINATION 1: G1+G2+EX+0,3EY

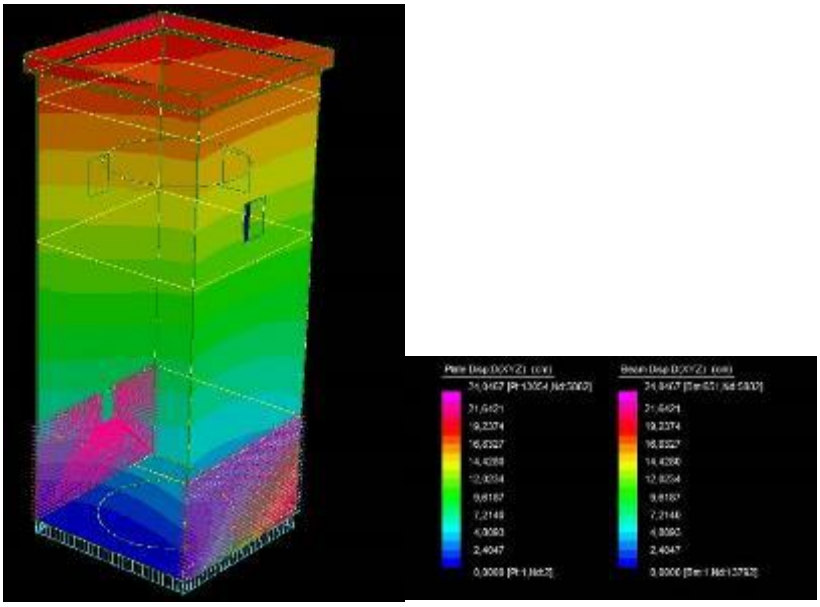

FIGURE 57 – NORTH-WEST VIEW OF THE TOWER, DEFORMATION WITH SEISMIC COMBINATION 2: G1+G2+EX-0,3EY

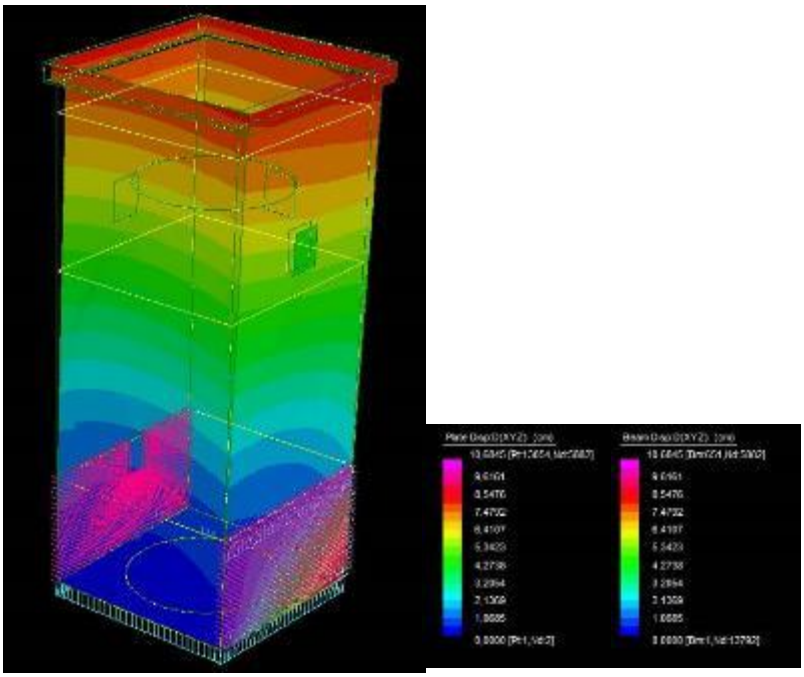

FIGURA58 – NORTH-WEST VIEW OF THE TOWER, DEFORMATION WITH SEISMIC COMBINATION 3: G1+G2-EX+0,3EY

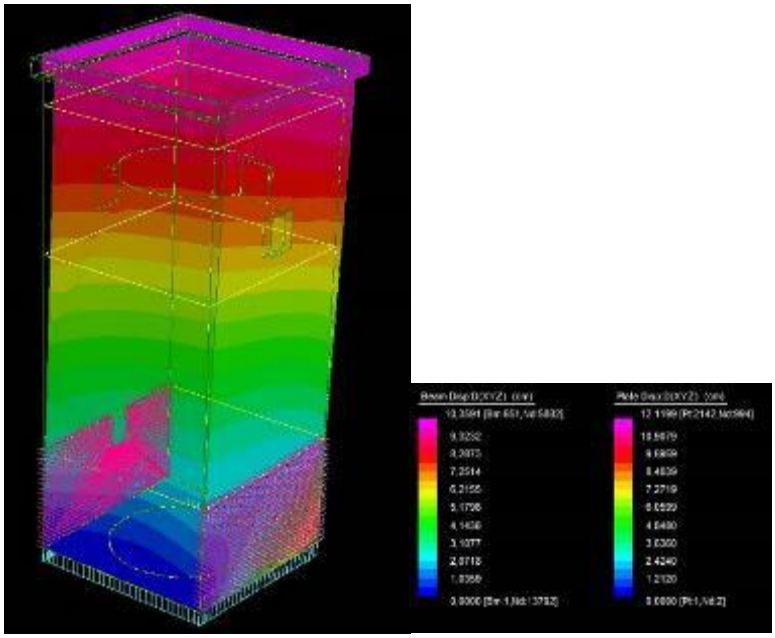

FIGURE 59 – NORTH-WEST VIEW OF THE TOWER, DEFORMATION WITH SEISMIC COMBINATION 4: G1+G2-EX-0,3EY

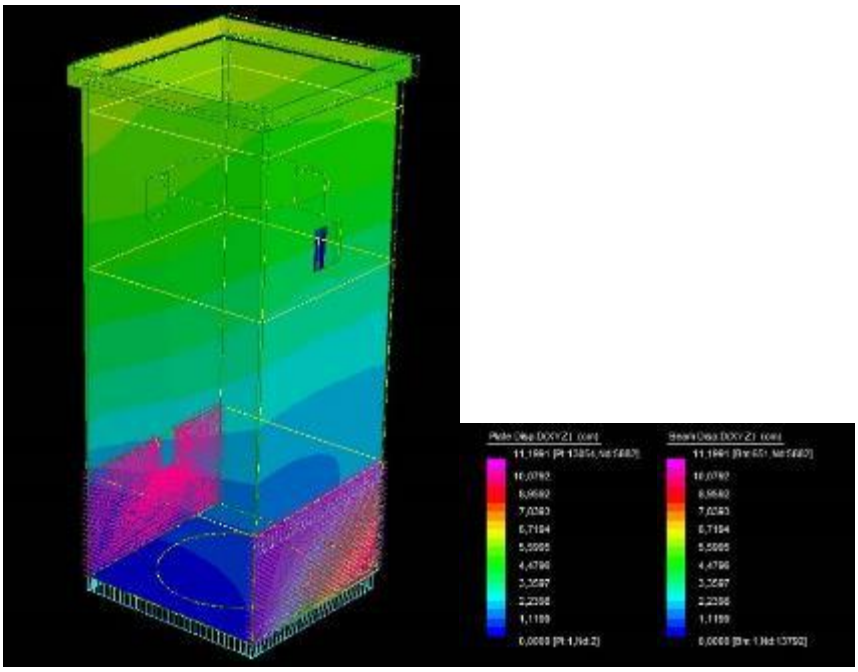

FIGURE 60 – NORTH-WEST VIEW OF THE TOWER, DEFORMATION WITH SEISMIC COMBINATION 5: G1+G2+EY+0,3EY

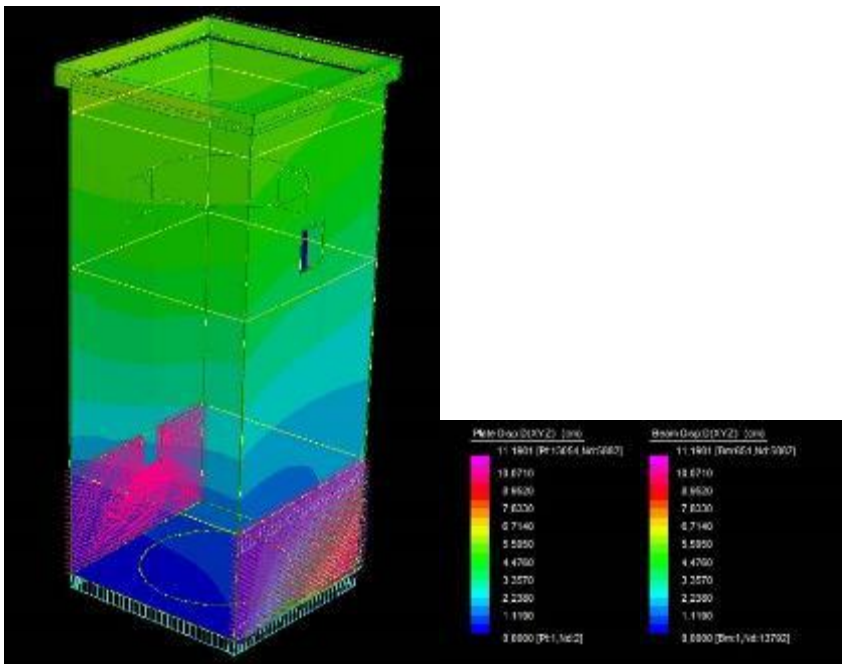

FIGURE 61 – NORTH-WEST VIEW OF THE TOWER, DEFORMATION WITH SEISMIC COMBINATION 6: G1+G2+EY-0,3EY

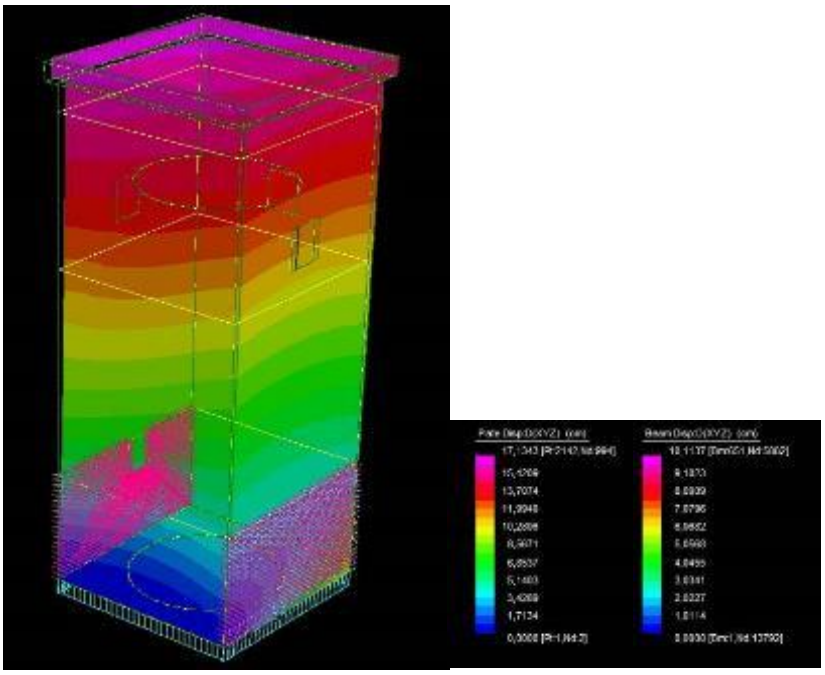

FIGURE 62 – NORTH-WEST VIEW OF THE TOWER, DEFORMATION WITH SEISMIC COMBINATION 7: G1+G2-EY+0,3EY

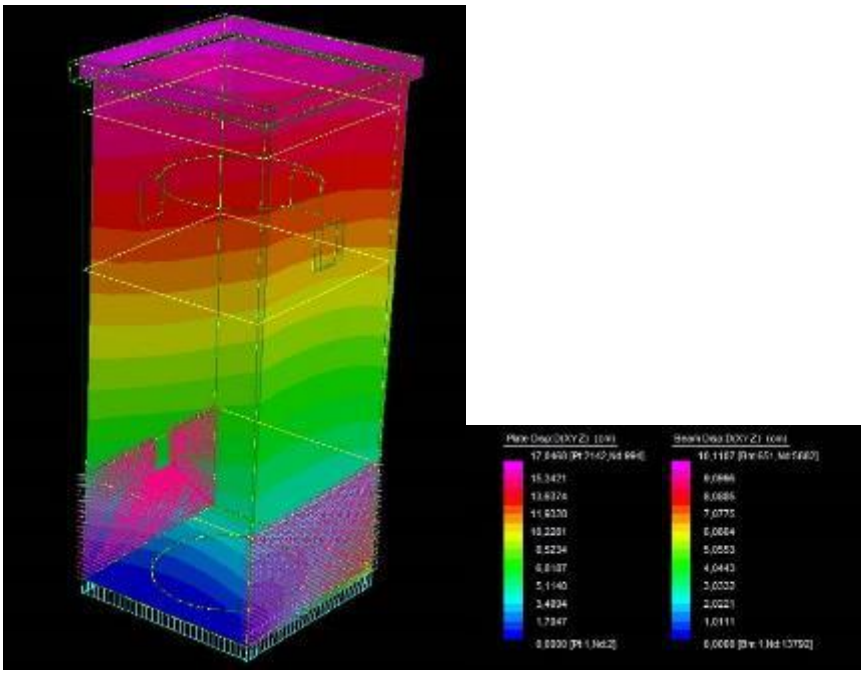

FIGURE 67 – NORTH-WEST VIEW OF THE TOWER, DEFORMATION WITH SEISMIC COMBINATION 8: G1+G2-EY+0,3EY

The completely different behavior of the masonry structure and the cistern made it necessary to compare the displacements of the two structures in the event of an earthquake and to check that there were no hammering problems. For this reason all the maximum displacements in three directions (dx, dy, dxyz) have been identified both for the spectral response of each single modal shape and for the final seismic combinations. After this analysis it was ascertained that as far as the two structures are concerned, they are not subject to hammering since the displacements of the tank are much smaller than those of the masonry structure and the order of magnitude is not comparable. For completeness it is reported that the prevalent displacements occur at the apex of the tower and along the y-axis, where there are no other building aggregates and therefore no restrictions adjacent to the structure. In particular, the greater displacement in the x direction alone is 9.54 cm, in the y direction alone it is 16.39 cm and considering the maximum spatial displacement in the three directions (with displacement prevalence along y) is equal to 18.02 cm.

II.8 Seismic risk assessment

In general, the seismic risk assesses the expected damage following a possible seismic event and depends on several factors, in fact the risk is expressed by the equation:

Risk = Hazard • Vulnerability • Exposition

where:

- Hazard, consists in the probability that an earthquake occurs and is linked to the seismic zone in which the object of study is located;

- Vulnerability, consists in the evaluation of the consequences of the earthquake and is linked to the capacity of resistance of the object of study;

- Exposition consists in the socio/economic evaluation of the consequences and is linked to the contexts of the communities.

The code indicates two alternative methods to determine the class of the seismic risk of a building, the conventional and the simplified method. For the Norman Tower the conventional method was applied, which is based on the application of the normal analysis methods envisaged by the current NCT 2018, in order to determine the risk class considering two parameters:

- The **expected average annual loss(PAM),** which takes into account the economic losses associated with the damage to the structural and non-structural elements, and referring to the **reconstruction cost (CR)** of the building without its content;
- The **safety index (IS-V)** of the structure, defined as the ratio between *peak ground acceleration* (PGA, *Peak Ground Acceleration*) capacity, which determines the achievement of the State of Life Protection Limit (SLV), and the *PGA demand* referring to the specific site where the construction is located and always to the SLV, which the standard indicates as a reference for the design of a new building. The structure's safety index (IS-V) is also known as the "Risk Index".

It follows that to calculate both PAM and IS-V of the Tower of Craco, it is necessary to determine the peak accelerations to the ground for which the various Limit States are reached (SL of Operation-SLO, SL of Damage-SLD , SL of Life Preservation- SLV, SL of Collapse prevention-SLC), using the usual limit states safety checks required by the Technical Standards for Construction.

In particular, PAM parameter can be assimilated to the cost of restoration, also known as **Cost of reconstruction (CR)**, of the damage caused by the seismic events that will occur during the life of the building, divided annually and expressed as a percentage of the cost of reconstruction. Therefore, PAM can be evaluated, like the area underlying the curve representing the direct economic losses, as a function of the average annual frequency of exceeding (equal to the inverse of the average return period) of the events that cause the reaching of a limit state for the structure. This curve, in the absence of more precise data, can be discretized by a broken line. The smaller the area subtended by this curve, the lower the expected average annual loss (PAM) (Fig. 63)

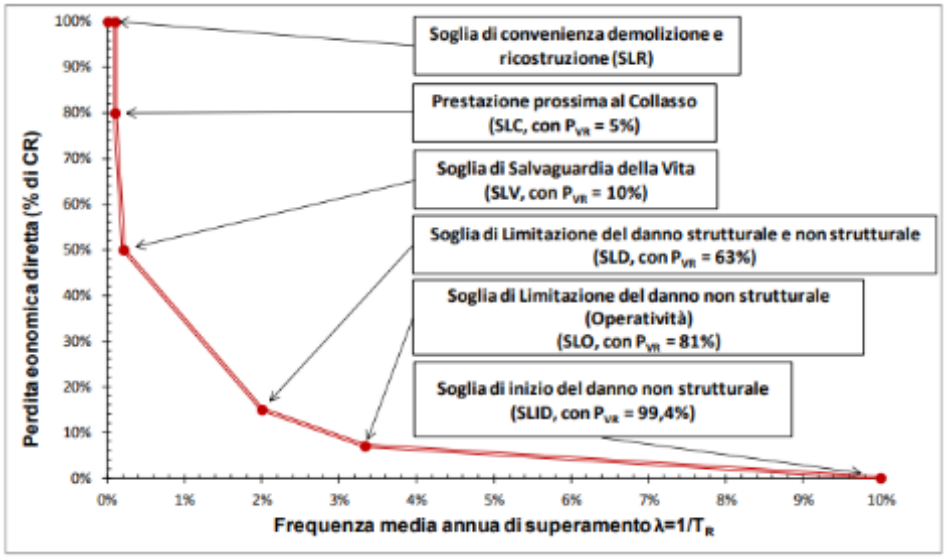

FIGURE 63. TREND OF THE CURVE THAT IDENTIFIES PAM, REFERRING TO A CONSTRUCTION WITH A NOMINAL LIFE OF 50 YEARS AND BELONGING TO THE USE CLASS II.

In the specific case of the Norman Tower, since this is a property with significant historical and cultural value, it is not plausible to hypothesize a cost of reconstruction alone. Its

reconstruction, however economically estimable, can in no way make up for the historical and cultural value lost in the event of its collapse and/or serious damage.

For this reason, the approach studied envisages the identification of a new **CR* parameter "New Reconstruction Cost",** sum of the mere cost of reconstruction CR and a parameter that takes into account the historical and social value of the Tower. In the case under study, the parameter is the **Fruity Loss (PF).**Therefore:

$$CR^* = CR + PF$$

Craco, in fact, as already mentioned, has become a tourist attraction center for its history, its social value and its historical and architectural heritage, thus becoming a symbolic ghost town; for this reason the "Scenographic Museum of Craco" was established, an organization that allows you to visit the historic center of Craco and in particular some of its symbolic structures including the Tower.

Assuming the collapse of the Tower, therefore, the loss of a symbolic element of the historical center is hypothesized and therefore its non-usability too; this non-visitability would have an effect on a monthly economic loss during the whole period which coincides with the "Recovery Time" of the structure.

Of course, this parameter cannot absolutely estimate the real historical-artistic value of the Tower, but it can be a first approach to consider parameters, important for the architectural heritage, unfortunately not estimable in the probabilistic way of structural safety, such as to create a gap in the current legislation , which is based on numerous analytical prescriptions.

The loss of usability was quantified by calculating the monthly number of tickets sold **(n),** the average ticket price **(c_b)** and the time to "Restore" the structure **(t),**ie.:

$$PF=n*c_b*t$$

These new parameters were then estimated. The monthly number of visitors (n), exponentially increasing in recent years (2009 to 2017), as can be seen from the graph, was extrapolated from the data of established annual visits, available from the museum website. In particular, the number of annual users of 2017 has been divided for the 12 months (last certain data)(Figure 64).

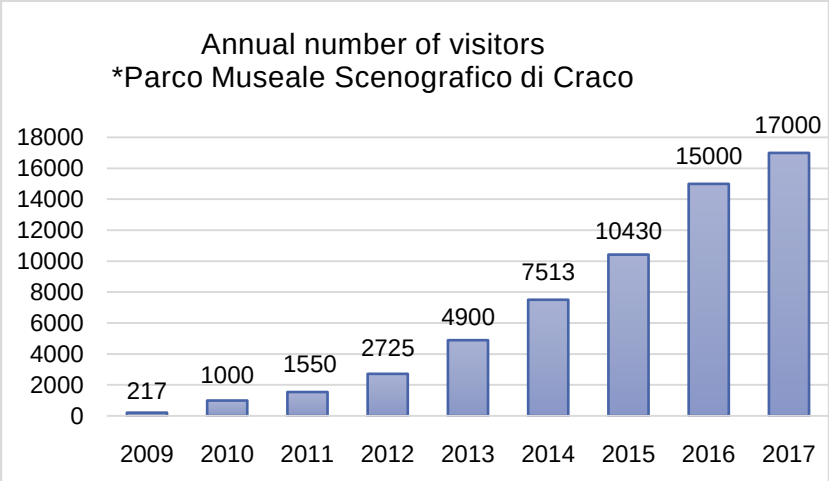

FIGURE 64. GRAPHIC OF ANNUAL NUMBER VISITORS

The number of annual visits was 17,000, so the monthly number is equal to:

$$n=1416$$

The ticket price was also found on the site of the "Parco ScenograficoMuseale di Craco"; it can cost from € 5.00 to € 20.00, but on average a standard ticket costs € 10.00, so the value taken into consideration is It was:

$$c_b= 10{,}00\ €$$

To identify a recovery time (t) and the mere Reconstruction Costs (CR) an intervention has been hypothesized, which foresees the faithful reconstruction of the "as it was, where it was" type, and therefore the realization:

- of the load-bearing stone masonry in its three different thicknesses (from 0.85 m, 1.7 m and 2.15 m);
- of the roof covering in reinforced concrete;
- of the concrete tank.

It was therefore estimated that this intervention:

- can last about 12 months, probably the shortest, to try to create the least possible discomfort at the museum: **t = 12 months**,
- have a **CR cost of € 316,468.00.**

Table 12 summarizes the CRs that have been calculated through the Regional Register of the Basilicata Region.

Cost of reconstruction Regional price list 2018 - Basilicata Region								
	thickness	h/wide	length	n	tot	U.M.	Unitary cost	
Masonry	2,15	13,61	8,46	2,00	495,10	mc	€ 178,37	€88.311,80
	2,15	13,61	8,76	2,00	512,66	mc	€ 178,37	€91.443,43
	1,70	7,56	8,46	2,00	217,46	mc	€ 178,37	€38.787,60
	1,70	7,56	8,76	2,00	225,17	mc	€ 178,37	€40.163,04
	0,85	0,76	9,20	2,00	11,89	mc	€	€2.120,18

							178,37	
	0,85	0,76	9,50	2,00	12,27	mc	€ 178,37	€2.189,31
								€263.015,37
Floor slab Cls Rck30	0,25	4,16	4,46		18,55	mq	€ 54,64	€1.013,77
	0,25	4,90	5,20		25,48	mq	€ 54,64	€1.392,23
								€2.406,00
Cistern Cls Rck25	0,35		r=3,20	area base cisterna	32,15	mq	€ 134,40	€4.320,96
	0,35	17,30		area laterale cisterna	347,66	mq	€ 134,40	€46.725,50
								€51.046,46
TOT								**€316.467,83**

TABLE 12. COSTS OF RECONSTRUCTIONS CR CALCULATED THROUGH THE REGIONAL REGISTER OF BASILICATA

Finally:

Cost of reconstruction	**CR**	**€ 316.468,00**
Loss of usability	PF	€ 170.000,00
Cost of reconstruction*	**CR***	**€ 486.468,00**

For the calculation of the Seismic Risk of the Tower, the analysis of the structure was carried out using PROSAP software [39], for which the Tower was modeled with the same characteristics of the model in STRAUS, this allowed to determine the values of ground accelerations of capacity , PGA_C (SLi), which induce to reach the limit states indicated by the standard (SLC, SLV, SLD, SLO). In a simplified way, the checks have been carried out limited to the SLV and the SLD, since the other two SLs can be determined according to the SLV and the SLD, and in particular it was found that:

PGA_{SLV}= 0.083g

PGA_{SLD}= 0.0336g

The return periods, T_{rC}, associated with earthquakes generating ground accelerations, PGA_{SLV} and PGA_{SLD} were then evaluated. The transition from PG_{AC} (PGA_{SLV} and PGA_{SLD}) to the values of the return period were performed using the following relationship, as indicated by the legislation:

$$T_{rC} = T_{rD} (PGA_C/PGA_D)^{\eta}$$

with ηequal to:

$\eta = 1/0{,}356$ for $0{,}15g \geq a_g \geq 0{,}05g$
$\eta = 1/0{,}34$ for $0{,}05g > a_g$

For each return period T_{rC} the average annual frequency of exceedancehas been defined:

$$\lambda = 1/T_{rC}$$

having conducted the analysis of the structure only for SLV and SLD limit states, it was possible to define the average annual frequency of exceedance for the limit states not investigated according to these simplified expressions:

$\lambda_{SLO} = 1{,}67\lambda_{SLD}$
$\lambda_{SLC} = 0{,}49\lambda_{SLV}$,

Finally, the minimum and maximum values of economic loss for the reconstruction of the Tower were defined as 0% and 100% of the **Reconstruction Cost** (CR) and were associated, as indicated by the Codes, to:

- the Start Damage Limit State (SLID), a zero economic loss (0%) at a seismic event with a return period conventionally assumed to be 10 years, i.e., $\lambda = 0.1$;

• the Restoration Limit State (SLR), an economic loss of 100%, that is, a demolition and reconstruction intervention with a return period conventionally equal to that of the Limit State of the Collapses (SLC), i.e., $\lambda = 0$.

For each of the Limit States considered, the value of the reconstruction cost percentage is associated with the corresponding value of λ.

According to Table 13, as indicated by the code:

LIMIT STATE	CR* (%)	COST (€)
SLR	100%	€486.468,00
SLC	80%	€389.174,00
SLV	50%	€194.587,00
SLD	15%	€29.188,00
SLO	7%	€2.043,00
SLID	0%	€0,00

TABLE 13. RECONSTRUCTION COSTS (CR)/RESTORATION, ASSOCIATED WITH THE ACHIEVEMENT OF EACH LIMIT STATE FOR THE TOWER OF CRACO, OBTAINED ACCORDING TO PERCENTAGE, AS PER REGULATIONS.

This relationship was then diagrammed and PAM (in percentage value) was defined as the area subtended by the broken line of the Average Expected Annual Loss, identified by the pairs of points (λ, CR), for each of the above-mentioned limit states, to which the point (λ=0, CR = 100%) is added through the following the expression:

$$PAM = \Sigma^{5}_{i=2} [\lambda(SL_i) - \lambda(SL_{i-1})]*[CR(SL_i) + CR(SL_{i-1})]/2 + \lambda(SLC)*CR(SLR)$$

where index “i” represents the generic limit state (i=5 for SLC and i=1 for SLID)

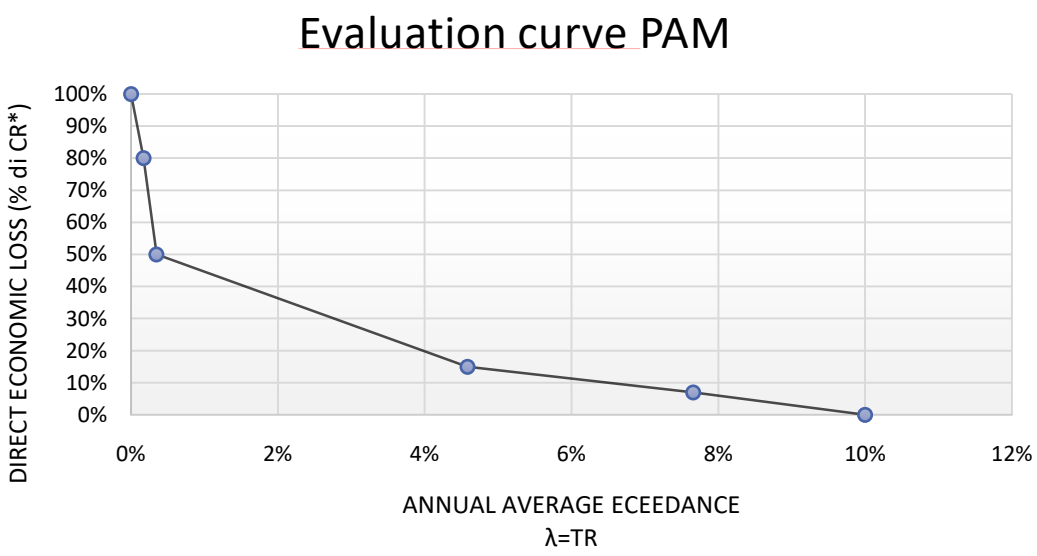

Average Expected Annual Loss (PAM):

ANNUAL AVERAGE ECEEDANCE $\lambda=1/T_R$			
SLR	100%	λ_{SLR}	0
SLC	80%	λ_{SLC}	0.002
SLV	50%	λ_{SLV}	0.003
SLD	15%	λ_{SLD}	0.046
SLO	7%	λ_{SLO}	0.077
SLID	0%	λ_{SLID}	0.100

AVERAGE ANNUAL FREQUENCY OF EXCEEDANCE

Finally, the PAM Class is identified by means of the table of the code that associates the class with the range of values assumed by the PAM (Table 14).

In our case **PAM = 2.07%**, therefore Class: **C_{PAM}**

Perdita Media Annua attesa (PAM)	Classe PAM
PAM ≤ 0,50%	A^{+}_{PAM}
0,50% < PAM ≤ 1,0%	A_{PAM}
1,0% < PAM ≤ 1,5%	B_{PAM}
1,5% < PAM ≤ 2,5%	C_{PAM}
2,5% < PAM ≤ 3,5%	D_{PAM}
3,5% < PAM ≤ 4,5%	E_{PAM}
4,5% < PAM ≤ 7,5%	F_{PAM}
7,5% ≤ PAM	G_{PAM}

TABLE 14. TREND OF THE CURVE THAT IDENTIFIES PAM, REFERRING TO A CONSTRUCTION WITH A NOMINAL LIFE OF 50 YEARS AND BELONGING TO THE USE CLASS II.

The safety index for life IS-V is determined, that is the ratio between PGA_C (of capacity) that made the building reach the state limit of safeguarding human life and PGA_D (of demand) of the site where the constructionis positioned, with reference to the same limit state, to then identify Class IS-V, by means of the following table present in the standard, which associates the class with the range of values assumed by IS-V Safety Index, evaluated as a ratio between PGA_C (SLV) and PGA_D (SLV). In our case **PGA_D = 0.103g** and **PGA_C = 0.083g**. So the ratio is equal to:

$$\mathbf{PGA_c/PGA_D = 81\%}$$

Indice di Sicurezza	Classe IS-V
100% < IS-V	$A^{+}_{IS\text{-}V}$
80% ≤ IS-V < 100%	$A_{IS\text{-}V}$
60% ≤ IS-V < 80%	$B_{IS\text{-}V}$
45% ≤ IS-V < 60%	$C_{IS\text{-}V}$
30% ≤ IS-V < 45%	$D_{IS\text{-}V}$
15% ≤ IS-V < 30%	$E_{IS\text{-}V}$
IS-V ≤ 15%	$F_{IS\text{-}V}$

TABLE 15 –ATTRIBUTION OF IS-V RISK CLASS ACCORDING TO THE EXTENT OF THE SECURITY INDEX

Therefore, according Table 15 “Attribution of IS-V Risk Class”, the Safety Index Class (IS-V) or Risk Index is equal to $\mathbf{A_{IS\text{-}V}}$.

It follows that the final **SEISMIC RISK CLASS** of the Tower is **C**, as it is equal to the worst/lowest class between the PAM Class and the IS-V Class, or the one corresponding to the highest risk. In our case, in fact, the PAM Class is equal to C and Class IS-V to A.

In conclusion, for the Norman Tower, being an asset with significant historical and cultural value, hypothesizing a cost of reconstruction alone is not plausible. Its reconstruction, however, economically estimable, can in no way make up for the historical and cultural value lost in the event of its collapse. The identified approach, therefore, for the estimation of the CR * parameter represents a possible proposal for the determination of an economic value of PAM, associated with types of buildings with high historical and cultural value and accessible to the public.

III. Multi-risk analysis

Italy is characterized by many heavily populated areas and a territory which, due to its specificities, is highly exposed to different natural risks, many of which concern the same area. In fact, the uncertainty of the occurrence of a natural event requires a study of risk analysis both single and multi-risk, as the territory, also due to its specific geomorphology, if involved in a natural event, could be subject to a cascade effect to further natural events, all linked together. The complexity of the possible scenarios that can occur is the result of the amplification of the effect of the events considered individually. In order to develop a model suitable for the prevention and minimization of effects, it is necessary to use algorithms that

allow, once the probability intensity distribution of the natural trigger event is determined, to derive the probabilities of the sequences of possible events that constitute the waterfall.

Thus the need to use multi-risk methods is born: a careful analysis that considers the interaction between the events, the possible cascade effects and the evaluation of all the elements affected, represents a useful starting point for monitoring and planning the development of a territory, also in terms of post-event emergency management.

In the previous sections, the landslide and seismic risk analyzes were carried out individually. In this section we will try to identify a methodology that allows us to compare the results obtained, associating the specific PGA values for the Norman Tower with the landslide risk indices, obtained by mapping the territory.

III.1 Starting values

III.1.1 Landslide risk

The landslide risk of the Municipality of Craco presents a varied mapping, as it is possible to identify the areas representative of the three risk levels assessed: high, average or low. In particular, from the Pai cartography [29] and from the analysis carried out by ENEA [28], the Norman Tower falls within the area characterized by low level.

As explained in the introduction, the combination of different events could amplify the natural effects found on the territory and on the built heritage, therefore, for the sediment area of the Norman Tower positioned on the sheer rock of the north-eastern slope and in correspondence with a niche of detachment of a slow flow active in the past, it is interesting to consider the possible scenarios that can be triggered, assessable through different Degrees of Risk.

For this reason, in this study, the hypothesized scenarios provided for the activation of only the type of landslide, the "slow flow" one, present on the same side of the Tower. The activation of this phenomenon could occur due to a joint seismic event. Instead, the rotational-translational sliding type was excluded as it is present on the South side of the Municipality of Craco, too far from the subject of the research.

Once the type of landslide and its hazard have been defined, it is necessary to identify the parameters that describe and evaluate the risk connected to the type of event considered and that take into account the factor linked to the exposure. The methodology adopted hypothesizes several possible scenarios through the definition of three degrees of damage (Tab.16), at the basis of the multi-risk analysis.

Risk grade	Real estate	Activity
Low	Minor aesthetic or functional damage	Socio-economic activities are not interrupted
Average	Functionaldamage	Interruption of socio-economic activities
High	Slight and relevant Structural damage, until the total collapse	Destruction of socio-economic activities

TABLE 16 – CLASSIFICATION OF DAMAGE GRADE FOR LANDSLIDE RISK.

III.1.2 Seismic risk

In Chapter II, the seismic risk of the Norman Tower was analyzed using the conventional method, determining the peak ground acceleration (PGA) for each limit state, from which, subsequently, it was possible to obtain all the return times (T_{rC}) and the various annual average frequencies of exceedance (λ_{Sli}). Through the latter (λ_{Sli}) and the percentages, indicated by the code, relating to the cost of reconstruction for the achievement of each limit state of the structure, the curve representing direct economic losses is identified. The area

underlying this curve represents the expected annual average loss PAM (Fig.65). Table 17 and Figure 70show that the proposed methodology divides the underlying area of the curve and therefore the possible damage scenarios, with respect to the achievement of the various Limit States, into three degrees of damage. This allows to distinguish the scenarios from structural and non-structural damage, in particular, the degree will be low if the scenarios foresee non-structural damage, average if they foresee non-structural damage and minor structural damage, high if they foresee serious structural damage leading to collapse or to the possible loss of human lives that benefit from the structure at the time of the seismic event.

Risk grade	State limit	Real estate	Activity
Low	SLID – SLO	No structural damage	Socio-economic activities are not interrupted
Average	SLO-SLD-SLV	Slight structural and unstructural damage	Interruption of socio-economic activities
High	SLV-SLC	Structural damage: from the human life preservation to close to collapse scenario	Destruction of socio-economic activities

TABLE 17 – CLASSIFICATION OF THE DAMAGE DEGREE FOR SEISMIC RISK.

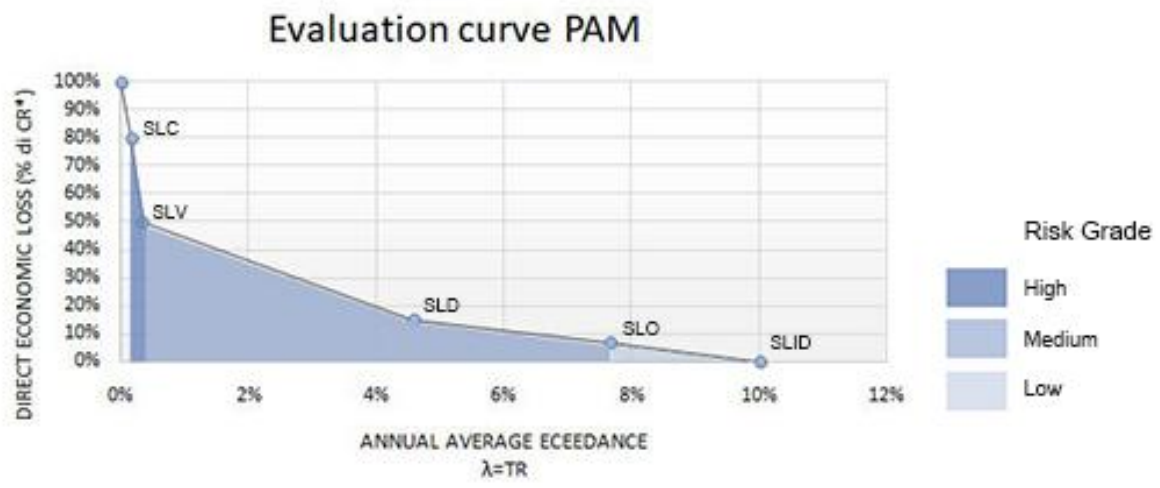

FIGURE 65– IDENTIFICATION OF THE DEGREES OF DAMAGE FOR SEISMIC RISK ON THE PAM CURVE.

Through this methodology, three degrees of damage were identified, attributable to the seismic risk, to be related to the multi-risk analysis with the three values emerged from the Landslide Risk.

III.2 Comparison of values

The comparison was made by taking the three degrees of possible damage, obtained previously, for both seismic and landslide risks.

The frequency and degree of the two individual risks were compared and combined, assessing the predominance of one risk over the other. This comparison made it possible to identify a “Multi-Risk Matrix” (table 18).

In any case, keep in mind that the Norman Tower suffers relatively the effects of the landslide risk. Therefore, the seismic risk, althoughnot high, isdominant.

Risk grade		**Landslide Hazard**		
		Low	Average	High
Earthquake Hazard	Low	El-Ll	El-La	El-Lh
	Average	Ea-Ll	Ea-La	Ea-Lh
	High	Eh-Ll	Eh-La	Eh-Lh

TABLE 18 – MULTI-RISK MATRIX.

Several scenarios are shown in the Table 18:

1. **El-Ll:** both Risks cause low level of damage, for which significant structural damage and interruption of use of the activity are not expected;
2. **Ea-Ll:** seismic risk is dominated by landslide risk, with slight structural and non-structural damage and the interruption of use;

3. **Eh-Ll:** the seismic risk is dominated by the landslide risk, with structural damage detected that could lead to the collapse and immediate interruption of use;
4. **El-La:**Average landslide risk predominant over the low seismic risk, the damages are only non-structural or functional, so there is only loss of ease;
5. **Ea-La:** the combination of both risks, seismic and landslide, at an average level leads to the non-use of the tower and to the presence of slight non-structural and structural damage;
6. **Eh-La:** the high seismic risk combined with a average landslide risk causes the non-use of the tower and the presence of significant structural damage up to the possible partial or total collapse of the structure;
7. **El-Lh:** the risk from high landslide predominated over the low seismic risk, for which the damages found are slight structural and lead to the non-usability of the tower;
8. **Ea-Lh:** High landslide risk and average seismic risk, the damages found are structurally significant and lead to the non-usability of the Tower;
9. **Eh-Lh:** both high Risks, the detectable damages are structural and significant up to the possible partial or total collapse of the structure and lead to the non-usability of the Tower.

III.3Hypothesis of involvement of the tower from the landslide front

A linear analysis of the stress state of the tower was also carried out.Starting from the historical data of the instabilities suffered in Craco (deformations of the ground) collected and analyzed in [28], three imposed vertical displacementhave been hypothesized at the base, in correspondence with the South side, that is the one closest to the landslide front. These

displacements can be associated with the three scenarios, which define in the previous chapter (III.1.1) the Damage Degrees of due to Landslide Risk:

- Low hazard: 200mm;
- Average hazard: 500 mm;
- High hazard: 1000 mm.

The model, visible in Fig. 66, has been subjected to a seismic analysis which also includes the three different displacements. Sothe results, visible fromFig. 67 for each displacement,outline the stress state of the tower in relation to the Linear Analysis carried out on Prosap [39] and highlight the combined behavior of the tower subjected to Heartquake Risk and a simulated Landslide Risk, or rather aMultirisk Analysis in the event of a determinate vertical displacement imposed on the basis of historical data collected.

FIGURE 66–PROSAP FE-MODEL OF THE TOWER WITH IMPOSED VERTICAL DISPLACEMENT

Vertical Displacement egual to 200mm

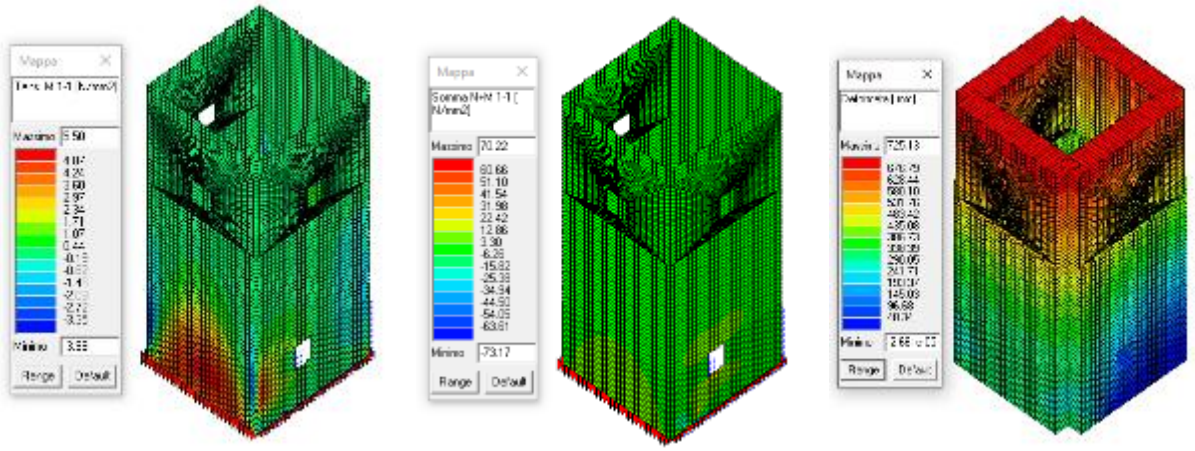

Vertical Displacement egual to 500mm

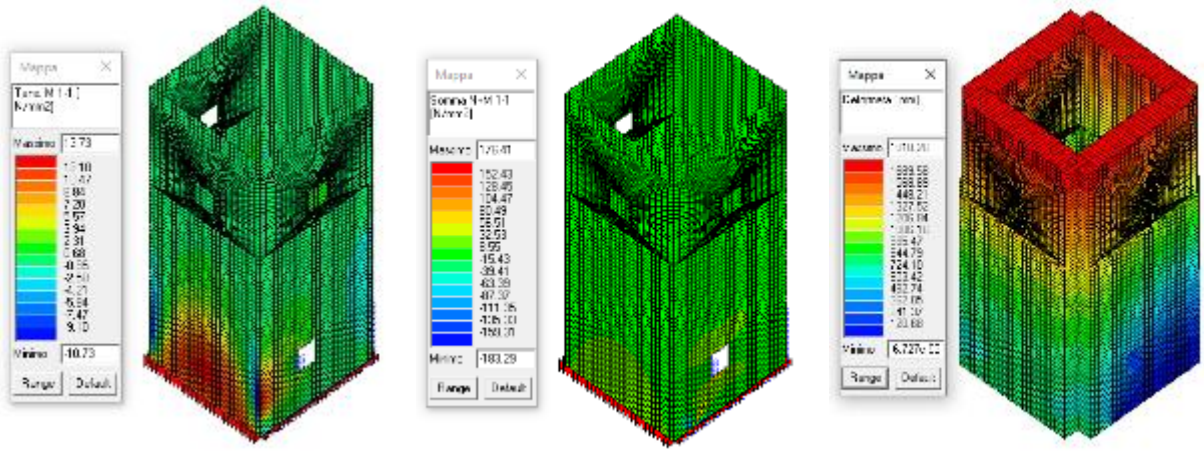

Vertical Displacement egual to 1000mm

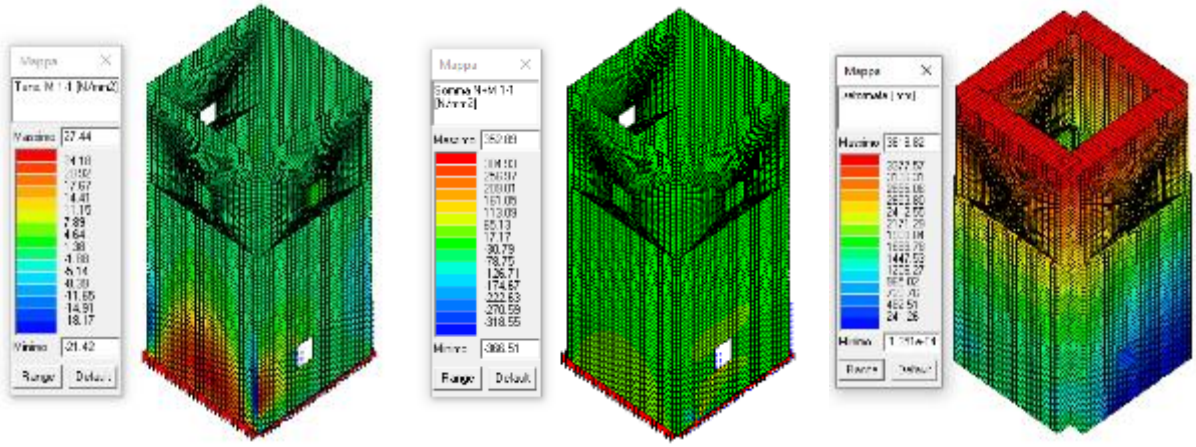

FIGURE 67–STRESS STATE AND DEFORMATION OF THE TOWER FOR DIFFERENT IMPOSED VERTICAL DISPLACEMENT.

In landslidecase,the hammering action of the tankRCfoundation on the masonry basement, could carry out possible scenarios.In particular, two different configuration were investigated in which several constraints at the base were partially removednear the landslide front. The figures 68-69outline, for each “constraint configuration”, the stress state of the tower in relation to the Linear Analysis carried out on Prosap [39] and highlight the combined behavior of the tower subjected to Heartquake Risk and a simulated Landslide Risk, or rather a Multirisk Analysis in the case of a determinated constraint configuartion imposed.

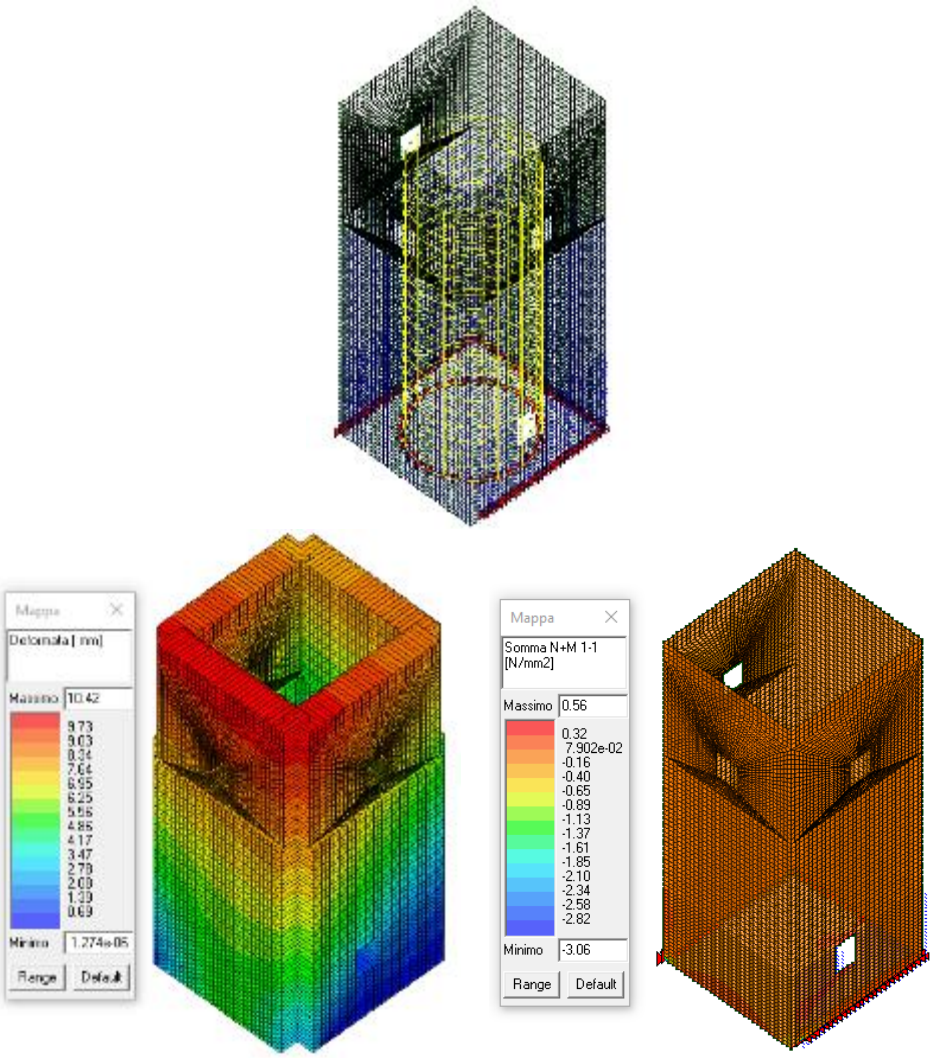

FIGURE 68–STRESS STATE AND DEFORMATION OF THE TOWER

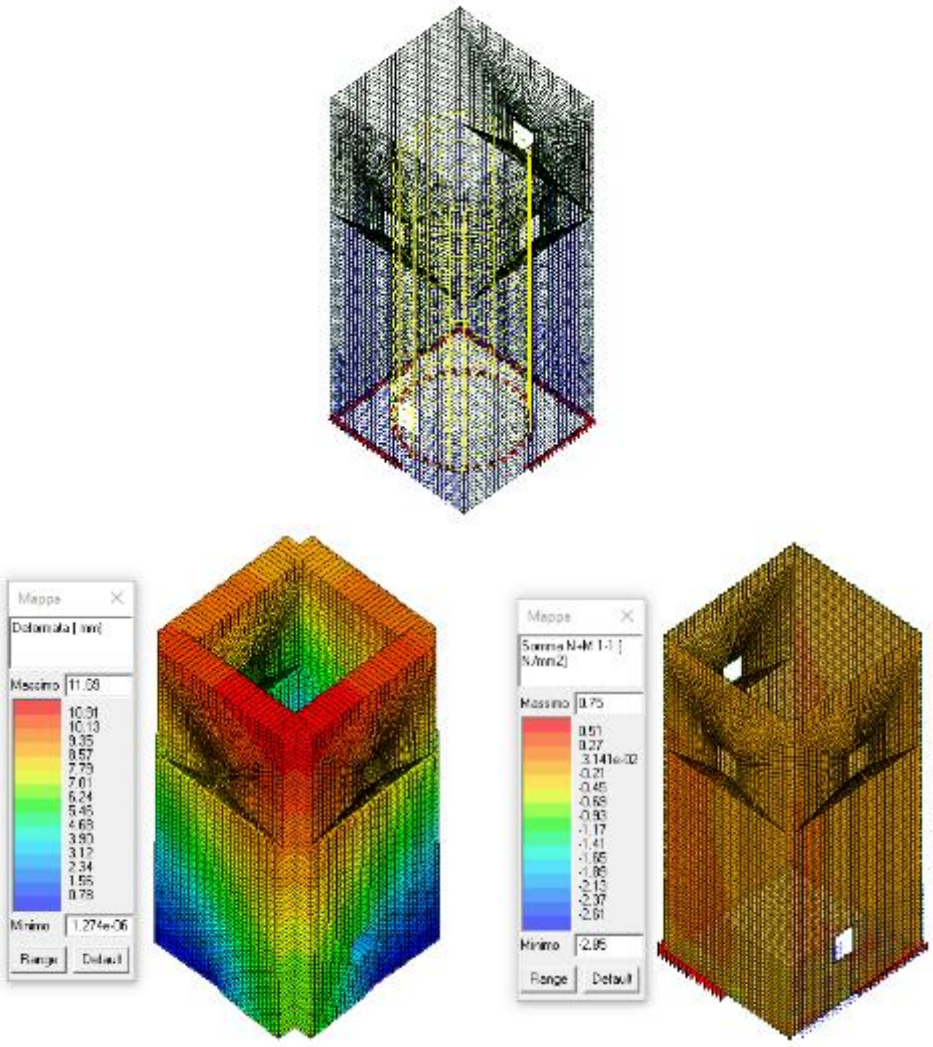

FIGURE 69–STRESS STATE AND DEFORMATION OF THE TOWER

IV. Risk Mitigation

The analyzes conducted in the previously described phases have made it possible to construct a detailed picture of the characteristics of both the phenomena of instability and the context within which they developed. In order to contain and mitigate the analyzed Risks, a monitoring system of the entire area of the Municipality of Craco and, specifically, of the investigated structure and a hypothesis of intervention of arrangement and consolidation of the land have been designed, in order to preserve and make it safe the Norman Tower.

Based on the design idea developed in [38] the areas on which it was deemed appropriate to provide for the installation of a monitoring system are those indicated as:

- Area of the historical center
- Convent area

The plans in Figs. 70-71 show the arrangement of the equipment and perforations to be made.

From a general point of view, a master acquisition unit (UMP) was planned to be installed in the Convent area, which is also the most suitable place for the installation of a weather station connected by cable. The weather station allows you to have a series of continuous data relating to temperatures and rainfall, such as to be able to make precise correlations with any displacements recorded by the kinematic monitoring system.

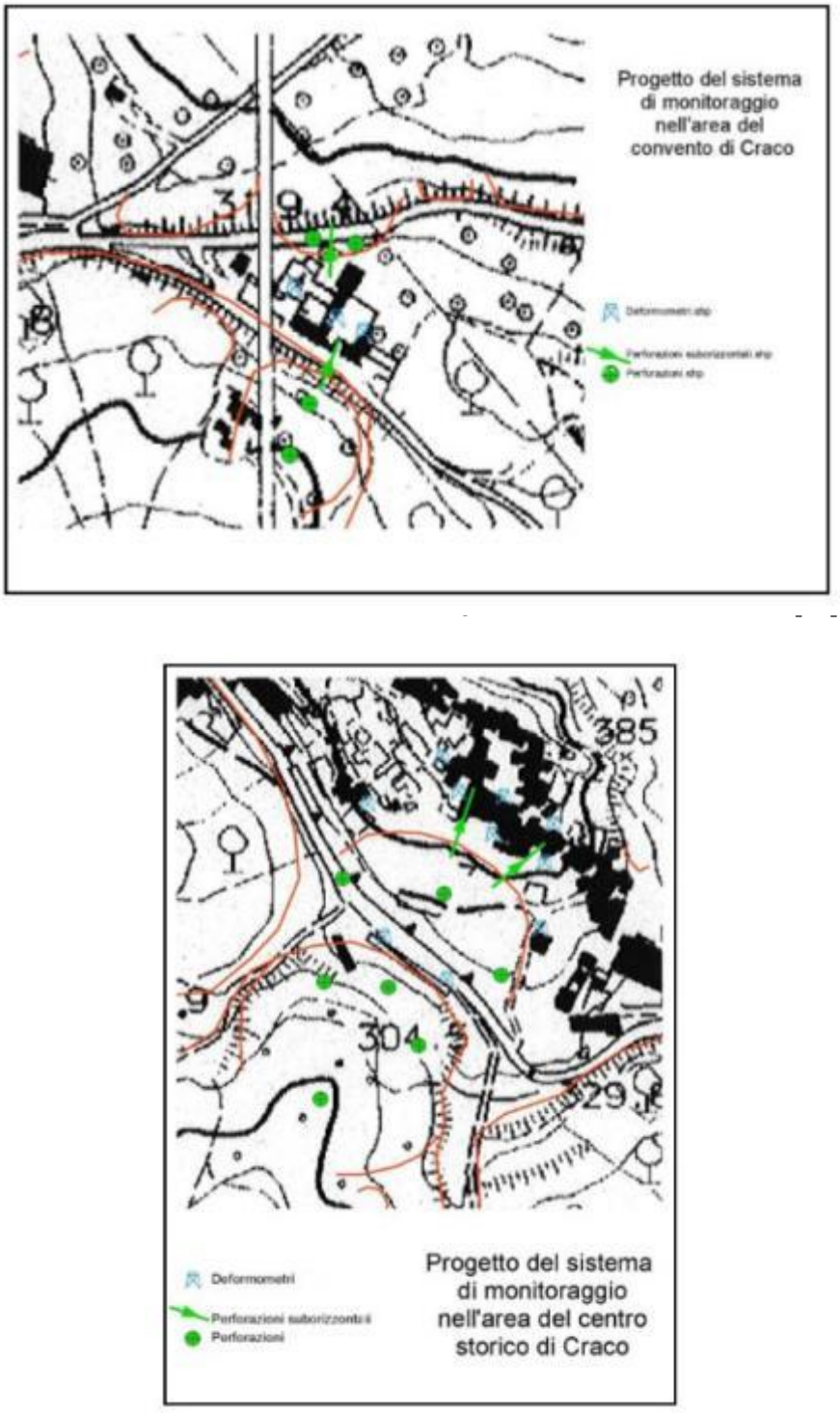

FIGURE 71 - ARRANGEMENT OF MONITORING EQUIPMENT IN THE HISTORICAL CENTRE AREA [38]

SITO HISTORIC-ARCHEOLOGIC MONITORING SYSTEM OF *CRACO*			
EQUIPMENT	**NUMBER**	**SURVEYS**	
		NUMBER	**TOTAL METERS**
Piezometer	6	6	120
Crack placement sensor	8		
Inclinometer	6	11	290
Extensometer	3	3 (sub-horizontal)	110
Meteo station	1		

TABLE 18. EQUIPMENT FOR KINEMATIC MONITORING OF THE TWO SECTORS OF THE HISTORIC CENTRE AND THE CONVENT OF CRACO

regards the area of the historic center, two separate data acquisition and transmission units (UMP) were planned to be connected via cable to the sensors located upstream and downstream of the road, respectively. The data must be transmitted to the master acquisition system in the Convent using appropriate radio modems.

In addition to recording the oscillations of the aquifer through a series of piezometers arranged in the two areas, the monitoring system provided will allow both measurements of displacements in depth through the installation in hole of strain gages, inclinometers and TDRs, and deformations of elements constituting the structures of the buildings of the Historic Center and the Convent.

As far as the perforations are concerned, surveys have been provided each for the installation of piezometric probes with inclinometer tubes and probes for deep strain gages.

On the Tower there will be n. 6 accelerometers arranged on several levels at the two opposite corners of the structure.

In addition to the rains, other factors that have contributed negatively to the stability of the slopes are attributable to anthropogenic factors such as:

- the abandonment of wells following the construction of the aqueduct network

- losses in the aqueduct and sewage networks, which produced additional water supplies in the land; infiltration was also favored by cuts and excavations produced by anthropic activity.

- the construction of the football field right inside the landslide niche; the construction of this work has in fact produced an increase in the stability conditions of the slope, in terms of an increase in the mobilizing forces acting on the slope;

- the support work on highway 103 close to the historic center.

The interventions proposed in [38] foresee both the quenching and tempering of the slopes of the Craco hill and the safety of the areas most affected by the phenomena on which goods that require protection actions insist. Overall, the regulation of most of the ditches along the slopes of the Craco hill and the construction of hydraulic works useful for removing the waters from the land along the slopes and in areas close to the Historic Center and the Conventmust be carried out.

The quenching and tempering of the slopes must include different drainage interventions:

• superficial and sub-superficial draining trenches;

• deep draining wells;

• arrangement of the ditch beds by possible remodeling and naturalistic engineering works.

The interventions must achieve the following results:

• to avoid, as far as possible, that the waters present in the aquifer of the conglomerate-sandy top unit affect the complex of varicolor clays and Pliocene clays;

• drain water deep into the areas of the most superficial landslides, in order to reduce interstitial pressures within the varicolor clays;

• reduce the imbibition of the surface blanket along the slopes by rainwater, in order to avoid feeding the deeper layers, whose excursions contribute to the instability of landslide bodies;

• avoid linear erosion along the rivers which contributes both to the development of badlands and to the undermining of the slopes at the foot;

• avoid that water leaks from the sewer and water network contribute to a further contribution in the conglomerate-sandy summit complex.

Conclusions

The present study focuses on the multi-risk analysis of a mixed structure made with masonry walls, which encloses an element in reinforced concrete, such as the Norman Tower of Craco.

In particular, the risks being assessed are: Earthquake Risk and Landslide Risk.

This choice depended on the typological nature of the soil on which the structure is based, falling within the “Average” seismicity area according to the Italian classification [40] and on the historical archive of landslides, which significantly affected the area in the last century.

The approach proposed for the study is concentrated in a first phase on the vulnerability of Tower about Landslide Risk. The latter was based on data collected in scientific literature [28] and on the PAI Italian legislation [29].

In a second phase, the Earthquake Monorisk was analyzed, on the basis of the structural characteristics and seismic parameters of the area and the economic value of the “Average Annual Loss” (in Italian “Perdita Media Annua: PAM”), thatis assessed in order to be able to classify the structure, which has some peculiarities being a historical-monumental building for museum use.

The results obtained from the two Mono-risk assessments made feasible the developmentof an approach aimed at the qualitative identification of possible damage scenarios as a result of the combination of the effects due to both the individual risks.

The uncertainty of these events motivated the development of a model for the numerical analysis of the Tower, which considers the Earthquake Risk and the Landslide Risk, through

the hypothesis of displacements at the base, so as to be able to quantify the damage on the structure, due to the co-presence of the two events.

References

[1] Ivorra S., Pallares F. - Dynamic investigations on a masonry bell tower, Eng Struct, 28(5) (2006) pp.660–667

[2]Meskouris K. - Structural dynamics, models, methods, examples, Ernst & Sohn, Berlin, 2000.

[3] Foti D., Debernardis M., Paparella V. - Structural Safety Control of Masonry Buildings: NonLinear Static Seismic Analysis with a Non-Linear Shear Strength Criterion, In: B.H.V. Topping, (Editor). Proc. of the Eleventh International Conference on Computational Structures Technology. Dubrovnik, 4-7 sept. 2012, STIRLINGSHIRE: Civil-Comp Press, doi: 10.4203/ccp.99.

[4] Foti D. - A New Experimental Approach to the Pushover Analysis of Masonry Buildings, Computers and Structures (2014).

[5] Modena C., Valluzzi M.R.,. TonginiFolli R, Binda L. - Design choices and intervention techniques for repairing and strengthening of the Monza cathedral bell-tower, Constr Build Mater, 16(7) (2002) 385–395.

[6] Castellano A., Foti P., Fraddosio A., Marzano S., Mininno G., PiccioniM.D. - Seismic Response of a Historic Masonry Construction Isolated by Stable Unbonded Fiber-Reinforced Elastomeric Isolators (SU-FREI), Key Engineering Materials (2014).

[7] Formisano A., Mazzolani F.M., Florio G., Landolfo R. - A quick methodology for seismic vulnerability assessment of historical masonry aggregates, in: Proc. of the COST Action C26 Final Conference “Urban Habitat Constructions under Catastrophic Events”, Federico M. Mazzolani, Chair, Naples, 16-18 September 2010, CRC Press, Taylor & Francis Group, London, 577- 582.

[8] Formisano A., Florio G., Landolfo R., Mazzolani F.M. - Numerical calibration of a simplified procedure for the seismic behaviour assessment of masonry building aggregates, in: Proc. of the 13th International Conference on Civil, Structural and Environmental Engineering Computing, CC 2011; Chania, Crete; 6 - 9 September 2011.

[9] FotiD. - Identification of the modalproperties of a Medieval tower next to a landslide, in press in: Proc International Forum “Le Vie dei Mercanti”, Editor La Scuola di Pitagora, in“Fabbrica della Conoscenza”, 12-14 June 2014, ID 184.

[10] Foti D., Gattulli V., Potenza F. - Output-only modal identification in unfavourable testing conditions and finite element model updating of a seismically damaged building, ComputerAided Civil And Infrastructure Engineering, 2014, Online ISSN: 1467-8667, doi: 10.1111/mice.12071.

[11] Foti D., Diaferio M., Giannoccaro N.I., Mongelli M. - Ambient Vibration Testing, Dynamic Identification and Model Updating of a Historic Tower, NDT&E Int.47 (2012) 88-95, doi:10.1016/ j.ndteint.2011.11.009.

[12] Foti D., Ivorra S., Bru D., Dimaggio G. - Dynamic Identification of a Pedestrian Bridge using OMA: Previous and Post-Reinforcing, In: B.H.V. Topping, (Editor). Proceedings of the Eleventh International Conference on Computational Structures Technology.

Dubrovnik, 4-7 sept. 2012, STIRLINGSHIRE: Civil-Comp Press, ISBN: 978-1-905088-54-6, doi: 10.4203/ccp.9.9

[13] Diaferio M., Foti D., Mongelli M., Giannoccaro N.I., Andersen P. - Operational Modal Analysis of a Historical Tower in Bari, in: Conference Proc. of the Society for Experimental Mechanics Series, "IMAC XXIX". 7 (2011) 335-342, doi: 10.1007/978-1-4419-9316-8_31, 31Jan.-3 Feb. 2011, Jacksonville, Florida, USA.

[14] Diaferio M., Foti D., Sepe V. - Dynamic Identification of the Tower of the Provincial Administration Building, Bari, Italy, in: Proc of the Eleventh International Conference on Civil, Structural and Environmental Engineering Computing, Malta, 18-21 Sept. 2007, paper n. 2.

[15] Lepidi M., Gattulli V. & Foti - Swinging-bell resonances and their cancellation identified by dynamical testing in D.a modern bell tower, Eng Struct, 31(7) (2009) 1486–1500.

[16] DPCM 02.09.2011. Valutazione e riduzione del rischio sismico del patrimonio culturale con riferimento alle Norme tecniche per le costruzioni di cui al DM 14/01/2008.

[17] Foti D., Ivorra S., Sabba' M.F. - Dynamic Investigation of an Ancient Bell Tower with Operational Modal Analysis, The Open Constr and Build Tech J, 6 (2012) 384-391, doi: 10.2174/1874836801206010384.

[18] Foti D., Diaferio M., Giannoccaro N.I. - Non-Destructive Monitoring of an Old Masonry Clock Tower with Forced and Environmental Actions, in press in: Proc International Forum "Le Vie dei Mercanti", Editor La Scuola di Pitagora, in "FabbricadellaConoscenza", 12-14 June 2014, ID 111.

[19] Balduzzi A., Casnedi R., Crescenti U., TonnaM. – Il Plio-Pleistocene nel sottosuolo del bacino pugliese (Avanfossa Appenninica). Geologica Romana, 1982

[20] Roure F., Casero P., Vialley R. – Growth process and melage formation in tje southern Appenninesacretionary wedge. Earth and Planet.Sc.Lett., 102: pp. 395-412, 1991

[21] Ciaranfi N., D'alessandro A., Marino M. – A candidate section for the Lower-Middle Pleistocene boundary (Appennine Foredeep, South Italy), 1997. In: W. Naiwen and J. Remane (Eds), Proceedings at the 30th International Geological Congress

[22] Bentivenga M., Coltorti M., Prosser G. – Il movimento gravitativo profondo di Craco (Basilicata Ionica). Il Quaternario, Italian Journal of Quaternary Sciences 17(2/2), 2004, pp. 613-625

[23] Carrara A., D'elia B., Semenza E. – Classificazione e nomenclatura dei fenomeni franosi. Fa parte di : Geologia Applicata e Idrogeologia, n° 20, II, pp. 223-243, Bari, 1985

[24] Carrara, A., &Cardinalli, M. (1991). GIS technology in mapping landslide hazard Carrara, A. and Guzzetti, F. Geographical Information Systems in Assessing Natural Hazard, Kluwer Academic Publisher (1995), 173-175.

[25] Hammond, C. (1992). Level I stability analysis (LISA) documentation for version 2.0 (Vol. 285). US Department of Agriculture, Forest Service, Intermountain Research Station.

[26] Montgomery, D. R., & Dietrich, W. E. (1994). A physically based model for the topographic control on shallow landsliding. Water resources research, 30(4), 1153-1171.

[27] Dietrich, W. E., & Montgomery, D. R. (1998). SHALSTAB: a digital terrain model for mapping shallow landslide potential. University of California.

[28] Corrado M., Delmonaco G., Falconi L., Margottini C., Martini G., Paolini S., Spizzichino D.- Linee guida per la salvaguardia dei beni culturali dai rischi naturali. Analisi per la valutazione del rischio di frana nell'area di Craco (MT). Consorzio Civita, Roma, ENEA C.R. Casaccia, Roma, ENEA C.R.

[29] Italian Law 183/89: the Plan for the Hydrogeological Structure (or PAI)

[30] Legislative Decree 152/2006: Consolidated Act on the Environment

[31] http://www.istat.it/it/mappa-rischi

[32] D. Foti, (2015) Non Destructive Techniques and Monitoring for the Evolutive Damage Detection of an Ancient Masonery Structure. Key Engineering Materials Vol. 628 pp. 168-177. Trans Tech Publications, Switzerland

[33] DPCM 02/09/2011 Valutazione e riduzione del rischio sismico del patrimonio culturale con riferimento alle Norme tecniche per le costruzioni di cui al DM 14/01/08

[34] A. Formisano, F. M. Mazzolani, G. Florio, R. Landolfo - A quick methodology for seismic vulnerability assessment of historical masonry aggregates. in: Proceedings of the COST Action C26 Final Conference "Urban Habitat Constructions under Catastrophic Events", Federico M. Mazzolani, Naples, 16-18 September 2010, CRC Press, Taylor & Francis Group, London

[35] C. Modena, M. R. Valluzzi, R. Tongini Folli. L. Binda - Design choices and intervention techniques for repairing and strengthening of the Monza cathedral bell-tower. Construction and Building Materials, Lambda, 2002, pp. 385–395

[36] LAB VIEW, National Instrument: Austin, TX (USA).

[37] STRAUS 7, v 2.3.3, Strand7 Pty Ltd (AUS).

[38] Craco. Linee guida per la salvaguardia dei beni culturali dai rischi naturali. https://www.afs.enea.it/protprev/www/cases/craco/craco.htm

[39]] 2S.I. ProSAP. PROfessional Structural Analysis Program 2017.

[40] DM 17 Gennaio 2018-Aggiornamento delle «Norme tecniche per le costruzioni». *Ministero delle Infrastrutture e dei Trasporti.Gazzetta Ufficiale della Repubblica Italiana*, n.*42*.

Publications produced within the project

S. IVORRA, N.I. GIANNOCCARO, D. FOTI, "Simple model for predicting the vibration transmission of a squat masonry tower by base forced vibrations", Structural Control and Health Monitoring, 2019, e2360; Doi:https://doi.org/10.1002/stc.2311

D. FOTI, M. LA SCALA, S. LAMONACA, V. VACCA : “Control of framed structures using intelligent monitoring networks”, MATEC Web of Conferences, Volume 125, article n. 05012, 04 October 2017. 21st International Conference on Circuits, Systems, Communications and Computers (CSCC 2017), DOI: https://doi.org/10.1051/matecconf/201712505012

M. DIAFERIO, D. FOTI, F. POTENZA: “Prediction of the fundamental frequencies and modal shapes of historic masonry towers by empirical equations based on experimental data”, Engineering Structures, vol. 156 (2018) 433–442.

M. DIAFERIO, D. FOTI, “Risk assessment of Trani’s Cathedral bell tower in Apulia, Italy”, International Journal of Advanced Structural Engineering (IJASE), September 2017, Vol. 9, Issue 3, pp 259–267. ISSN: 2008-3556, DOI: 10.1007/s40091-017-0162-0.

FOTI, D., LA SCALA, M., LAMONACA, S., VACCA, V., “An energy router for structural monitoring of framed buildings and real-time shutdown of power and gas supply during earthquakes”, WSEAS Transactions on Environment and Development, 2017, 13, pp. 405-502.

M. DIAFERIO, D. FOTI, N. I. GIANNOCCARO, S. IVORRA, “A nonlinear numerical model of a historical slender structure”, Proc. of the 4th International Conference on Mechanical Models in Structural Engineering CMMoST2017, 29th Nov.- 1st Dec. 2017, Madrid, Spain.

D. FOTI, V. VACCA, “Rocking of Multiblock stone classical columns”, Earthquake Resistant Engineering Structures XI, WIT Transactions on The Built Environment, Vol 172,2017, pp.11-13, ISBN: 978-1-78466-203-5.